CRACK PROPAGATION IN FINITE BODIES

A THESIS

Presented to

The Faculty of the Division of Graduate Studies

By

John Francis Malluck

In Partial Fulfillment

of the Requirements for the Degree

Doctor of Philosophy in the

School of Engineering Science and Mechanics

Georgia Institute of Technology

July, 1976

CRACK PROPAGATION IN FINITE BODIES

Approved:

W. W. King, Chairman

J. M. Anderson

J. A. Aberson

Date approved by Chairman 8/23/76

This thesis is dedicated

to my wife, Sandra, and my daughter, Lisa.

ACKNOWLEDGMENTS

I would like to express my gratitude to Dr. Wilton W. King, my advisor, for his guidance and encouragement throughout the course of this thesis. My sincere appreciation is due Dr. James A. Aberson, and Dr. Jerry M. Anderson for their assistance and suggestions. A special note of thanks is due Dr. James A. Aberson for performing the finite-element analysis required for a portion of this work, through the use of a computer program he and Dr. Joseph D. Morgan, III developed at Georgia Tech. Finally, I would like to thank all the above as well as Dr. Satya N. Atluri, Dr. John T. Berry, and Dr. Michael P. Stallybrass for reading and reviewing my thesis.

I gratefully wish to acknowledge the financial support of the National Science Foundation Traineeship program, the Ford Foundation, and the School of Engineering Science and Mechanics during my graduate studies.

My deepest appreciation goes to my wife, Sandra, and daughter, Lisa, for their encouragement, devotion, and understanding during the entire period of my studies. Completion of this thesis could not have been possible without their help.

I would also like to thank Mrs. Peggy Moore and Mrs. Jackie Van Hook for typing the preliminary draft of this thesis. A special note of thanks goes to Mrs. Jackie Van Hook for typing the final manuscript.

TABLE OF CONTENTS

TABLE OF CONTENTS (Continued)

LIST OF TABLES

LIST OF ILLUSTRATIONS

LIST OF ILLUSTRATIONS (Continued)

LIST OF ILLUSTRATIONS (Continued)

LIST OF SYMBOLS

Symbol	Definition
A	Cross-sectional area of the beam
A_b	Energy absorbed due to crack extension
$\hat{A}$	Constant given in equation (3.8)
$\hat{A}_n$	Coefficients of the eigenfunctions
a	Crack length
a_r	Crack arrest length
$a_1, a_2, \ldots, a_6$	Integration constants
$\hat{B}$	Constant given in equation (3.8)
b	Width of the beam
c	Crack speed
c_o	Bar wave speed
c_1	Dilatational wave speed
c_2	Shear wave speed
c_R	Rayleigh wave speed
COD	Crack opening displacement
DCB	Double cantilever beam
$d(\ )$	Total derivative
E	Elastic modulus
E_T	Total system energy
$F(\ )$	Interpolate function defined in equation (B.1)
$F_1(s_1, s_2)$	Function defined by equation (3.28)
$\underset{\approx}{F}$	Matrix of eigenfunctions

$F(s_i)$	Function defined by equation (3.31)
G	Shear modulus
G_q	Static strain energy release rate
$g(s_i)$	Function defined by equation (3.31)
h	Height of beam
I	Moment of inertia
j	Summation index
K_D	Dynamic stress-intensity factor
K_n	n^{th} coefficient of the eigenfunctions
K_q	Static stress intensity factor
$\underset{\sim}{K}$	Vector of coefficients K_n
$\bar{K}_e, \bar{K}_r$	Dimensionless elastic foundation parameters
k	Shear deflection coefficient of the beam
k_e	Extensional stiffness of the elastic foundation
k_r	Rotational stiffness of the elastic foundation
k_1	Stress-intensity factor as given in equation (3.28)
L	Length
ℓ	Summation index
M	Bending moment
M_T	Imposed moment at the crack tip
M_1, M_2	M defined in each beam section used for the static solution
m	Eigenvalues
N	Preselected number of eigenfunctions
n	Eigenvalues
P	Applied shear load

p	Constant (= 1)
Q_T	Load imposed at the crack tip
q	Constant ($= \sqrt{5}$)
R	Energy absorbed per unit area of crack extension
s_1, s_2	Parameters defined by equation (3.6)
T	Kinetic energy
t	Time
U	Strain energy
U^*	Lineal strain energy density
u_x	x component of displacement
u_y	y component of displacement
u_{x_n}	n^{th} eigenfunction for u_x
u_{y_n}	n^{th} eigenfunction for u_y
$\underset{\sim}{u}$	Vector of displacement components
V	Transverse shear
V_1, V_2	V defined in each beam section used for the static solution
v	Transverse velocity
v_e	Imposed velocity
W	Work due to external loads
w	z component of displacement
w_1, w_2	w defined in each beam section used for the static solution
X, Y, Z	Fixed Cartesian coordinate
x, y, z	Cartesian coordinates traveling with the moving crack tip

y_1, y_2	Coordinates defined by equation (3.5)
(r, θ)	Polar coordinate system traveling with the crack tip
(r_1, θ_1)	Polar coordinate system defined by equation (3.9)
(r_2, θ_2)	Polar coordinate system defined by equation (3.9)
α	Inverse slope of the II^+ characteristic lines
$\bar{\gamma}_1, \bar{\gamma}_2, \ldots, \bar{\gamma}_6$	Constants used in the static solution
δ	Prescribed deflection
δ_a, δ_b	Deflections given in Figure 25
∇^2	Laplacian operator defined by equation (3.1)
∇_1^2, ∇_2^2	Laplacian operators defined by equation (3.7)
Δ	Discrete increment
λ	Lamé constant
μ	Shear modulus
ν	Poisson's ratio
ξ	Dimensionless X coordinate
ρ	Mass density
σ_{xx}	Normal stress in the x-direction
σ_{yy}	Normal stress in the y-direction
σ_{xx_n}	n^{th} eigenfunction for σ_{xx}
σ_{yy_n}	n^{th} eigenfunction for σ_{yy}
τ	Dimensionless time
τ_{max}	Maximum shear stress
τ_{xy}	Shear stress in the xy plane
τ_{xy_n}	n^{th} eigenfunction for τ_{xy}
Φ	Displacement potential
Ψ	Displacement potential

ψ	Mean angle of rotation of the beam cross section about the neutral axis
ψ_1, ψ_2	ψ defined in each beam section used for the static solution
Ω	Angular velocity
$(\bar{\ })$	Superscript bar indicates non-dimensional quantity
$(\ )_o$	Subscript zero indicates initial value

SUMMARY

The inherent complexity of finding solutions for elastodynamic problems involving running-cracks in finite bodies has motivated many analysts to employ approximate methods. Two approximate methods are considered in this thesis. First, the crack behavior exhibited by a popular one-dimensional model is examined. Second, a solution technique is developed to extract dynamic stress-intensity factors for a running crack from a finite-element simulation of crack propagation.

A critique of Kanninen's one-dimensional beam-on-elastic foundation model is undertaken to determine the capability of the model to characterize crack propagation in the Double Cantilever Beam (DCB) Test Specimen. First, a semi-infinite model is used to examine the long time behavior of propagation initiating from a sharp crack. Crack behavior is determined for two loading conditions: dead-load, and constant end-deflection-rate. The crack behavior is qualitatively in agreement with Bilek and Burns' analysis which predicts the crack length to be proportional to the square root of the time. Second, a finite length model subjected to fixed-grips conditions and incorporating a blunt starter-notch is used to study rapid crack extension. Two alternate methods are considered for modeling the bluntness of the starter-notch. The resulting crack behavior is qualitatively in agreement with the experimentally observed phenomena. However, the crack behavior appears to be sensitive to the method selected to simulate the bluntness of the starter-notch. All solutions are obtained by the method of characteristics.

Currently, more sophisticated methods are being investigated to predict crack propagation in non-beam-type structures. Guided by the success and convenience of Williams' static eigenfunctions used in conjunction with finite-element methods, analyses of running-crack problems are anticipated through analogous techniques. First, the entire sequence of eigenfunctions for a crack propagating at constant velocity is obtained using a procedure outlined by Rice. The eigenfunctions are then manipulated into forms which reduce to Williams' static eigenfunctions as the crack speed approaches zero. The dependence of the singular ($r^{-1/2}$) stress eigenfunctions and the corresponding ($r^{1/2}$) displacement eigenfunctions upon the crack speed is examined. Finally, a procedure is developed to extract stress-intensity factors from finite-element nodal displacements through the use of the displacement eigenfunctions. The viability of the procedure is investigated through a finite-element simulation of Broberg's problem. The calculated stress-intensity factors are in reasonable accord with Broberg's solution.

CHAPTER I

INTRODUCTION

In the field of fracture mechanics, the methodology for predicting the initiation of fracture has been well developed. However, the study of the ensuing phenomenon of crack propagation is still in its infancy. It has only been within the past twenty-five years that even the simplest crack propagation problems have been approached.

Obviously when discussing crack propagation, it is the rate at which the crack tip extends, that is, the crack speed, which dictates the type of analysis which is appropriate. If the crack speed is small enough, such that inertia effects brought about by crack extension are insignificant, a quasi-static analysis may suffice. On the other hand, when the crack speed increases to the extent that the associated inertia effects cannot be ignored, a true elastodynamic problem must be considered. Often the term "rapid crack extension" is identified with this phenomenon. The word rapid is used because crack speeds have been measured which are of the order of twenty percent of the dilatational wave speed of the material. Clearly, under such circumstances the failure of a structure may occur within the passing of a few microseconds. It is this phenomenon of rapid crack extension which is the central concern of this thesis. In addition, the discussion which follows will be restricted to opening-mode, or Mode I, crack propagation. References and discussion of the extensive literature existing on anti-plane strain (Mode III) propagation,

may be found in a survey article by Achenbach [1].

Because rapid crack extension may bring about the immediate catastrophic failure of a structure, many analysts and experimentalists have directed their research towards developing a methodology for predicting and controlling this phenomenon. Since the concepts of stress-intensity factor and static strain energy release rate have proved to be reliable indicators for the initiation of fracture, it is natural to examine these same parameters in dynamic crack propagation. Needless to say, the majority of analyses avoid the complications associated with the boundary reflections of stress waves in finite bodies by dealing with fundamental problems involving semi-infinite cracks in infinite bodies.

The first solutions for elastodynamic problems involving moving cracks were produced by Yoffe [2] and Craggs [3]. Yoffe investigated a constant length crack traveling at constant speed in an infinite body. The physical significance of this problem is lost however, because the analysis requires the crack to extend at one crack tip and heal itself at the other tip to maintain a constant crack length. Craggs studied a semi-infinite crack traveling at constant speed in an infinite body. The crack is being driven by wedging forces traveling on the crack faces. Unfortunately, the solution for each of these problems is not applicable during the initiation of crack propagation, simply because the solutions are presumed to be steady state, that is, the patterns of stress and deformation are time-invariant with respect to a coordinate system moving with the crack tip.

Subsequently, other analysts have solved initial-value elastodynamics problems involving moving cracks. These analyses are for the

most part limited to constant velocity crack extension. Broberg [4] considered an infinite elastic body initially in equilibrium with a uniform uniaxial tension prior to crack extension. At time zero a crack extends symmetrically from an initially zero length. Each crack tip, one traveling to the left and the other to the right, extends at constant rate. Broberg's analysis leads to the conclusion that the ratio of dynamic stress-intensity factor to the corresponding static stress-intensity factor is only a function of the crack speed and the material properties of the body. In fact, this ratio is shown to be a decreasing function of crack speed, which vanishes at the Rayleigh wave speed.

Tsai [5] succeeded in developing integral sclutions for a crack propagating at a varying crack speed in an infinite body under the action of an arbitrary pressure on the crack faces. However, the equations are solved only for the explicit cases of constant velocity and constant acceleration with uniform pressure acting on the crack face. As expected, the constant velocity case yields results for dynamic stress-intensity factors which are in agreement with Broberg's results. The more interesting situation occurs for the constant acceleration crack propagation. For this situation the ratio of dynamic to static stress-intensity factors does not decrease as rapidly with crack speed as the constant velocity situation indicates. Unfortunately, Tsai does not explicitly state the value of acceleration used in the analysis. There is no reason to believe the behavior of the accelerating crack is independent of the acceleration.

Another interesting initial-value problem was solved by Baker [6]. He considered a semi-infinite crack appearing and propagating at constant velocity in an infinite body. While the sudden appearance of a crack in

an elastic body seems to be a very artificial problem, recently Achenbach and Nuismer [7] have shown that Baker's solution is also the solution for a step-stress pulse incident on a half-plane crack.

As stated, the previously discussed initial-value problems are restricted to crack propagation occurring at constant velocity. Consequently, analysts have recently considered problems involving a crack moving at a variable velocity. Freund [8,9] has investigated the behavior of a semi-infinite crack extending uniformly and non-uniformly in an infinite elastic body subjected to time independent loading. Freund has also been able to use his solution technique, which entails superposition, to produce a solution for a stress wave impinging upon a crack [10,11]. A more general problem has been solved by Kostrov [12], who considered a semi-infinite crack extending non-uniformly in an elastic body under time varying loading. Freund's solution can be obtained as a special case of Kostrov's solution. In addition, Kostrov formulates a solution for a finite crack, such as the Broberg crack, but does not explicitly obtain a solution.

The works of Freund and Kostrov are the most general solutions available for elastodynamic problems involving moving cracks. Despite their generality these solutions are still limited in application to finite body problems until wave reflections occurring at a boundary, or at another crack tip, influence the crack behavour. When the finite dimensions of a body cannot be ignored, solutions for an infinite body cannot adequately characterize the crack behavior, except perhaps by use of superposition. This fact has motivated many analysts to seek

alternative methods for studying crack propagation in finite bodies.

A practical approach for studying crack propagation in particular test specimens has been the development of specialized models. Because beam models have proved to be adequate to analyze static crack problems for beam-type structures, several investigators have attempted to extend these models to study dynamic crack propagation [13,14,15]. In particular, the Double Cantilever Beam (DCB) Test Specimen has proven popular with both experimentalists and analysts. The name of this specimen is derived from its geometry. As shown in Figure 1, the specimen resembles two beams which are joined together along the proposed crack trajectory. Clearly, analysts favor the geometry of this particular specimen because one-dimensional beam theory may be used for a model. Experimentalists favor this specimen because sizable regions of straight crack extension occur without the necessity of sidegrooving the test specimen when wedge-type loading is applied.

The analysis of Bilek and Burns [16,17,18] produces a similarity solution for crack extension in the DCB specimen. The arms of the DCB specimen are modeled as built-in Bernoulli-Euler beams with the location of the crack tip corresponding to the location of the built-in ends of the beams. The remaining uncracked region of the specimen is not modeled in their analysis. The crack extension process is simulated by allowing the length of the beam to increase with time. In addition, a critical bending moment at the crack tip is adopted as a crack extension criterion. Thus, the crack speed is not predetermined in their analysis, which means that the crack extension will occur at a rate consistent with the model

and the initial conditions of the problem. For loading conditions of dead-load and constant end-deflection rate, they conclude that the crack length is simply proportional to the square root of time. Unfortunately, Bilek and Burns analysis suffers from several limitations. First, the similarity solution forces the analysis to begin with zero crack length and an undeformed specimen. Clearly, beam theory is not applicable when the crack length is short compared to the specimen's height. In addition, the restriction that the model be initially undeformed precludes an analysis of any experiment in which the specimen is initially deformed. Furthermore, Bilek and Burns' analysis only considers three loading conditions: constant load, constant end-deflection-rate, and constant applied bending moment. The first two cases are of interest for they simulate the conditions encountered in a laboratory.

Fortunately, other models are available which allow the inclusion of the appropriate initial conditions and initial crack length. Kanninen [19-24] has developed a beam-on-elastic foundation model to analyze crack propagation in the DCB specimen. In essence, his model consists of two Timoshenko beams joined together along their lengths by an elastic foundation. The elastic foundation represents the crack trajectory. In addition, a critical value of strain energy density in the elastic foundation at the crack tip is adopted as a crack extension criterion. The crack extension process is then simulated by removing those segments of the elastic foundation in which the crack extension criterion is exceeded. Dynamic stress-intensity factors are also determined from an energy balance within the model. Kanninen's DCB model will be discussed in detail in Chapter II of this thesis.

The use of these specialized beam models, however, precludes any application to non-beam-type structures. An alternative is to use one of the many existing numerical techniques, such as the finite-difference method, or the finite-element method, to study crack extension in finite bodies.

Wilkins' analysis [25] is the earliest known examination of crack propagation by finite differences. Wilkins investigated the behavior of the stress distribution in a sheet as a crack propagates at constant velocity. However, the investigation of dynamic stress-intensity factors or dynamic energy release rates are not included in his analysis.

A finite-difference scheme was also used by Shmuely and Alterman [26] to analyze crack propagation in a central-cracked elastic sheet. Recently, Shmuely and Peretz [27] have used this same technique to analyze crack propagation in a DCB model. In both of these analyses a critical stress ahead of the crack tip is adopted as a crack extension criterion. Thus, crack speed is not predisposed. While the analysis does yield behavior which agrees with the experimentally observed phenomenon, they do not attempt to establish the behavior of such quantities as dynamic stress-intensity factors, or dynamic energy release rates.

Kobayashi [28] has simulated the fracture of edge-notched Homalite-100 plates through the use of the finite-element method. Dynamic energy release rates are computed based upon the stresses and displacements in the vicinity of the crack tip. Dynamic stress-intensity factors are then deduced from the energy release rates.

An alternative to this straight-forward application of the

finite-element method and the finite-difference method to crack propagation problems, is to devise a technique which incorporates the near-tip behavior of stress and deformation associated with a propagating crack. Such a technique is motivated by the success of Williams' [29] eigenfunctions used in conjunction with the finite-element method for extracting stress-intensity factors for stationary cracks in finite bodies [30,31]. Reliable stress-intensity factors have been deduced for stationary cracks both for static and dynamic loading. Thus, a procedure based upon use of finite elements and the eigenfunctions associated with a propagating crack is expected to yield reliable dynamic stress-intensity factors for running-cracks.

The local behavior of a propagating crack was first investigated by Cotterell [32]. He presents numerical results for the angular behavior of the singular $(r^{-\frac{1}{2}})$ stresses at a crack tip moving at a constant speed. Rice [33] outlines the development of dynamic eigenfunctions for a crack propagating at constant velocity. The singular $(r^{-\frac{1}{2}})$ stress eigenfunctions, and the associated $(r^{\frac{1}{2}})$ displacement eigenfunctions are explicitly stated. Using the procedure outlined by Rice, a sequence of eigenfunctions can be generated for a crack propagating at constant velocity.

The implementation of these constant velocity eigenfunctions may well be of value even for the case of unsteady propagation because recently, Nilsson [34] has shown that singular $(r^{-\frac{1}{2}})$ stress eigenfunctions and the associated $(r^{\frac{1}{2}})$ displacement eigenfunctions are not dependent upon the acceleration of the crack tip. Even though the other terms in the sequence of eigenfunctions may depend on the

acceleration of the crack, the behavior of stress and displacement for an accelerating crack can be adequately characterized in the immediate vicinity of the crack tip. This is so, simply because the $(r^{-\frac{1}{2}})$ stress eigenfunctions and the $(r^{\frac{1}{2}})$ displacement eigenfunction dominate the solution as $r \to 0$.

In light of the previous discussion, it is reasonable to presume that numerical methods will play an increasingly important role in understanding the phenomenon of rapid crack propagations. As such, the objectives of this thesis are twofold. First, a critique of Kanninen's DCB model is undertaken. Second, a convenient solution technique is devised to enable the calculation of stress-intensity factors from finite-element nodal displacements.

A critique of Kanninen's DCB model is undertaken to determine the capability of this one-dimensional model to characterize crack propagation in the DCB test specimen. First, a semi-infinite model is used to examine the long time behavior of propagation initiating from a sharp crack. The resulting crack length-time behavior is compared with the analysis of Bilek and Burns [17,18] for the loading conditions of dead-load, and constant end-deflection-rate. Next, a finite length model is used to simulate Kanninen's analysis. The model is subjected to fixed-grips boundary conditions, and crack extension is said to initiate from a blunt notch. Two alternate methods are utilized to simulate the initial notch bluntness. All solutions are obtained by the method of characteristics.

The second objective of this thesis is to devise a procedure to extract stress-intensity factors from finite-element nodal displacements.

First, the entire sequence of eigenfunctions for a crack propagating at constant velocity is obtained using the procedure outlined by Rice. Next, the eigenfunctions are manipulated into a form which will reduce to the appropriate static eigenfunctions as obtained by Williams. The dependence of the singular $(r^{-\frac{1}{2}})$ stress eigenfunctions and the corresponding $(r^{\frac{1}{2}})$ displacement eigenfunctions upon the crack speed is then examined. Finally, a procedure is developed to exact stress-intensity factors from finite-element nodal displacements by fitting the nodal displacements to a selected number of eigenfunctions. The viability of this procedure is investigated through a finite-element simulation of Broberg's problem.

CHAPTER II

A CRITIQUE OF KANNINEN'S DCB MODEL

The analysis conducted at the Battelle Laboratories by Kanninen utilizes a simple beam-on-elastic foundation model to simulate rapid crack propagation in the DCB test specimen. The motivation for developing such a model is to establish a correlation between experimentally measured and analytically predicted crack speeds and crack arrest lengths. Clearly, once such a correlation has been established, the necessity and complexity of gathering reliable experimental data can be eliminated.

Figure 1 shows the DCB specimen used in the Battelle analysis. The laboratory experiment essentially consists of slowly advancing a wedge between loading pins which are placed in the holes located in the specimen arms. The key-hole notch shown is the starter-notch or initial crack. The key-hole notch shown in the figure is meant to draw attention to the fact that the starter-notch has a finite radius of curvature at the end. Thus, as the wedge is advanced between the pins, a gradual increase of strain energy occurs in the specimen. The finite radius of the starter-notch tip allows more strain energy to accumulate than would be possible with a sharp initial crack. It is this excess of strain energy which results in rapid crack propagation when fracture initiates. As the rate of advance of the loading wedge is extremely small in comparison with the crack speed, the process is said to occur under

fixed-grips, or constant end-deflection conditions. If the blunt notch is not used, stable crack growth occurs as the wedge advances between the pins, since for fixed pin displacements the stress-intensity factor decreases with crack length. Such behavior might be expected because a static analysis of the DCB specimen indicates the stability of the crack extension process depends on the loading conditions. Figure 2 shows the behavior of static stress-intensity factor in a DCB model under both fixed-grips and dead-load. Clearly, the fixed-grips condition indicates stable crack extension, while the dead-load situation indicates unstable growth. Thus if a true dead-load could be applied to a laboratory specimen, rapid crack extension would presumably occur. On the other hand, if fixed-grips conditions are used, only slow crack extension can be attained. Thus, the Battelle analysis of the DCB model has circumvented the problem of using fixed-grips conditions, by incorporating a blunt starter-notch which allows excess energy to be stored in the specimen.

Kanninen's model of the DCB specimen is shown in Figure 3. The beam is intended to represent the upper half of the specimen, and the elastic foundation represents the crack trajectory. Kanninen's current analysis makes use of a Timoshenko beam and a generalized elastic foundation, that is, an elastic foundation which possesses both extensional and rotational stiffness. Kanninen's earlier analysis [19] used a Bernoulli-Euler beam supported by a Winkler (extensional) foundation to deduce static strain energy release rates. To achieve satisfactory dynamic response, the model has evolved into its present form and is being used to predict crack speed and dynamic fracture toughness [22-24].

As stated previously, an attractive feature of the Kanninen model is that the crack speed is not predisposed. That is, rather than specifying a crack speed, a crack extension criterion is established to govern the advance of the crack through the elastic foundation. In his analysis, Kanninen has adopted a critical value of strain energy density in the elastic foundation to be the crack extension criterion. Thus, crack extension is accomplished by simply removing that section of the elastic foundation in which the criterion is violated. Such a criterion is also attractive from the fact that some means must be taken to model the bluntness of the starter-notch. Thus, this may be easily accomplished by initially prescribing end-deflections which will cause the strain energy density at the crack tip to exceed the critical value by a prescribed amount. Such a procedure is also identical to prescribing a deflection which produces an initial static strain energy release rate which exceeds the corresponding static strain energy release rate, if a sharp crack existed. This equivalence will be discussed in a later section. However, the current Battelle analysis also introduces a pinching force and restoring moment acting upon the beam above the crack tip in addition to the prescribed deflections. The purpose of this force and moment is to "relieve" the crack tip, that is, confine the excess deformation to the arms of the specimen, such that the crack extension criterion is not initially violated at the crack tip. It should be pointed out that the method chosen to simulate the bluntness is arbitrary, and that the current method used at the Battelle laboratories is simply one of many possibilities. The process used to simulate crack propagation in the Battelle analysis is shown in Figure 4. Crack

extension begins by removing the force and moment at the crack tip. Crack arrest occurs when the crack extension criterion is no longer violated. All solutions were obtained through use of finite-differences.

Several of the more important predictions concerning rapid crack propagation in the DCB test specimen made in the Battelle analysis [23] follow:

1. "The crack propagates at an essentially constant, steady-state velocity from the start. This is confirmed by the velocity measurements."

2. "The steady-state velocity is not an invariant, but depends on the initial conditions, i.e., the bluntness of the starter slot. This is confirmed by measurements."

3. "For a given DCB configuration, material density and modulus, the crack velocity and arrest length are separate single-valued functions of R," (the energy absorbed at the crack tip per unit area of crack extension), "or K_d," (the dynamic stress-intensity factor). "This means that R- or K_d-values can be inferred independently from the velocity and from the arrest length."

4. "Alternatively, the theory predicts a unique relation between crack velocity and the length of the crack at arrest, that is independent of the dynamic toughness of the material."

A critique of the Kanninen DCB model is now undertaken to investigate the validity of these conclusions, in particular the third conclusion. The model used in the analysis is a duplicate of Kanninen's model. Since the governing equations are hyperbolic the solution technique to be used is the method of characteristics, rather than the finite-difference technique used by Kanninen. First, a semi-infinite model is used to

examine the crack length-time behavior occurring in two of the loading conditions considered by Bilek and Burns [17,18], that is dead-load, and constant-end-deflection rate. Next, a finite length model is used to simulate Kanninen's analysis. The model is subjected to fixed-grips conditions, and the crack extension is said to initiate from a blunt notch. Two alternate methods are used to simulate the bluntness of the starter-notch.

2.1 Formulation of Kanninen's DCB Model

2.1.1 Governing Equations

The free-body diagram and notation used for a Timoshenko beam supported by a generalized elastic foundation are shown in Figure 5. The constitutive relations may be expressed as:

$$M = - EI\ \psi_{,X} \quad \text{and} \quad V = k\ GA(w_{,X} - \psi) \tag{2.1}$$

The equations of motion are then:

$$\rho\ A\ \ddot{w} = V_{,X} - k_e\ w$$

and (2.2)

$$\rho\ I\ddot{\psi} = V - M_{,X} - k_r\ \psi$$

where the dots indicate partial derivatives with respect to time.

2.1.2 Selection of Elastic Foundation Stiffnesses

For the purpose of duplicating the existing DCB model, the foundation stiffnesses are chosen to be identical to values used in the Battelle analysis. That is

$$k_e = \frac{2Eb}{h} \qquad \text{and} \qquad k_r = \frac{kGA}{2} \tag{2.3}$$

These stiffnesses are essentially evaluated by means of a one-dimensional "tensile specimen" picture of the foundation elements. A more detailed discussion concerning the selection of these elastic constants is found in [22]. It suffices here to say that the above constants produce satisfactory correlation between stress-intensity factors calculated using this model, and those calculated using two-dimensional elasticity theory.

2.1.3 Crack Extension Criterion

As discussed previously, the crack extension criterion adopted in Kanninen's analysis is a critical value of the lineal strain energy density, U^*, at the crack tip in the elastic foundation. In terms of the notation given in Figure 4,

$$U^* = k_e w^2 + k_r \psi^2 > U^*_{critical} \tag{2.4}$$

at the crack tip for propagation. Crack extension is then accomplished by simply removing the region in the elastic foundation in which the extension criterion is exceeded. Crack extension will then occur at a rate consistent with the model and the initial conditions of the problem.

The analysis conducted by Kanninen takes advantage of a convenient non-dimensionalization of the crack extension criterion. Because the critical value of U^* is generally unknown, a non-dimensionalization with respect to $U^*_{critical}$ is performed. U^* is simply related to the energy absorbed per unit area of crack extension, R, by the equation

$$U^*_{critical} = b\,R \tag{2.5}$$

where b is the width of the specimen. The crack extension criterion then becomes:

$$\bar{U}^* = \frac{U^*}{U^*_{critical}} > 1 \tag{2.6}$$

at the crack tip in the elastic foundation for propagation to occur.

It should be noted that the value of R is presumed to be a constant in the majority of the analyses conducted by Kanninen. A limited amount of study has been performed for a crack-speed dependent R [24]. However, the analysis indicates essentially the same constant speed crack behavior. In this analysis R is presumed to be a constant.

2.2 The Method of Characteristics as Applied to the DCB Model

Because of the hyperbolic nature of the system of governing differential equations, (2.1) and (2.2), these equations are naturally suited for solution by the method of characteristics. Such a solution method should yield the same crack behavior as obtained by Kanninen through the finite-difference method.

2.2.1 Development of the Characteristic Curves

Letting $v = w_{,t}$ and $\Omega = \psi_{,t}$ the model consists of the following six coupled first order linear differential equations:

$$M_{,t} + EI\,\Omega_{,x} = 0$$

$$V_{,t} - k\,GA(v_{,x} - \Omega) = 0$$

$$
\begin{aligned}
&M_{,x} + \rho I \Omega_{,t} - V + k_r \psi = 0 \\
&V_{,x} - \rho A v_{,t} - k_e w = 0 \\
&v = w_{,t} \\
&\Omega = \psi_{,t}
\end{aligned}
\tag{2.7}
$$

Assuming the beam to be of rectangular cross-section, the shear deflection coefficient is taken by Kanninen to be $k = \frac{1}{3}\frac{E}{G}$, which is exact for $\nu = \frac{3}{11}$.

The following non-dimensionalizations are then made:

$$
\begin{aligned}
&\xi = \frac{X}{h} \quad , && \tau = \left(\frac{E}{\rho}\right)^{1/2} \frac{t}{h} \\
&\bar{w} = \left(\frac{2E}{hR}\right)^{1/2} w \quad , && \bar{\psi} = \left(\frac{2Eh}{R}\right)^{1/2} \psi \\
&\bar{V} = \frac{3}{b}\left(\frac{2}{REh}\right)^{1/2} V \quad , && \bar{M} = \frac{12}{bh}\left(\frac{2}{REh}\right)^{1/2} M \\
&\bar{v} = \left(\frac{2\rho h}{R}\right)^{1/2} v \quad , && \bar{\Omega} = \left(\frac{2\rho h}{R}\right)^{1/2} h\,\Omega
\end{aligned}
\tag{2.8}
$$

Using the foundation elastic stiffnesses (2.3), and the above non-dimensionalizations, the crack extension criterion (2.6) becomes

$$
\bar{U}^* = \bar{w}^2 + \frac{1}{12}\bar{\psi}^2 > 1 \tag{2.9}
$$

at the crack tip in the elastic foundation for propagation to occur.

Use of the Interior Derivative Approach [35] results in the characteristic curves appropriate for the system of equations (2.7).

Two sets of characteristic curves result, $I\pm$ and $II\pm$. The resulting equations are:

$$I\pm: \quad \pm d\bar{M} + d\bar{\Omega} = (4\bar{V} - 2\bar{\psi})d\tau$$

$$\text{along the direction } \frac{d\bar{\xi}}{d\tau} = \pm 1$$

$$II\pm: \quad \pm \frac{1}{\sqrt{3}} d\bar{V} - d\bar{v} = \left(2\bar{w} \mp \frac{1}{\sqrt{3}} \bar{\Omega}\right) d\tau \tag{2.10}$$

$$\text{along the direction } \frac{d\bar{\xi}}{d\tau} = \pm \frac{1}{\sqrt{3}}$$

A similar set of characteristic curves are developed for the unsupported section of the beam by setting $k_e = k_r = 0$ in equations (2.7) and proceeding in an analogous manner. The resulting equations are:

$$I\pm: \quad \pm d\bar{M} + d\bar{\Omega} = 4\bar{V}\, d\tau$$

$$\text{along the direction } \frac{d\bar{\xi}}{d\tau} = \pm 1$$

$$II\pm: \quad \pm \frac{1}{\sqrt{3}} d\bar{V} - d\bar{v} = \mp \frac{1}{\sqrt{3}} \bar{\Omega}\, d\tau \tag{2.11}$$

$$\text{along the direction } \frac{d\bar{\xi}}{d\tau} = \pm \frac{1}{\sqrt{3}}$$

2.2.2 Advancing the Crack Through the Network of Characteristic Curves

The network of characteristic curves used in this analysis, and a typical element of the network are shown in Figure 6. The solution process begins at time zero with appropriate initial values for the problem to be considered. Appendix A gives the procedure for obtaining

a static solution for the DCB model. The numerical scheme used to obtain a solution throughout the gridwork of characteristic curves is discussed in Appendix B.

Within the network of characteristic curves two cases are encountered when implementing the crack extension criterion at the crack tip. They are shown in Figure 6. In essence, the figure shows the two possible situations occurring at the interface of the supported and unsupported sections of the beam. Figure 6a depicts the situation occurring when one-half of the element lies in the foundation region. The procedure followed is to first evaluate the six unknowns ($\bar{w}$, $\bar{\psi}$, $\bar{M}$, $\bar{V}$, $\bar{v}$, $\bar{\Omega}$) at point 1. The dimensionless form of the crack extension criterion is then evaluated. If $\bar{U}^* > 1$, the crack tip is then advanced by the increment $\Delta\tau$. The six unknowns at point 1 are then recalculated as if the entire element is located in a region unsupported by the elastic foundation.

Figure 6b depicts the situation occurring when the entire element lies within the elastic foundation region. The procedure followed is to first evaluate the six unknowns at point 1. The dimensionless form of the crack extension criterion is then evaluated. If $\bar{U}^* > 1$, the crack tip is then advanced by the increment $\Delta\tau$. The six unknowns are then recalculated at point 1 as if one-half of the element is not supported by the elastic foundation. The procedure then follows the discussion as for Figure 6a. It should be noted that although the provision is made for crack growth to occur under the conditions of this second situation, no such advancing of the crack-tip ever occurred in practice. Crack extension always occurred as discussed for Figure 6a.

The possibility exists that the procedure for advancing the crack through the network of characteristic curves may influence the crack behavior. For this reason, an alternative procedure is implemented. The procedure for advancing the crack is identical to that discussed previously, except the six unknowns at point 1 are not recalculated after the crack tip is advanced to the next node. This procedure is subsequently referred to as "the modified crack extension procedure". As will be seen, no significant alteration in crack behavior occurs when this alternate procedure is implemented.

2.3 Response of a Semi-Infinite DCB Model

Before undertaking a study of crack propagation in the blunt-notched DCB specimen, the behavior of a semi-infinite model is studied under various loading conditions. The semi-infinite model is of particular interest because a comparison with Bilek and Burns' analysis [17,18] is possible.

Bilek and Burns' analysis produces a similarity solution for the equations of motion of a built-in Bernoulli-Euler beam. In essence, their model represents only the arms of the DCB specimen. These arms lengthen as the crack grows. Their model also differs from Kanninen's DCB model in that a critical bending moment at the crack tip is adopted as a crack extension criterion, and in that all initial conditions including the initial crack length must be zero.

Bilek and Burns' analysis is of particular interest because they have considered two loading conditions which are approximations of laboratory test conditions, dead-load, and constant end-deflection-rate.

The dead-load situation is of concern because a static analysis of the DCB specimen indicates that dead-load is an inherently unstable loading condition. As such, if rapid crack extension is possible from a sharp crack, it might be expected to occur under dead-load conditions. The constant end-deflection-rate loading condition is of interest because it approximates the conditions for a high speed impact test. The primary conclusion of the Bilek and Burns analysis is that the crack length is proportional to the square root of time for both of these loading conditions.

A semi-infinite version of Kanninen's DCB model is examined under both dead-load and constant end-deflection-rate loading conditions. The semi-infinite model conveniently removes the influence of the rear boundary upon the crack behavior, thus allowing long time crack behavior to occur as in the Bilek and Burns' analysis. Crack propagation is said to initiate from a sharp crack in that the critical crack extension criterion is not initially violated at the crack tip.

An initial dimensionless crack length of one grid spacing is used to approximate the zero initial crack length used in Bilek and Burns' analysis. The values prescribed for the geometry of the model are found in Table 1. Other than the initial crack length; the geometry used in this analysis was selected to represent as closely as possible the dimensionless geometry used in Kanninen's analysis.

The solution procedure used for the dead-load loading condition is as follows. First, the static solution is determined by prescribing a dimensionless load $\bar{P}_o$ at the end of the arm of the model which results in the crack extension criterion reaching the critical value at the

crack tip, i.e., $\bar{U}^* = 1$. The details required for determining the dimensionless applied load for the initial crack length used in this analysis are given in Appendix D. Next, the load is increased by a pre-set percentage during the first boundary calculation. The new dimensionless load, $\bar{P}$, is then maintained constant for all subsequent boundary calculations. The equations appropriate for the dead-load boundary element are given in Appendix C.

In order to minimize the computer time required to produce a solution, and to verify that incrementing the load in one time step does not influence the resulting crack behavior, an alternative load application procedure is investigated. This procedure is subsequently referred to as "the modified load application procedure." For selected problems, the percent increase in load is applied before producing the static solution. This results in a static solution which has a region of the elastic foundation in which the crack extension criterion is violated. In essence a "small" amount of initial bluntness is tolerated. The dimensionless load $\bar{P}$ is then maintained constant throughout all boundary calculations.

The solution procedure for the constant end-deflection-rate loading condition is as follows. First, all initial conditions are prescribed to be zero. Next, a prescribed dimensionless end-deflection-rate is imposed during the first boundary calculation. This dimensionless end-deflection-rate is then maintained constant during all subsequent boundary calculations. The equations for the constant end-deflection-rate boundary element are given in Appendix C. A detailed discussion of the selection of the magnitude of the imposed dimensionless

end-deflection-rates is given in Appendix G.

Solutions obtained for dead-load and constant end-deflection-rate are discussed in the following sections.

2.3.1 Dead-Load

The crack length-time behavior of Kanninen's DCB model when used to simulate the dead-load condition of Bilek's and Burns' analysis is shown in Figure 7. The behavior exhibited in this figure corresponds to having prescribed a ten percent increase in the dimensionless load $\bar{P}_o$ during the first boundary calculation. Clearly, the greatest crack speeds occur immediately after initiation, and then continually diminish as the extension process continues. Thus, reasonable agreement exists between the crack behavior shown in this figure and the crack behavior predicted by Bilek and Burns, that is, that the crack length is proportional to the square root of the time, despite the fact that the models used in each analysis differ considerably. Unfortunately, the analysis indicates that sustained rapid crack extension initiating from a sharp crack cannot be achieved in the DCB specimen even under the severe loading conditions of dead-load.

Also shown in the figure is the crack behavior resulting when the modified load application procedure is implemented. The actual crack behavior is not shown in the figure, only selected points are plotted to show the trend. Refer to the squares in the figure. The resulting crack behavior is identical for all practical purposes to the crack behavior which occurs when the original procedure is used. Thus, there is no indication of the load application procedure influencing the crack behavior.

The influence of the initial crack length upon the crack behavior is also shown in Figure 7. The circles plotted on the figure show the resulting crack length-time behavior when an initial crack length typical of the Battelle analysis is used. Table 1 gives the dimensionless value of crack length used. It should be noted that the final load, $\bar{P}$, corresponding to the crack behavior indicated by the circles, is within four percent of the final load used for the shorter crack length. Thus, for all practical purposes, the loads in these two cases are identical, only the initial crack lengths differ. As is evident in the figure, the initially longer crack length only influences the crack behavior during the first one-hundred and fifty microseconds. After this time, the crack behavior does not reflect the influence of the initial crack length.

The effect of magnitude of the dead-load imposed upon the model is investigated next. The following five figures show the resulting crack length-time behavior of Kanninen's DCB model when subjected to various magnitudes of dead-load. The initial crack length is selected to be a value typical of the Battelle analysis. Figures 8, 9, 10, 11 and 12 correspond to ten, twenty-five, fifty, one hundred and two hundred percent increases respectively in the applied load during the first boundary calculation. The first two of these figures show the crack behavior for time durations in the range of the analysis of Bilek and Burns. The latter figures are limited to time spans in the range of Kanninen's analysis. As the figures indicate, there exists a tendency to develop increasing crack speed with an increasing magnitude of dead load. However, the magnitude of the crack speed remains below twenty percent of the bar wave speed, c_o, even for the most severe dead-load situation

which amounted to a two hundred percent increase in the applied load. Thus, sustained rapid crack extension is not observed in the DCB Model under dead-load conditions.

For each of the preceeding dead-load cases discussed, the total system energy is monitored to act as a check of the numerical solution. Appendix F gives the equations required to determine the kinetic energy, strain energy, energy absorbed by crack extension, and work due to external loads.

2.3.2 Constant End-Deflection-Rate

Crack length-time behavior of Kanninen's DCB model when used to simulate the conditions of Bilek and Burns' analysis for constant end-deflection-rate is shown in Figure 13. The magnitudes of the two imposed dimensionless velocities considered in this analysis are discussed in more detail in Appendix G. The crack length-time behavior shown in the figure is in excellent agreement with Bilek and Burns conclusion, that the crack length is proportional to the square root of the time. Obviously, from the figure the constant of proportionality must be dependent upon the magnitude of the velocity among other factors. As evident in the figure, the highest crack speed occurs immediately after initiation, then continually diminish as the crack extension process continues.

Crack length-time behavior of Kanninen's DCB model is also examined when the initial crack length is chosen to duplicate the crack length used in the Battelle analysis (See Table 1).

The imposed dimensionless end-velocities are identical to those

used for the shorter initial crack length. As seen, the initially longer crack length has very little effect upon the gross crack length-time behavior of the model under constant end-deflection-rate conditions.

For each constant end-deflection-rate case discussed, the total system energy is monitored to act as a check of the numerical solution. Appendix F gives the appropriate equations required to determine the kinetic energy, strain energy, energy absorbed by crack extension, and work due to external loads.

2.3.3 Conclusions and Comments

The analysis of a semi-infinite DCB model under dead-load and constant end-deflection-rate leads to the conclusion that rapid crack extension, that is greater than twenty percent of the bar wave speed, initiating from a sharp crack cannot be sustained in a DCB test specimen. As anticipated from the analysis of Bilek and Burns, the greatest crack speed occurs shortly after the initiation of crack growth, but diminishes as the extension process continues. Experiments conducted by Shah [36] confirm this conclusion, although the experimental loading device can only approximate dead-load. In addition, for both initial crack lengths considered in this analysis, the crack length-time behavior follows Bilek and Burns result, that the crack length is proportional to the square root of the time.

2.4 Response of a Blunt-Notched Finite DCB Model

Kanninen's DCB model as used in the Battelle analysis is primarily intended to study rapid crack propagation in the DCB specimen initiating from a blunt starter-notch. As such, a finite length DCB

model can conveniently be used under fixed displacement boundary conditions to simulate the actual test specimen. However, the details of modeling the bluntness of the starter-notch must be discussed in some depth, as it is not clear what represents a natural way of modeling this bluntness.

The most current analysis conducted at the Battelle Laboratories models the initial notch bluntness by first prescribing a fixed-grips boundary deflection which causes the critical value of strain energy density to be exceeded by a prescribed amount at the crack tip, i.e., the leading springs on the elastic foundation. Next, a force and moment are applied on the beam directly over the crack tip in order to suppress this "overstretch" in the elastic foundation. By an appropriate selection of the magnitudes for this force and moment, the value of the strain energy density at the crack tip may be made to equal the critical value. Additional requirements must now be specified to determine the actual values for this force and moment acting above the crack tip. The Battelle analysis requires that "the strain energy of the system is initially a minimum" [22]. However, the logic behind minimizing the strain energy with respect to the force and moment acting above the crack tip is not at all clear because all equilibrium configurations produce a minimum of the strain energy functional.

Due to the ambiguity discussed above and because the method of modeling the bluntness of the starter-notch is arbitrary, two alternative methods for modeling the bluntness are included in this analysis. The first method used to simulate the starter-notch bluntness consists of prescribing fixed end-deflections which give rise to a strain energy

density at the crack tip which exceeds the critical value. Thus, the bluntness is modeled by allowing the existence of a segment of the elastic foundation in which the crack extension criterion is exceeded. In essence, a region of the elastic foundation is initially allowed to be overstretched. The second method used to simulate the bluntness of the starter notch is to again prescribe fixed end-deflections which cause the strain energy density at the crack tip to exceed the critical value. In this case, the existence of the overstretched region in the elastic foundation is suppressed by the application of a pinching force and restoring moment on the beam above the crack tip. Obviously, each of the two methods has advantages and disadvantages. The first method which allows the initial overstretch in the elastic foundation offers the advantage of having an initial strain energy distribution which is consistent with the static beam model. The disadvantage of this procedure is that instantaneous crack formation occurs at the start of the numerical process. Consequently, discontinuities in strain energy and kinetic energy release rates also occur. The method of simulating the bluntness which imposes the force and moment above the crack tip offers the advantage of producing a finite crack propagation rate at the start of the numerical procedure. Unfortunately, the strain energy distribution is inconsistent with the static model, since the imposed load and moment acting at the crack tip are not included in the calculation of the static strain energy.

It should be noted at this point that the values of the imposed pinching force and restoring moment acting above the crack tip used in this analysis differ from the values used in Kanninen's analysis

primarily because of the ambiguity in Kanninen's discussion of the selection of these quantities. The force and moment used in this analysis are obtained by requiring that all subsequent deformation of the DCB model be confined to the arms of the model once the critical value of strain energy density has been reached at the crack tip. These two methods used to simulate the notch bluntness represent extremes. In one case there is absolutely no restriction upon the deformation of the model. In the second case the deformation is restricted to the arms of the model once the critical value of the strain energy density has been reached at the crack tip. Kanninen's method for selection of the force and moment probably lies somewhere between these extremes. The values of the end-deflections and the applied forces and moments used in the analysis are given in Appendices D and E. A more detailed discussion of the procedure used to determine the values for the force and moment acting at the crack tip is presented in Appendix E.

It should be noted that prescribing end-deflections which give rise to a strain energy density at the crack tip which exceeds the critical value may be interpreted in terms of quantities of more physical relevance in the field of fracture mechanics. That is, specifying values of dimensionless lineal strain energy density is equivalent to specifying the ratio G_q/R or K_q/K_D, where G_q and K_q are the static strain energy release rate and the static stress intensity factor respectively when blunting of the notch is not assumed, and R and K_D are the energy absorbed per unit area of crack extension, and dynamic stress-intensity factor. The equivalence of the quantities is discussed in Appendix H.

The method for modeling the bluntness of the starter notch should prove to be inconsequential, if generalizations are to be made about crack behavior. It is interesting to note that the first method used to model the notch bluntness was originally used in an earlier DCB analysis at the Battelle Laboratories [20]. This procedure was subsequently abandoned in favor of a procedure which suppresses the overstretched region in the elastic foundation, although no explanation is given for such a preference.

2.4.1 Crack Behavior When an Overstretched Foundation is Permitted

The crack length-time behavior and the system energy-time behavior of a finite DCB model, when allowing the bluntness of the starter notch to be simulated by an overstretched region of the elastic foundation, are shown in Figures 14 through 19. Three successively "blunter" starter notches are considered in this analysis by allowing the lineal strain energy density at the crack tip in the elastic foundation to exceed the critical value by factors of two, four, and six, i.e., $\bar{U}^{*} = 2, 4$, and 6, or $G_q/R = 2,4,6$. (See Appendix H).

The general features of the crack behavior exhibited by the model agree with the experimentally observed phenomena. In each case the crack rapidly accelerates, then continues to propagate at essentially constant velocity until crack arrest occurs. As anticipated, crack speeds and crack arrest lengths increase with increasing levels of initial energy overstorage.

The system energy-time behavior of the DCB model for each of the three "blunt" initial conditions are shown in Figures 15, 17 and 19. The initial instantaneous releasing of the overstretched segment of the

elastic foundation does result in an immediate loss of energy in the system. However, the total system energy is preserved during the crack extension process following initiation.

As shown in the three figures, the strain energy of the system, U, is observed to decrease as the crack extends, the kinetic energy, T, is observed first to increase, but then to be recovered by the system as the crack extends, and the energy absorbed due to crack extension, A_b, is observed to be monotonically increasing as expected.

As stated previously, a modified procedure is implemented to advance the crack tip through the network of charcteristic curves. Figure 16 shows the resulting crack length-time behavior when this modified procedure is implemented. No appreciable alteration in the crack behavior is detectable.

2.4.2 Crack Behavior When the Overstretched Foundation is Suppressed

The resulting crack length-time behavior of the DCB model, when the initial overstretch of the elastic foundation is suppressed by the application of a force and moment upon the beam above the crack tip, are shown in Figure 20 through 22. The end-deflections prescribed are identical to those used in the preceding analysis, i.e., Figures 14 through 19. The solution procedure begins by removing the force and moment acting above the crack tip.

Once again, the general features of the crack behavior exhibited by the model agree with the experimentally observed phenomena. In each case, the crack propagates at essentially constant velocity following crack initiation. The crack speeds and crack arrest lengths increase with increasing magnitudes of the prescribed end-deflections. The most

striking feature of the crack behavior is the apparent crack arrest and reinitiation occurring during the crack extension process. Figure 21 shows one region in which crack arrest and reinitiation occurs. Two such regions are evident in Figure 22.

The system energy-time behavior is not reported for the DCB model when the second method is used to simulate the initial notch bluntness because a decay (approximately ten percent) of the total system energy is observed to occur as the numerical solution process proceeds. This energy decay is believed to be attributable to the discontinuities in shear and in moment which are generated when the force and moment are removed from the crack tip. As in the Battelle analysis, no provision is made to account for these discontinuities in the numerical computations. However, while acknowledging the unfavorable presence of these discontinuities, the Battelle analysis does not report a system energy decay [23].

The effects of implementing the modified crack extension procedure, and the effects of grid retirement are shown in Figure 21. As before, the effect of using the modified crack extension procedure does not give rise to appreciable differences in crack behavior. The effect of using a gridwork of characteristic curves which is four times as fine as the original network also results in essentially the same crack behavior. Thus, the grid spacing used in the analysis is sufficiently fine to guarantee reliable crack behavior, i.e., crack behavior which will not be significantly altered by further grid refinement.

In addition, as a semi-infinite DCB model conveniently removes the influence of the rear boundary of the model, a cursory examination

of the effect of the rear boundary is made by using a semi-infinite DCB model subjected to fixed grips conditions. Figure 23 shows the crack length-time behavior for the identical fixed grips conditions as in Figure 22. As seen, the rear boundary of the model has little effect upon the crack behavior.

2.4.3 A Comparison Between Crack Behaviors for Each Method of Simulating the Starter Notch Bluntness

A comparison of the crack behavior for each method used to simulate the initial notch bluntness clearly indicates the sensitivity of the DCB model to the initial conditions used. A direct comparison of Figures 14, 16 and 18 with Figures 20, 21 and 22 indicates markedly different crack behaviors. The latter series of figures exhibits an increasing tendency towards discontinuous crack growth, i.e., arrest and reinitiation, whereas the former series of figures does not indicate this behavior. The gross features of the crack extension process, crack speeds and crack arrest lengths, for each of the six figures are shown in Table 2. As the table indicates sizable differences occur in both crack speeds and crack arrest lengths. Crack speeds differ by as much as thirty-five percent, and crack arrest lengths differ by as much as sixteen percent.

A comparison of the gross features of the crack extension process is now made with the behavior obtained by Kanninen [23]. First, the behavior of the crack arrest length for increasing levels of initial energy overstorage is examined. Figure 26 shows dimensionless crack arrest length versus the parameter G_q/R for each of the two methods used to simulate the started notch bluntness in this analysis, as well as

those obtained in Kanninen's analysis. As is evident, the method used to simulate the bluntness of the notch makes a sizable difference in the relationship between crack arrest length and the initial energy overstorage level. Thus, for a given experiment, that is given values of h, a_r, and G_q, three different values of R can be deduced, each depending upon the method of simulating the initial notch bluntness. This dependence upon the method used to simulate the notch bluntness is also evident in Figure 27 which shows the behavior of crack speed for increasing levels of initial energy overstorage. Again, an experimentally measured crack speed would result in an R-value which depends upon the method used to simulate the initial notch bluntness. Finally, a comparison is made of crack speeds and crack arrest lengths, through the elimination of the parameter G_q/R. Figure 28 shows the crack speed versus the dimensionless crack arrest length for each method used to simulate the notch bluntness in this analysis, as well as Kanninen's analysis. Again, the sensitivity of the model to the method used to simulate the notch bluntness is evident in this figure. Thus, one must conclude from the comparisons made in Figures 26, 27, and 28, that Kanninen's DCB model exhibits an appreciable sensitivity to the simulation of the starter-notch bluntness.

2.4.4 Conclusions and Comments

An immediate observation which needs comment is the nature of the crack extension process shown in each of the Figures 13-17 and 19-21. The process of advancing the crack tip through the network of characteristic curves in discrete increments results in the crack pausing at a fixed crack length for several time increments during each

discrete advance of the crack tip in the solution process. That is, once the crack tip has been advanced to the next node in the gridwork, a period of time must elapse before the crack extension criterion is again satisfied at the crack tip and the crack tip is allowed to advance to the next node.

This inherent pausing character of the crack extension process is not evident in the crack length-time behavior as presented by Kanninen [23]. The pausing character of the crack extension process must also be inherent in Kanninen's analysis, as the finite-difference scheme employed to obtain a solution requires $\frac{dx}{dt} > c_o$ to assure numerical stability. Clearly, given a unit time increment Δt, the smallest spatial increment allowable must be $\Delta x > c_o \Delta t$. Because the crack speeds observed are substantially less than the bar wave speed, c_o, the increment $c_o \Delta t$ or Δx must be farther than the crack could advance in any one time increment. Thus, the crack tip must remain at a fixed position for several time increments. The behavior of the crack presented by Kanninen may represent some mean value of the crack tip location, which in effect would smooth out the crack length-time behavior.

In light of this discussion, the discontinuous crack growth observed in some cases previously discussed in this analysis and in Kanninen's analysis, may simply be a characteristic of the model when subjected to particular initial conditions. Thus, these regions previously identified as crack arrest and reinitiation regions may be nothing more than "longer" pauses in the numerical crack extension process, and not actual behavior to be expected in the laboratory. Clearly, additional investigation needs to be undertaken. In

be inconsequential for the majority of the crack extension process during the time span studied. Thus, wave reflections occurring at the front boundary of the specimen arm are believed to be the cause of the oscillatory nature of the crack behavior and the arrest and reinitiation phenomenon.

However, a much more serious criticism of the model can be made because of its sensitivity to the means used to simulate the initial notch bluntness. As shown, the relationship between crack speed and initial energy overstorage, (c/c_o vs. G_q/R) and the relationship between crack arrest length and initial energy overstorage (a_r/h vs. G_q/R) are dependent upon the simulation of the starter-notch bluntness. Thus, an attempt to extract R-values from experimental data by using one of these two relationships may not be successful. In addition, it has been shown that the relationship between crack arrest length and crack speed is not unique, but also depends upon the method used to simulate the notch bluntness. This fact has been confirmed recently by a two-dimensional finite-difference analysis of the DCB specimen performed by Shmuely and Peretz [27]. Their crack arrest length and crack speed relationship departs substantially from Kanninen's relationship.

In conclusion, the DCB analysis presented here demonstrates that the model as formulated by Kanninen is sensitive to variations in the simulation of the starter notch bluntness. Due to this fact, generalizations about crack behavior with regard to interpreting experimental data, or with regard to developing an understanding of the crack arrest phonomenon, must be subject to careful scrutiny.

particular, other initial conditions should be studied to see if the arrest and reinitiation regions occur.

A close examination of the six figures displaying the crack behavior in the finite DCB model, indicates an oscillatory character in the crack length-time behavior. The crack behavior appears to oscillate about the straight line segment indicating constant crack speed. In the DCB analysis conducted at the Battelle Laboratories, attempts are made to correlate the period of the oscillations, and the period of the crack arrest and reinitiation occurrences, with wave reflections caused by the lateral surfaces of the specimen arms [22]. Other attempts are made to explain these oscillations by attributing them to the influence of the mass of the loading pins [23]. These correlations as made in the Battelle analysis are subject to dispute. First, the beam model only allows wave propagation along the axis of the beam. Thus, there are no wave reflections from the lateral surfaces of the beam arms. If the period of these oscillations does correlate with the wave transit time between the lateral surfaces in the specimen arms, it is by chance and not by actual wave reflections. Secondly, the oscillatory nature of the crack length-time behavior is not related to the mass of the loading pins because the oscillations occur in this analysis even when the pins are not modeled. Thus, the oscillatory nature of the crack behavior, and the regions of crack arrest and reinitiation, are best attributed to wave reflections caused by the front and rear boundaries of the model. In fact, when comparing the crack behavior of the semi-infinite model and the finite model subjected to fixed-grips conditions, the influence of the rear boundary appears to

CHAPTER III

AN APPLICATION OF RUNNING-CRACK EIGENFUNCTIONS TO A FINITE-ELEMENT SIMULATION OF RAPID CRACK PROPAGATION

As the conclusions given in Chapter II point out, a one-dimensional model is not a completely satisfactory model for predicting crack propagation in the DCB Test specimen. This fact, with the additional observation that an extension of this one-dimensional beam-type model to include other types of geometries is not at all obvious, has led many analysts to consider alternative means to simulate crack propagation in structures.

In particular, Williams' [29] static eigenfunctions when used in conjunction with the finite-element method [30,31] have been highly successful and convenient for determining approximate solutions for stress-intensity factors for stationary cracks. An analogous technique is anticipated to be successful for deducing stress-intensity factors for running cracks in finite bodies. The development of dynamic eigen-solutions for the two-dimensional opening-mode propagation of a crack at constant velocity is outlined by Rice [33]. These constant velocity eigenfunctions are of particular interest because Nilsson [34] has shown that the singular ($r^{-1/2}$) stress terms do not depend upon the acceleration of the crack tip, but only depend upon the crack tip's instantaneous velocity. Thus, the singular ($r^{-1/2}$) stress eigenfunctions and the corresponding ($r^{1/2}$) displacement eigenfunctions obtained for the special case of constant crack speed remain unchanged if the

crack speed is varying. With this fact in mind and as the other eigenfunctions corresponding to constant crack speed do satisfy the equations of motion and boundary conditions of stress-free crack faces, it is reasonable to anticipate that a numerical application of the constant velocity eigenfunctions should produce reliable dynamic stress-intensity factors, not only for problems for which the crack speed has been specified to be constant, but also for problems in which the crack speed does not vary "too rapidly".

In order to verify the ability of the constant velocity eigenfunctions to adequately predict dynamic stress-intensity factors, a procedure is developed to extract the stress-intensity factor from finite element nodal displacements for a problem solved by Broberg [4]. Broberg's problem was selected because it is one of the few true initial value problems for which a solution is readily available.

Extraction of stress-intensity-factors from finite-element nodal displacements when using conventional finite elements has proven difficult for static problems involving cracks, because the conventional plane-stress or plane-strain element cannot provide displacements which converge to the $r^{1/2}$ behavior in the vicinity of the crack tip. This problem is overcome by considering displacements in a "not-too-near" neighborhood of the crack tip. That is, nodal displacements too near the crack tip will reflect the inability of the conventional element to fit the $r^{1/2}$ variation in displacements. On the other hand, nodal displacements too far from the crack tip will not be adequately represented by the $r^{1/2}$ eigenfunction. This difficulty is addressed by considering finite-element nodal displacements at three different radial

distances from the crack tip and by including terms other than the $r^{1/2}$ displacement eigenfunction.

Although the capability for determining dynamic stress-intensity-factors is not severely tested by using a simulation of Broberg's problem which is a constant velocity crack propagation problem, it is a necessary task if confidence is to be gained in using these eigenfunctions when an exact solution does not exist. In addition, because the exact solution is known, numerical experimentation can be undertaken by comparing the stress-intensity factors as obtained by Broberg with values obtained by varying the number of terms of the eigensolution to be used, and by considering various radial nodal patterns.

3.1 Development of the Eigenfunctions

When considering plane-strain deformation of a homogeneous, isotropic, linear elastic solid, the field equations of elastodynamics are satisfied if the displacement potentials Φ and Ψ satisfy the wave equations. (Refer to Fung [37])

$$c_1^2 \nabla^2 \Phi = \Phi_{,tt}$$

and

$$\nabla^2 = \frac{\partial^2}{\partial X^2} + \frac{\partial^2}{\partial Y^2} \tag{3.1}$$

$$c_2^2 \nabla^2 \Psi = \Psi_{,tt}$$

where c_1 and c_2 are the dilatational and shear wave speeds respectively. In terms of the Lamé constant, λ, the shear modulus, μ, and the material density, ρ, c_1 and c_2 are given by:

$$c_1^2 = \frac{\lambda + 2\mu}{\rho} , \qquad c_2^2 = \frac{\mu}{\rho} \tag{3.2}$$

Components of displacement, u_X and u_Y, are related to the two potentials through the relations:

$$u_X = \Phi_{,X} + \Psi_{,Y} \quad \text{and} \quad u_Y = \Phi_{,Y} - \Psi_{,X} \tag{3.3}$$

where X and Y are fixed rectangular coordinates.

Let us consider a crack traveling in an infinite body at constant speed c, and let us introduce a coordinate system traveling with the crack tip, $x = X - ct$, $y = Y$. Figure 29 shows the various coordinate systems discussed in this development.

Following Rice [33], we seek solutions to the wave equations (3.1) in which Φ and Ψ are functions only of x and y. This restriction on the solutions for Φ and Ψ results in stress and deformation patterns which are convected through the body at constant speed, or appear time-independent to an observer traveling with the crack-tip. The wave equation then become

$$(1 - c^2/c_1^2)\Phi_{,xx} + \Phi_{,yy} = 0$$

and (3.4)

$$(1 - c^2/c_2^2)\Psi_{,xx} + \Psi_{,yy} = 0$$

The transformations

$$y_1 = S_1 y \quad \text{and} \quad y_2 = S_2 y \tag{3.5}$$

where

$$s_1^2 = 1 - c^2/c_1^2 \quad \text{and} \quad s_2^2 = 1 - c^2/c_2^2 \tag{3.6}$$

are introduced to reduce the wave equations to the Laplace equations. (Refer to Fung [37])

$$\nabla_1^2 = \frac{\partial^2}{\partial x^2} + \frac{\partial^2}{\partial y_1^2}$$

$$s_1^2 \nabla_1^2 \Phi = 0 \qquad s_2^2 \nabla_2^2 \Psi = 0 \tag{3.7}$$

$$\nabla_2^2 = \frac{\partial^2}{\partial x^2} + \frac{\partial^2}{\partial y_2^2}$$

For the symmetric opening-mode extension of a crack along the x-axis, solutions for Φ and Ψ are

$$\Phi = \hat{A}\, r_1^m \cos m\, \theta_1$$

$$\Psi = \hat{B}\, r_2^m \sin m\, \theta_2 \tag{3.8}$$

where $\hat{A}$ and $\hat{B}$ are unknown constants, and the polar coordinate systems (r_1, θ_1) and (r_2, θ_2) are given by

$$r_1 e^{i\theta_1} = x + i\, y_1 \quad \text{and} \quad r_2 e^{i\theta_2} = x + i\, y_2 \tag{3.9}$$

Such solutions lead to displacements

$$u_x = \hat{A}\, m\, r_1^{(m-1)} \cos((m-1)\theta_1) + \hat{B} m\, S_2\, r_2^{(m-1)} \cos((m-1)\theta_2) \tag{3.10}$$

$$u_y = -\hat{A}m\, S_1 r_1^{(m-1)} \sin((m-1)\theta_1) - \hat{B}m\, r_2^{(m-1)} \sin((m-1)\theta_2)$$

and stresses

$$\begin{aligned}
\sigma_{xx} &= -\mu m(1-m)[(2s_1^2 - s_2^2 + 1)\hat{A} r_1^{(m-2)} \cos((m-2)\theta_1) \\
&\qquad + 2s_2 \hat{B}\, r_2^{(m-2)} \cos((m-2)\theta_2)] \\
\sigma_{yy} &= \mu m(1-m)[(1 + s_2^2)\hat{A} r_1^{(m-2)} \cos((m-2)\theta_1) \\
&\qquad + 2s_2 \hat{B} r_2^{(m-2)} \cos((m-2)\theta_2)] \\
\tau_{xy} &= \mu m(1-m)[2s_1 \hat{A} r_1^{(m-2)} \sin((m-2)\theta_1) \\
&\qquad + (1 + s_2^2)\hat{B}\, r_2^{m-2} \sin((m-2)\theta_2)]
\end{aligned} \tag{3.11}$$

Applying the boundary conditions for traction-free crack faces, that is

$$\sigma_{yy} = \tau_{xy} = 0 \qquad \text{on} \qquad (x < 0, \quad Y = 0^+, \; 0^-) \tag{3.12}$$

leads to two homogeneous linear algebraic equations in the constants $\hat{A}$ and $\hat{B}$.

$$\begin{aligned}
0 &= \mu m(1-m)[(1 + s_2^2)\hat{A} \cos((m-2)\pi) + 2s_2\, \hat{B} \cos((m-2)\pi)] \\
0 &= \mu m(1-m)[2s_1 \hat{A} \sin((m-2)\pi) + (1 + s_2^2)\hat{B} \sin((m-2)\pi)]
\end{aligned} \tag{3.13}$$

For a non-trivial solution to exist, the determinant of the coefficients

must vanish. This results in the characteristic equation

$$[(1 + s_2^2)^2 - 4s_1 s_2]m^2(1-m)^2 \sin(2m\pi) = 0 \tag{3.14}$$

The leading factor of this equation which is a function of crack speed is recognized as the Rayleigh function [38], and will not vanish except for zero crack speed or the Rayleigh wave speed.

The characteristic equation then results in the following eigenvalues

$$m = 0, \pm 1/2, \pm 1, \pm 3/2, \pm 2, \pm 5/2, \cdots \tag{3.15}$$

An examination of the displacement relations (3.10) forces the restriction $m \geq 1$ to insure bounded displacements at the origin ($r = 0$). The resulting eigenvalues are

$$m = 1 + 1/2\, n \quad , \qquad n = 0, 1, 2, 3, \cdots \tag{3.16}$$

Incorporating those eigenvalues into the homogeneous equations (3.13) to relate the constants $\hat{A}$ and $\hat{B}$, then eliminating the constant B in relations (3.10, 3.11) results in the following eigenfunctions

$$u_{x_n} = \hat{A}_n(\tfrac{1}{2} n + 1)\{r_1^{\frac{1}{2}n} \cos(\tfrac{1}{2} n \theta_1) - \tfrac{1}{2} g(n) r_2^{\frac{1}{2}n} \cos(\tfrac{1}{2} n \theta_2)\}$$

$$u_{y_n} = \hat{A}_n(\tfrac{1}{2} n + 1)\{-s_1 r_1^{\frac{1}{2}n} \sin(\tfrac{1}{2} n \theta_1) + \tfrac{1}{2} (g(n)/s_2) r_2^{\frac{1}{2}n} \sin(\tfrac{1}{2} n \theta_2)\}$$

$$\sigma_{xx_n} = \hat{A}_n \mu(\tfrac{1}{2} n)(\tfrac{1}{2} n + 1)\{(2s_1^2 - s_2^2 + 1) r_1^{(\frac{1}{2} n - 1)} \cos((\tfrac{1}{2} n - 1)\theta_1)$$

$$- g(n)r_2^{(\frac{1}{2}n - 1)}\cos((\tfrac{1}{2}n - 1)\theta_2)\}$$

$$\sigma_{yy_n} = \hat{A}_n\ \mu(\tfrac{1}{2}n)(\tfrac{1}{2}n + 1)\{-(1 + s_2^2)r_1^{(\frac{1}{2}n - 1)}\cos((\tfrac{1}{2}n - 1)\theta_1) \quad (3.17)$$

$$+ g(n)r_2^{(\frac{1}{2}n - 1)}\cos((\tfrac{1}{2}n - 1)\theta_2)\}$$

$$\tau_{xy_n} = \hat{A}_n\ \mu(\tfrac{1}{2}n)(\tfrac{1}{2}n + 1)\{-2s_1 r_1^{(\frac{1}{2}n - 1)}\sin((\tfrac{1}{2}n - 1)\theta_1)$$

$$+ \tfrac{1}{2}((1 + s_2^2)/s_2)g(n)r_2^{(\frac{1}{2}n - 1)}\sin((\tfrac{1}{2}n - 1)\theta_2)\}$$

where

$$g(n) = \begin{cases} 4s_1 s_2/(1 + s_2^2), & n \text{ odd} \\ 1 + s_2^2, & n \text{ even} \end{cases} \quad (3.18)$$

where $\hat{A}_n$ are undetermined constants.

It is interesting to note that the eigenvalue n = 0 recovers the rigid-body translation term along the x-axis. The next eigenvalue n = 1 produces singular stresses of the usual $r^{-1/2}$ form, as in the stationary crack problem.

Dynamic stress intensity factors are obtained by relating K_D to the constant A_1. Defining the dynamic stress-intensity factor as

$$K_D = \lim_{x \to 0^+} [\sqrt{2\pi x}\ \sigma_{yy}(x,0)] \quad (3.19)$$

Then

$$K_D = \frac{3\sqrt{2\pi}}{4}\ \mu\left[\frac{4s_1 s_2 - (1 + s_2^2)^2}{(1 + s_2^2)}\right]\hat{A}_1 \quad (3.20)$$

As discussed previously, the eigenfunctions developed, depend upon the Rayleigh function, $(1 + s_2^2)^2 - 4s_1s_2$, not vanishing. However, it is reasonable to anticipate that Williams' static eigenfunctions [29] will result if the proper limiting procedure is followed when allowing the crack speed to approach zero. Formally taking the limit as $c \to 0$ in the eigenfunctions (3.17) results in zero stresses and displacements, if the constants A_n are assumed to be of finite magnitude. In addition, the stress-intensity factor K_D also becomes identically zero, if the constants A_n are again finite. This difficulty is overcome by eliminating the constants $\hat{A}_n$, in favor of the new constants K_n, given by

$$K_n = \frac{3\sqrt{2\pi}}{4}\,\mu\left[\frac{4s_1s_2 - (1 + s_2^2)^2}{(1 + s_2^2)}\right]\hat{A}_n \tag{3.21}$$

The eigenfunctions then are written

$$u_{x_n} = \frac{4}{3\sqrt{2\pi}}\,\frac{K_n}{\mu}\,\frac{(1 + s_2^2)}{4s_1s_2 - (1 + s_2^2)^2}\,(\tfrac{1}{2}\,n + 1)\{r_1^{\frac{1}{2}n}\cos(\tfrac{1}{2}\,n\,\theta_1)$$

$$- \tfrac{1}{2}\,g(n)r_2^{\frac{1}{2}n}\cos(\tfrac{1}{2}\,n\,\theta_2)\}$$

$$u_{y_n} = \frac{4}{3\sqrt{2\pi}}\,\frac{K_n}{\mu}\,\frac{(1 + s_2^2)}{4s_1s_2 - (1 + s_2^2)^2}\,(\tfrac{1}{2}\,n + 1)\{-s_1r_1^{\frac{1}{2}n}\sin(\tfrac{1}{2}\,n\,\theta_1) \tag{3.22}$$

$$+ \tfrac{1}{2}(g(n)/s_2)r_2^{\frac{1}{2}n}\sin(\tfrac{1}{2}\,n\,\theta_2)\}$$

$$\sigma_{xx_n} = \frac{4}{3\sqrt{2\pi}}\,K_n\,\frac{(1 + s_2^2)}{4s_1s_2 - (1 + s_2^2)^2}\,(\tfrac{1}{2}\,n)(\tfrac{1}{2}\,n + 1)\{(2s_1^2 - s_2^2 + 1)r_1^{(\frac{1}{2}n - 1)}$$

$$\cos((\tfrac{1}{2}\,n - 1)\theta_1) - g(n)r_2^{(\frac{1}{2}n - 1)}\cos((\tfrac{1}{2}\,n - 1)\theta_2)\}$$

$$\sigma_{yy_n} = \frac{4}{3\sqrt{2\pi}} K_n \frac{(1 + s_2^2)}{4s_1s_2 - (1 + s_2^2)^2} (\tfrac{1}{2} n)(\tfrac{1}{2} n + 1)$$

$$\{- (1 + s_2^2) r_1^{(\frac{1}{2} n - 1)} \cos((\tfrac{1}{2} n - 1)\theta_1)$$

$$+ g(n)\, r_2^{(\frac{1}{2} n - 1)} \cos((\tfrac{1}{2} n - 1)\theta_2)\}$$

$$\tau_{xy_n} = \frac{4}{3\sqrt{2\pi}} K_n \frac{(1 + s_2^2)}{4s_1s_2 - (1 + s_2^2)^2} (\tfrac{1}{2} n)(\tfrac{1}{2} n + 1)$$

$$\{- 2s_1 r_1^{(\frac{1}{2} n - 1)} \sin((\tfrac{1}{2} n - 1)\theta_1)$$

$$+ \tfrac{1}{2} ((1 + s_2^2)/s_2) g(n) r_2^{(\frac{1}{2} n - 1)} \sin((\tfrac{1}{2} n - 1)\theta_2)\}$$

The constant K_1 now becomes the dynamic stress-intensity factor K_D.

A limiting process is now applied by allowing $c \to o$ that is $s_1, s_2 \to 1$. An indeterminate form results for each eigenfunction (3.22). Use of l'Hôpital's Rule resolves the indeterminacy, and the appropriate static eigenfunctions are obtained, which are equivalent to Williams' function.

$$u_{x_n} = \frac{1}{3\sqrt{2\pi}} \frac{K_n}{\mu} (\tfrac{1}{2} n + 1)\, r^{n/2} \left\{(\tfrac{1}{2} n - 4\nu + 3 + (-1)^n)\cos(\tfrac{1}{2} n\, \theta) - \tfrac{1}{2} n \cos\left(\left(\frac{n-4}{2}\right)\theta\right)\right\}$$

$$u_{y_n} = \frac{1}{3\sqrt{2\pi}} \frac{K_n}{\mu} (\tfrac{1}{2} n + 1) r^{n/2} \left\{- (\tfrac{1}{2} n + 4\nu - 3 + (-1)^n) \sin(\tfrac{1}{2} n\, \theta) + \tfrac{1}{2} n \sin\left(\left(\frac{n-4}{2}\right)\theta\right)\right\} \qquad (3.23)$$

$$\sigma_{xx_n} = \frac{1}{3\sqrt{2\pi}} K_n(\tfrac{1}{2}n + 1)(\tfrac{1}{2}n)r^{\left(\frac{n-2}{2}\right)}\left\{(n + 4 + 2(-1)^n)\cos\left(\left(\frac{n-2}{2}\right)\theta\right)\right.$$

$$\left. - (n - 2)\cos\left(\left(\frac{n-6}{2}\right)\theta\right)\right\}$$

$$\sigma_{yy_n} = \frac{1}{3\sqrt{2\pi}} K_n(\tfrac{1}{2}n + 1)(\tfrac{1}{2}n)r^{\left(\frac{n-2}{2}\right)}\left\{-(n + 4 + 2(-1)^n)\cos\left(\left(\frac{n-2}{2}\right)\theta\right)\right.$$

$$\left. + (n - 2)\cos\left(\left(\frac{n-6}{2}\right)\theta\right)\right\}$$

$$\tau_{xy_n} = \frac{1}{3\sqrt{2\pi}} K_n(\tfrac{1}{2}n + 1)(\tfrac{1}{2}n)r^{\left(\frac{n-2}{2}\right)}\left\{-(n + 2(-1)^n)\sin\left(\left(\frac{n-2}{2}\right)\theta\right)\right.$$

$$\left. + (n - 2)\sin\left(\left(\frac{n-6}{2}\right)\theta\right)\right\}$$

3.2 General Features of the Dynamic Eigenfunctions in the Vicinity of the Crack Tip

A study of the behavior of both stress and displacement in the vicinity of the moving crack tip reveals a dependence upon the crack speed. The singular stress eigenfunctions are given explicitly by

$$\sigma_{xx} = \frac{K_1}{\sqrt{2\pi}} \frac{(1 + s_2^2)}{4s_1s_2 - (1 + s_2^2)^2}\left\{(2s_1^2 - s_2^2 + 1)r_1^{-1/2}\cos(1/2\ \theta_1)\right.$$

$$\left. - \frac{4s_1s_2}{1 + s_2^2} r_2^{-1/2}\cos(1/2\ \theta_2)\right\}$$

$$\sigma_{yy} = \frac{K_1}{\sqrt{2\pi}} \frac{(1 + s_2^2)}{4s_1s_2 - (1 + s_2^2)^2} \left\{ - (1 + s_2^2) r_1^{-1/2} \cos(1/2\ \theta_1) \right.$$

$$\left. + \frac{4s_1s_2}{1 + s_2^2} r_2^{-1/2} \cos(1/2\ \theta_2) \right\} \qquad (3.24)$$

$$\tau_{xy} = \frac{K_1}{\sqrt{2\pi}} \frac{(1 + s_2^2)}{4s_1s_1 - (1 + s_2^2)^2} \left\{ 2s_1 r_1^{-1/2} \sin(1/2\ \theta_1) - 2s_1 r_2^{-1/2} \sin(1/2\ \theta_2) \right\}$$

The corresponding $\sqrt{r}$ displacement eigenfunctions are given by

$$u_x = \frac{2K_1}{\sqrt{2\pi}\ \mu} \frac{(1 + s_2^2)}{4s_1s_2 - (1 + s_2^2)^2} \left[\sqrt{r_1} \cos(1/2\ \theta_1) \right.$$

$$\left. - \frac{2s_1s_2}{1 + s_2^2} \sqrt{r_2} \cos(1/2\ \theta_2) \right] \qquad (3.25)$$

$$u_y = \frac{2K_1}{\sqrt{2\pi}\ \mu} \frac{(1 + s_2^2)}{4s_1s_2 - (1 + s_2^2)^2} \left[- s_1\sqrt{r_1} \sin(1/2\ \theta_1) \right.$$

$$\left. + \frac{2s_1}{1 + s_2^2} \sqrt{r_2} \sin(1/2\ \theta_2) \right]$$

Figures 30 - 34 show the angular variation of each of these eigenfunctions for the crack speeds $c/c_2 = 0.8$, 0.6, 0.4 and 0.2. Also shown in each figure is the variation of each of the corresponding static eigenfunctions. Material properties have been selected such that

Poisson's ratio is taken to be $\nu = 1/3$. This results in the ratio of wave speeds $c_1/c_2 = 2$, which is a close approximation for most engineering materials. As is evident in each figure, the increase of crack speed results in an increasing departure from the static distributions, although, the lowest crack speed considered, $c/c_2 = 0.2$ results in stress and displacement patterns which can be reasonably well approximated by the static eigenfunctions.

One area of potential use for the dynamic eigenfunctions given above is in the field of dynamic photoelasticity. Williams' static eigenfunctions have already received extensive use in this field [39] to determine stress intensity factors from photoelastic experiments. The solution technique has essentially been to match the isochromatic lines, which are lines of constant maximum shear stress, observed in a photoelastic experiment with the isochromatic line predicted by Williams' [29] singular stress eigenfunctions and a uniform stress term. The assumption is made that the isochromatic lines can be photographically resolved sufficiently close to the crack tip such that the use of the singular ($r^{-1/2}$) eigenfunctions suffices to represent the state of stress. A natural area of application for the dynamic eigenfunctions lies in interpreting isochromatic lines observed in dynamic photoelastic experiments.

The maximum shear stress τ_{max} is related to the state of stress σ_{xx}, σ_{yy}, and τ_{xy} through the relation

$$\tau_{max}^2 = \left(\frac{\sigma_{yy} - \sigma_{xx}}{2}\right)^2 + \tau_{xy}^2 \qquad (3.26)$$

Isochromatic lines are then produced by substituting the singular eigenfunctions (3.24) into the above equation.

Figure 35 shows a polar plot of the parameter $(\tau_{max}\sqrt{2\pi r}/K_1)$ for crack speeds $c/c_2 = 0.8$, 0.6, 0.4 and 0.2. For comparison the static isochromatic line

$$\tau_{max} = \frac{1}{2}\frac{K_1}{\sqrt{2\pi r}} \sin\theta \qquad (3.27)$$

is also shown on the figure. Obviously, for crack speeds $c/c_2 > 0.2$ the static isochromatic line proves to be totally inadequate to describe the state of stress in the vicinity of the crack tip.

However, it should be mentioned that the characteristics exhibited by the isochromatics differ in several ways from the isochromatic observed in dynamic photoelastic experiments. First, while the isochromatics shown here exhibit a tendency to lean towards the left, the experimentally observed isochromatic lines lean toward the right. This difference may be resolved simply by realizing that the experimentally observed isochromatic lines may not be sufficiently close to the crack tip such that the singular stress terms dominate. Thus, the rightward inclination of the experimentally observed isochromatic lines may indicate the inability to photographically resolve the isochromatics close enough to the crack tip. In addition, the double-lobed shape of the isochromatic line for the crack speed $c/c_2 = 0.8$ has never been observed experimentally, simply because an experiment has not yet been devised which allows a crack to propagate this rapidly.

In conclusion, it can be said that the use of these constant velocity eigenfunctions to extract stress-intensity factors from running crack photoelastic experiments should result in a considerable improvement to the method now being used, which is based upon static isochromatics.

3.3 Comments Concerning Other Solution Forms

The eigenfunctions (3.22) are a convenient form for expressing the stress and displacement fields in the vicinity of the moving crack tip. Neglecting the rigid body terms, as the crack tip is approached, the dominant term of the eigenfunction becomes the $r^{1/2}$ term for displacements and the $r^{-1/2}$ term for stress. Obviously these particular terms of the dynamic eigenfunctions have been of great interest to many analysts [27 - 30]. Other expressions currently being advocated to allow expressing the stress and displacement fields in the vicinity of the propagating crack tip are in a more cumbersome form. For example, Sih [40] advocates the use of the following forms for the $r^{-1/2}$ stress terms and $r^{1/2}$ displacement terms.

$$\sigma_{xx} = \frac{k_1}{\sqrt{2r}} F_1(s_1,s_2)[(1 + s_2^2)(2s_1^2 + 1 - s_2^2)f(s_1) - 4s_1s_2\, f(s_2)]$$

$$\sigma_{yy} = \frac{k_1}{\sqrt{2r}} F_1(s_1,s_2)[4s_1s_2\, f(s_2) - (1 + s_2^2)^2\, f(s_1)] \qquad (3.28)$$

$$\tau_{xy} = \frac{k_1}{\sqrt{2r}} F_1(s_1,s_2)2s_1(1 + s_2^2)[g(s_1) - g(s_2)]$$

$$\mu\, u_x = k_1\sqrt{2r}\, F_1(s_1,s_2)[(1 + s_2^2)(\cos^2\theta + s_1^2\sin^2\theta)^{1/2}f(s_1)$$

$$- 2s_1 s_2(\cos^2\theta + s_2^2 \sin^2\theta)^{1/2} f(s_2)]$$

$$\mu u_y = k_1\sqrt{2r}\, F_1(s_1,s_2)[s_1(1 + s_2^2)(\cos^2\theta + \sin^2\theta)^{1/2} g(s_1)$$

$$- 2s_1(\cos^2\theta + s_2^2 \sin^2\theta)^{1/2} g(s_2)]$$

where

$$s_j = [1 - (c/c_j)^2]^{1/2} , \quad j = 1,2 \tag{3.29}$$

and

$$f^2(s_j) + g^2(s_j) = \sec\theta(1 + s_j^2 \tan^2\theta)^{-1/2} \tag{3.30}$$

$$f^2(s_j) - g^2(s_j) = \sec\theta(1 + s_j^2 \tan^2\theta)^{-1} \tag{3.30}$$

k_1 is the stress-intensity factor and "The function $F_1(s_1,s_2)$ varies from one problem to the next depending upon the boundary conditions". Sih's expressions may be reduced to the form of the eigenfunctions. First, $f(s_j)$ and $g(s_j)$ are solved for

$$f^2(s_j) = \tfrac{1}{2}\sec\theta\{(1 + s_j^2 \tan^2\theta)^{-1/2} + (1 + s_j^2 \tan^2\theta)^{-1}\}$$

$$g^2(s_j) = \tfrac{1}{2}\sec\theta\{(1 + s_j^2 \tan^2\theta)^{-1/2} - (1 + s_j^2 \tan^2\theta)^{-1}\} \tag{3.31}$$

Using the relation

$$\tan\theta_j = s_j \tan\theta \tag{3.32}$$

and the half-angle trigonometric identify

$$\cos^2\alpha = 1/2(1 + \cos 2\alpha) \tag{3.33}$$

$f(s_j)$ and $g(s_j)$ are expressed as

$$f^2(s_j) = \sec\theta \cos\theta_j \cos^2(1/2\ \theta_j)$$

$$g^2(s_j) = \sec\theta \cos\theta_j \sin^2(1/2\ \theta_j) \tag{3.34}$$

or in a more convenient form for further manipulation

$$f(s_j) = (\cos^2\theta + s_j^2 \sin^2\theta)^{-1/4}\cos(1/2\ \theta_j)$$

$$g(s_j) = (\cos^2\theta + s_j^2 \sin^2\theta)^{-1/4}\sin(1/2\ \theta_j) \tag{3.35}$$

Making use of the relation

$$r_j = r(\cos^2\theta + s_j^2 \sin^2\theta)^{1/2} \tag{3.36}$$

and making the observations

$$\frac{f(s_j)}{\sqrt{r}} = \frac{\cos(1/2\ \theta_j)}{\sqrt{r_j}}$$

$$\frac{g(s_j)}{\sqrt{r}} = \frac{\sin(1/2\ \theta_j)}{\sqrt{r_j}} \tag{3.37}$$

$$\sqrt{r}(\cos^2\theta + s_j^2 \sin^2\theta)f(s_j) = \sqrt{r_j}\cos 1/2\ \theta_j$$

$$\sqrt{r}(\cos^2\theta + s_j^2 \sin^2\theta)g(s_j) = \sqrt{r_j}\sin 1/2\ \theta_j$$

Sih's equations can be expressed as

$$\sigma_{xx} = \frac{k_1}{\sqrt{2}} F_1(s_1,s_2)(1+s_2^2)\left[(2s_1^2+1-s_2^2)\frac{\cos(1/2\ \theta_1)}{\sqrt{r_1}}\right.$$

$$\left. - \frac{4s_1s_2}{(1+s_2^2)}\frac{\cos(1/2\ \theta_2)}{\sqrt{r_2}}\right]$$

$$\sigma_{yy} = \frac{k_1}{\sqrt{2}} F_1(s_1,s_2)(1+s_2^2)\left[-(1+s_2^2)\frac{\cos(1/2\ \theta_1)}{\sqrt{r_1}}\right.$$

$$\left. + \frac{4s_1s_2}{(1+s_2^2)}\frac{\cos(1/2\ \theta_2)}{\sqrt{r_2}}\right]$$

$$\tau_{xy} = \frac{k_1}{\sqrt{2}} F_1(s_1,s_2)(1+s_2^2)\left[2s_1\frac{\sin(1/2\ \theta_1)}{\sqrt{r_1}} - 2s_1\frac{\sin(1/2\ \theta_2)}{\sqrt{r_2}}\right]$$

$$\mu u_x = \sqrt{2}k_1 F_1(s_1,s_2)(1+s_2^2)\left[\sqrt{r_1}\cos(1/2\ \theta_1) - \frac{2s_1s_2}{1+s_2^2}\sqrt{r_2}\cos(1/2\ \theta_2)\right]$$

$$\mu u_y = \sqrt{2}k_1 F_1(s_1,s_2)(1+s_2^2)\left[s_1\sqrt{r_1}\sin(1/2\ \theta_1) - \frac{2s_1}{1+s_2^2}\sqrt{r_2}\sin(1/2\ \theta_2)\right]$$

Again, defining the stress-intensity factor K_D as

$$K_D = \lim_{r\to 0}\left(\sqrt{2\pi r}\ \sigma_{yy}(r,0)\right) \tag{3.39}$$

Then

$$K_D = k_1\sqrt{\pi}\ F_1(s_1,s_2)\ (4s_1s_2 - (1+s_2^2)^2) \tag{3.40}$$

Clearly

$$F_1(s_1,s_2) = \frac{1}{\sqrt{\pi}\,(4s_1s_2 - (1+s_2^2)^2)} \tag{3.41}$$

in order that the stress-intensity factors agree. Thus, $F_1(s_1,s_2)$ is not an arbitrary function varying from problem to problem as stated by Sih [40], but may simply be interpreted as the arbitrary constant in the eigenfunction solution, after the Rayleigh wave speed function has been factored out.

It is worthwhile to note that the half-angle trigonometric identity necessary to reduce Sih's expressions to the form of the eigenfunctions are appropriate only for these particular terms. The ability to express the other eigenfunctions in terms of $f(s_j)$ and $g(s_j)$ would be extremely awkward, if possible at all.

3.4 A Finite-Element Analysis of Broberg's Problem

The capability for extracting dynamic stress-intensity factors through the use of a finite element analysis of a running crack will now be demonstrated by simulating a problem solved by Broberg. This particular problem is selected because it is one of the few true initial value problems of physically meaningful crack extension for which a solution is readily available.

3.4.1 Broberg's Problem

Broberg's problem, as illustrated in Figure 36, consists of an infinite body initially in equilibrium with a uniform uniaxial tension $\sigma_{yy} = \sigma$ prior to crack extension. Initially, the body does not contain

a crack. At time zero, a crack begins to extend symmetrically through the body with each crack tip traveling at constant speed c . Broberg's analysis indicates that the ratio of dynamic to static stress-intensity factors is only a function of the crack speed and the material properties of the body. This stress-intensity factor ratio decreases monotonically from the value of one for the statics problem, to a value of zero at the Rayleigh wave speed.

3.4.2 The Finite-Element Model

A discussion of the finite-element model and the computational procedure used to simulate Broberg's problem follows. It should be mentioned that the finite-element simulation of Broberg's problem was not in itself a portion of this thesis. Rather, finite element nodal displacements were provided by Dr. James A. Aberson through use of an existing finite-element computer program to enable the calculation of dynamic stress-intensity factors for Broberg's problem. The reader may refer to [31] for more information regarding the use of finite elements to simulate dynamic problems.

Shown in Figure 37 is a finite-element model of one quadrant of Broberg's problem. The size of the body is selected such that for the time intervals of interest, the finite-model will represent the infinite space of Broberg's problem. That is, in a continuum analysis, a disturbance arising at the crack tip will not have sufficient time to travel to the boundary and return to the crack tip during the time interval of the finite-element analysis. Crack propagation is simulated simply by the sequential removal of restraints on the nodes at the base of the model which is the crack tip trajectory. Each element of the

model is a constant-strain triangle. The equations of motion are integrated numerically between nodal releases using the Newmark-β ($\beta = 1/4$) method [41]. Material properties are selected such that $c_1/c_2 = 2$ yielding a Rayleigh wave speed $c_R = 0.933\ c_2$. Crack speeds $c/c_2 = 0.2$, 0.4, 0.6 and 0.8 are considered in the analysis.

The characteristic length L shown in the figure is the largest half-length of the crack. The smallest spacing between nodes is then L/10. A total of ten nodal releases are then performed to simulate crack extension from an initial value of zero to a final value of L. During the time interval between each of those nodal releases, the equations of motion are integrated numerically for ten time steps. Introducing dimensionless time $\tau = c_2 t/L$. The size of each time step, $\Delta\tau$ is given below for each of the four crack speeds

c/c_2	$\Delta\tau$
0.2	0.0500
0.4	0.0250
0.6	0.0166
0.8	0.0125

The use of different time steps in the numerical integrations is not likely to have influenced the results significantly, since the largest time step used is the transit time of a longitudinal wave across the smallest of the finite elements. Past experience with using finite-elements to obtain solutions to dynamic problems [31] has led to this conclusion.

3.4.3 Computational Procedure

1) Nodal displacements for the equilibrium configuration of the uncracked body (all base nodes restrained against vertical displacement) are determined.

2) With the nodal displacements described above as initial values and with initial velocities of zero, numerical time integration is carried out for the model with node 1 (base nodes numbered 1,2,3,... from left to right) unrestrained and the other base nodes restrained. Integration is terminated at the time corresponding to the crack tip's arrival at the location of node 2.

3) Displacements and velocities at the end of the first interval of integration are taken as initial values for the second interval during which nodes 1 and 2 are unrestrained. Integration is terminated at the time corresponding to the crack tip arrival at the location of node 3. This process is repeated for time intervals corresponding to the presence of the crack tip between successive nodes.

Thus the numerical procedure is one in which a sequence of transient problems, each associated with a stationary crack, are solved. It should be noted that except at the end of each integration interval, the apparent crack length in the finite-element model is greater than that of the continuously expanding crack which is being simulated.

3.5 Calculation of Dynamic Stress-Intensity Factors

Dynamic stress-intensity factors are determined by matching nodal displacements in the neighborhood of the crack tip with a preselected number of displacement eigenfunctions.

The first and simplest technique used to determine stress-intensity factors is a crack-opening-displacement (COD) calculation. This is easily performed by noting that in the neighborhood of the crack tip, the u_y component of displacement may be adequately represented by the $r^{1/2}$ eigenfunction, that is

$$u_y = \frac{2}{\sqrt{2\pi}} \frac{K_1}{\mu} \frac{1}{4s_1 s_2 - (1 + s_2^2)^2} \{-s_1(1 + s_2^2) r_1^{1/2} \sin(1/2\ \theta_1) + 2s_1 r_2^{1/2} \sin(1/2\ \theta_1)\} \tag{3.42}$$

On the crack faces $\theta_1 = \theta_2 = \pi$ and $r_1 = r_2 = r$. Then this expression simplifies to

$$u_y = \frac{2}{\sqrt{2\pi}} \frac{K_1}{\mu} \frac{s_1(1 - s_2^2)}{4s_1 s_2 - (1 + s_2^2)^2} \sqrt{r} \tag{3.43}$$

Since the crack speed and material properties are specified, i.e. μ, s_1, and s_2 are known, this expression may be used to determine K_1 from finite-element nodal displacement for those nodes which lie on the crack face. The value of the radius, r, used in the above expression is the distance between the node coinciding with the crack tip and the node lying on the crack face. Figures 38 and 39 show the stress-intensity factors determined in this manner for each of two nodes lying on the crack faces.

Figure 38 shows the stress-intensity factors which result from this COD calculation when the node nearest to the crack tip is used.

In this case, the best results obtained are for the highest crack speed. Stress-intensity factors fall within 18 percent of Broberg's value for $c/c_2 = 0.8$. The worst results obtained are for the crack speed $c/c_2 = 0.2$ in which case stress-intensity factors depart from Broberg's results by 41 percent. A summary of the error may be found in Table 3. Also evident in the figure is an increasing scatter in the stress-intensity factors as the crack speed decreases. An explanation for this increase in scatter with decreasing crack speed may lie in the fact that the nodal releases which simulate the continuous crack extension, are in effect a more discontinuous process for the lower crack speeds.

For comparison the next node on the crack face is also used for COD calculations. The stress intensity factors resulting from these calculations are shown in Figure 39. In this case, the best results obtained are for the crack speed $c/c_2 = 0.6$ for which the error is 24 percent. The worst case occurs for the highest crack speed, $c/c_2 = 0.8$ for which the error is 40 percent. Once again the scatter in the calculated stress-intensity factors appears to increase with decreasing crack speed. A summary of the error in the calculated stress-intensity factor for each crack speed is found in Table 3.

A comparison of Figures 38 and 39 indicates that the stress-intensity factors for the node which lies two grid spacing from the crack tip are substantially lower in level than the values predicted by Broberg. The values of stress intensity factor based on the displacement from the node nearest the crack tip gives a level of stress-intensity factor which is in good agreement with Broberg particularly

for the highest crack speed. Such behavior is not surprising in that the $r^{1/2}$ behavior of displacement must become less dominant as one leaves the vicinity of the crack tip. Thus, stress-intensity factors based solely on the $r^{1/2}$ displacement term are limited to regions in which this displacement behavior dominates. However, as was discussed previously, the finite-element itself cannot produce a $r^{1/2}$ behavior of displacement in the vicinity of the crack tip because linear displacements are assumed. Thus, the displacements in the near vicinity of the crack tip are subject to suspicion. For these two reasons, a method for calculating stress intensity is explored which allows using displacements from nodes removed from the vicinity of the crack tip. This is achieved by incorporating terms other than just the $r^{1/2}$ displacement eigenfunction.

Three nodal patterns which surround the crack tip are selected for the analysis. Figures 40, 43 and 48 show the three patterns. Note that each pattern is located at increasing radial distances from the crack tip. These three patterns are subsequently referred to as the inner, middle, and outer nodal patterns.

After a particular pattern of nodes is selected, a finite number of terms of the eigenfunctions ($n = 0,1,2,\ldots$) are selected to represent the displacement pattern in the vicinity of the crack tip. Every node in each of the nodal patterns passes two degrees of freedom (u_x and u_y) except for the node which lies on the prolongation which has only one degree of freedom (u_x). Clearly, when the number of eigenfunction used to represent the displacements equals the total degrees of freedom in the nodal pattern, a simple matrix inversion may be

applied to obtain the coefficients of the eigenfunctions (K_n). When the number of eigenfunctions used are less than the total number of degrees of freedom in the nodal pattern, a least-squares fit [42] of the eigenfunctions to the displacements is sought. Details of both procedures are found in Appendix I. A discussion of the stress-intensity factors based on these nodal patterns follow.

Those nodes which immediately surround the crack tip are called the inner nodal pattern. This particular pattern contains a total of nine degrees of freedom. Figure 40 gives the stress-intensity factors when the first nine eigenfunctions ($n = 0,1,2,...8$) for displacements are used. Once again the best results occur for the highest crack speed $c/c_2 = 0.8$ for which the error is 18 percent. The worst case is again the slowest speed $c/c_2 = 0.2$ for which the error is 82 percent. Again appreciable scatter results for the lower crack speeds. The levels of the calculated stress intensity factors agree with Broberg's values.

One would expect that in the immediate vicinity of the crack tip, as the inner nodal pattern is, the participation of all nine eigenfunctions would not be needed to describe the displacement behavior. For this reason a two term ($n = 0,1$) and a four term ($n = 0,1,2,3$) least-squares fit of the nodal displacements to the eigenfunctions is performed. Figures 41 and 42 show the stress-intensity factors resulting from a two and four term least-squares fit respectively. Marked improvement is achieved for the lowest two crack speed $c/c_2 = 0.2$ and 0.4 when compared to the nine term fit. In addition, the scatter in stress-intensity values for the lower crack

speeds also shows improvement when compared to the nine term fit. Table 3 gives the error for each case.

The second pattern of nodes used in this analyses lie approximately two grid spacings around the crack tip. This pattern is referred to as the middle nodal pattern. This particular pattern contains a total of thirteen degrees of freedom. Thus, a straightforward fit of the thirteen nodal displacements to thirteen eigenfunctions ($n = 0,1,2,\ldots,12$) is performed. The resulting stress-intensity factors are shown in Figure 43. Once again, the higher crack speeds give good agreement with Broberg's results, whereas the lower crack speeds show more error and more scatter.

As discussed for the inner nodal pattern, one expects that all thirteen eigenfunctions are not needed to describe a displacement pattern for nodes located close to the crack tip. For this reason, stress-intensity factors are calculated based on two, three, four, and five term least-squares fits to the nodal displacements. The resulting stress-intensity factors are given in Figures 44, 45, 46 and 47 respectively. The best results obtained correspond to the four term least-squares fit. For this case, the errors given are about the same for each speed and the level of the stress-intensity values falls remarkably close to Broberg's results. It is interesting to note that the level of the stress-intensity factors for the two and three term least-squares fit fall somewhat below Broberg's values, whereas the five term fit falls above Broberg's values. Thus, there is some indication that a four term least-squares fit may be the optimum number of terms to select for this particular nodal pattern.

The third and final nodal pattern to be investigated is called the outer nodal pattern because it lies approximately four grid spacings from the crack tip. This particular pattern, however, could be used for only two crack lengths a = 0.5 and 0.7 because the finite element model did not possess sufficient grid refinement in the vicinity of the crack tip. The two cracks lengths 0.5, and 0.7 are the only crack lengths for which this pattern could be applied. As a consequence, the stress-intensity factors which are calculated can only give indications about the error or scatter.

The outer node pattern contains eleven degrees of freedom. The first attempt to calculate stress-intensity factors involves the use of eleven displacement eigenfunctions (n = 0,1,2,...,10). The resulting stress-intensity factors are shown in Figure 48. Next, a two term (n = 0,1) are four term (n = 0,1,2,3) least-squares fits are performed. The resulting stress-intensity factors are given in Figure 49 and 50 respectively. Once again, the four-term fit appears to give the best results. However, stress-intensity factors corresponding to additional crack lengths should be determined before conclusions are drawn. Table 3 give the error for each of figures.

3.6 Conclusions and Comments

The stress-intensity factors extracted from a finite-element model of Broberg's problem are in reasonable accord with the exact solution. Although the viability of the procedure for extracting dynamic stress-intensity factors has not been severely tested here because Broberg's problem involves crack propagation at constant

velocity, these constant velocity eigenfunctions do indeed adequately characterize a problem which is non-convective in nature. Obviously the potential of these constant velocity eigenfunctions for characterizing arbitrary crack motions must be investigated through a great deal of numerical experimentation.

Since the eigenfunctions adequately characterize a non-convective constant velocity crack propagation, the potential application of these functions to accelerating crack problems could be made through simulating an analysis of Tsai [5] for crack propagating at constant acceleration. In addition, an investigation should be undertaken of the nodal pattern used. A variety of patterns could be considered, until an optimum configuration is arrived at. Also, the effect of varying the number of eigenfunctions used to fit the displacement should be studied.

Should additional numerical experimentation prove successful for characterizing arbitrary crack motions, there are immediate applications for this procedure to extract dynamic stress-intensity factors. For example, a finite-element model of the DCB Test specimen could be for formed. A node releasing sequence could then be implemented which simulates the actual crack behavior in the DCB specimen. Finally, stress-intensity factors could be determined through the use of a procedure which is similar to that used for Broberg's problem.

APPENDICES

APPENDIX A

STATIC DCB SOLUTION

The static solution for the DCB model is produced by considering the total model to be composed of two sections, a cantilever beam section, and beam-on-elastic foundation section. Figure 24 shows the configuration for which the static solution is sought.

Clearly, the conditions which must be met at the interface of the two sections are

$$\begin{aligned} w_1(0) &= w_2(0) \\ \psi_1(0) &= \psi_2(0) \\ M_1(0^-) &= M_2(0^+) + M \\ V_1(0^-) &= V_2(0^+) + Q \end{aligned} \tag{A.1}$$

where the subscripts 1 and 2 refer to the respective section of the model.

Within section 2, the unsupported beam, the governing equations are

$$\begin{aligned} M &= - EI\ \psi_{,X} \\ V &= k\ GA(w_{,X} - \psi) \qquad (-a \leq X < 0) \\ V_{,X} &= 0 \\ V &= M_{,X} \end{aligned} \tag{A.2}$$

Incorporating the boundary conditions at X = -a. That is

$$M(-a) = 0, \qquad V(-a) = P \tag{A.3}$$

The dimensionless form of the solution can be expressed as

$$\begin{aligned}
\bar{M}_1 &= 4\,\bar{P}\,(\xi + \bar{a}) \\
\bar{V}_1 &= \bar{P} \qquad\qquad\qquad\qquad -\bar{a} \le \xi < 0 \\
\bar{\psi}_1 &= -2\bar{P}\,\xi^2 - 4\bar{P}\,\bar{a}\,\xi - \bar{P} + \gamma_1 \\
\bar{w}_1 &= -2/3\,\bar{P}\,\xi^3 - 2\,\bar{P}\,\bar{a}\,\xi^2 + \gamma_1\,\xi + \gamma_2
\end{aligned} \tag{A.4}$$

where $\bar{\gamma}_1$ and $\bar{\gamma}_2$ are as yet undetermined constants. The dimensionless form of all quantities are given explicitly by equations (8) in the text.

Within section 2, the beam-on-elastic foundation section of the model, the governing equations are

$$\begin{aligned}
M &= -EI\,\psi_{,X} \\
V &= kGA(w_{,X} - \psi) \\
0 &= V_{,X} - k_e\,w \\
0 &= V - M_{,X} - k_r\,\psi
\end{aligned} \tag{A.5}$$

A convenient dimensionless form of the solution for a semi-infinite model can be written as

$$\bar{\psi}_2 = e^{p\xi}[\gamma_3 \sin(q\xi) + \gamma_4 \cos(q\xi)] + e^{-p\xi}[\gamma_5 \sin(q\xi) + \gamma_6 \cos(q\xi)] \tag{A.6}$$

and similar expression for $\bar{W}_2$, $\bar{M}_2$ and $\bar{V}_2$. γ_3, γ_4, γ_5 and γ_6 are as yet undetermined constants. The constants p and q are related to the elastic foundation stiffnesses, and the shear deflection coefficient. That is, $p = 1$ and $q = \sqrt{5}$ for the values of the elastic foundation and shear deflection coefficient used in the text. The appropriate boundary conditions for the semi-infinite model are

$$w_2(X) \to 0 \quad \text{and} \quad \psi_2(X) \to 0 \quad \text{as} \quad X \to \infty .$$

A convenient dimensionless form of the solution for a finite model can be written as

$$\bar{\psi}_2 = \gamma_3 \sin(q\xi) \sinh(p\xi) + \gamma_4 \cos(q\xi) \sinh(p\xi)$$

$$+ \gamma_5 \sin(q\xi) \cosh(p\xi) + \gamma_6 \cos(q\xi) \cosh(p\xi) \qquad (A.7)$$

and similar expression for $\bar{W}_2$, $\bar{M}_2$, and $\bar{V}_2$ where again γ_3, γ_4, γ_5, and γ_6 and as yet undetermined constants, and $p = 1$, $q = \sqrt{5}$ as discussed previously.

The appropriate boundary conditions for the finite model are

$$M_2(L) = 0 \quad \text{and} \quad V_2(L) = 0 \quad \text{at} \quad X = L \qquad (A.8)$$

Clearly, the problem now reduces to determining the six constants γ_1 through γ_6 from the four conditions which must be met at the interface, and the two boundary condition at $X = L$ or as $X \to \infty$.

APPENDIX B

SOLUTION PROCEDURE FOR A TYPICAL ELEMENT IN THE NETWORK OF CHARACTERISTIC CURVES

A typical element in the network of characteristic curves is shown in Figure 6. All six quantities of concern ($\bar{w}$, $\bar{\psi}$, $\bar{M}$, $\bar{V}$, $\bar{v}$, $\bar{\Omega}$) are known at points 2, 3, and 4. Linear interpolation may then be used to determine these six quantities at points 5 and 6. Clearly,

$$F(5) = F(4) + \frac{2\alpha}{1+\alpha}\,[F(2) - F(4)]$$
$$F(6) = F(4) + \frac{2\alpha}{1+\alpha}\,[F(3) - F(4)] \qquad \text{(B.1)}$$

Integration is then performed along each of the four characteristic curves, I $\pm$, II $\pm$.

Along I +:

$$\bar{M}(1) - \bar{M}(2) + \bar{\Omega}(1) - \bar{\Omega}(2) = \int_2^1 (4\bar{V} - 2\bar{K}_r\bar{\psi})d\tau = a_1 \qquad \text{(B.2)}$$

Along I -:

$$-\bar{M}(1) + \bar{M}(3) + \bar{\Omega}(1) - \bar{\Omega}(3) = \int_3^1 (4\bar{V} - 2\bar{K}_r\bar{\psi})d\tau = a_2 \qquad \text{(B.3)}$$

Along II +:

$$\frac{1}{3\alpha}(\bar{V}(1) - \bar{V}(5)) - (\bar{v}(1) - \bar{v}(5)) = \int_5^1 (2\bar{K}_e\bar{w} - \alpha\bar{\Omega})d\tau = a_3 \qquad \text{(B.4)}$$

Along II -:

$$-\frac{1}{3\alpha}(\bar{V}(1)-\bar{V}(6))-(\bar{v}(1)-\bar{v}(6))=\int_6^1(2\bar{K}_e\bar{w}+\alpha\bar{\Omega})d\tau=a_4 \qquad (B.5)$$

which $\bar{K}_e=\bar{K}_r=\begin{cases}1 & \text{integrating in an elastic foundation region}\\ 0 & \text{integrating out of the elastic foundation region}\end{cases}$

and where $\alpha=\frac{1}{\sqrt{3}}$, the inverse slope of II + lines.

Integration is also performed along the direction

$$\frac{d\xi}{d\tau}=0$$

such that

$$\bar{\psi}(1)-\bar{\psi}(4)=\int_4^1\bar{\Omega}\,d\tau=a_5 \qquad (B.6)$$

$$\bar{w}(1)-\bar{w}(4)=\int_4^1\bar{v}\,d\tau=a_6 \qquad (B.7)$$

The integrations shown in the above six equations are performed by Trapezoid rule.

Thus, the integration constants a_1 - a_6 become

$$\begin{aligned}a_1&=[4(\bar{V}(1)+\bar{V}(2))-2\bar{K}_e(\bar{\psi}(1)+\bar{\psi}(2))]\frac{\Delta\tau}{2}\\ a_2&=[4(\bar{V}(1)+\bar{V}(3))-2\bar{K}_e(\bar{\psi}(1)+\bar{\psi}(3))]\frac{\Delta\tau}{2}\end{aligned} \qquad (B.8)$$

$$a_3 = [2\bar{K}_e(\bar{w}(1) + \bar{w}(5)) - \alpha(\bar{\Omega}(1) + \bar{\Omega}(5))] \frac{\Delta\tau}{1+\alpha}$$

$$a_4 = [2\bar{K}_e(\bar{w}(1) + \bar{w}(6)) + \alpha(\bar{\Omega}(1) + \bar{\Omega}(6))] \frac{\Delta\tau}{1+\alpha} \qquad (B.8)$$

$$a_5 = (\bar{\Omega}(1) + \bar{\Omega}(4))\ \Delta\tau$$

$$a_6 = (\bar{v}(1) + \bar{v}(4))\ \Delta\tau$$

A slight rearranging of the equations is undertaken to enable the use of an iterative solution technique. Combining equations (B.2) and (B.3)

$$\bar{\Omega}(1) = \tfrac{1}{2}[a_1 + a_2 + \bar{M}(2) - \bar{M}(3) + \bar{\Omega}(2) + \bar{\Omega}(3)] \qquad (B.9)$$

Combining equation (B.4) and (B.5)

$$\bar{v}(1) = \tfrac{1}{2}\left[\frac{1}{3\alpha}(\bar{V}(6) - \bar{V}(5)) + \bar{v}(5) + \bar{v}(6) - a_3 - a_4\right] \qquad (B.10)$$

Regarding $\bar{\Omega}(1)$ and $\bar{v}(1)$ as having been solved for in equations (B.9) and (B.10), equation (B.2) is rewritten as

$$\bar{M}(1) = a_1 - \bar{\Omega}(1) + \bar{M}(2) + \bar{\Omega}(2) \qquad (B.11)$$

Equation (B.4) is rewritten as

$$\bar{V}(1) = \bar{V}(5) + 3\alpha(a_3 + \bar{v}(1) - \bar{v}(5)) \qquad (B.12)$$

Equations (B.6) and (B.7) then are written as

$$\bar{\psi}(1) = \bar{\psi}(4) + a_5 \qquad (B.13)$$

$$\bar{w}(1) = \bar{w}(4) + a_6 \qquad (B.14)$$

To employ an iterative technique, initially all six quantities of concern at point 1 are assumed to be equal to their values at point 4. i.e.

$$\begin{aligned} \bar{w}(1) &= \bar{w}(4) \\ \bar{\psi}(1) &= \bar{\psi}(4) \\ &\vdots \\ \bar{\Omega}(1) &= \bar{\Omega}(4) \end{aligned} \tag{B.15}$$

The constant a_1 - a_6 are then evaluated. The quantities at point 1 are then calculated through the use of equation (B.9) to (B.14). The calculated values for point 1 are then compared to the assumed values. If the difference between the assumed and calculated quantities at point 1 is less than a specified tolerance (usually 10^{-6}), the iteration ceases. If the tolerance is exceeded by the difference in the assumed and calculated value of any one or more quantities, the iteration continues. That is, the calculated values become the new assumed values, the constants a_1 - a_6 are updated, and new values are calculated at point 1. The process repeats itself until all calculated values satisfy the specified tolerance.

APPENDIX C

GOVERNING EQUATIONS FOR BOUNDARY ELEMENTS

Four types of boundary elements are used in the analysis. The solution procedure is identical to the discussion in the preceeding appendix except that the equations used in the interative solution process are as follows:

1) Dead-Load Boundary Element

$$\begin{aligned}
\bar{V}(1) &= \bar{P} \\
\bar{M}(1) &= 0 \\
\bar{w}(1) &= \bar{w}(4) + a_6 \\
\bar{\Psi}(1) &= \bar{\Psi}(4) + a_5 \\
\bar{\Omega}(1) &= \bar{\Omega}(3) - \bar{M}(3) + a_2 \\
\bar{v}(1) &= \bar{v}(6) - a_4 - \frac{1}{3\alpha}\left(\bar{P} - \bar{V}(6)\right)
\end{aligned} \tag{C.1}$$

2) Constant End-Deflection-Rate Boundary Element

$$\begin{aligned}
\bar{v}(1) &= \bar{v}_e \\
\bar{M}(1) &= 0 \\
\bar{w}(1) &= \bar{w}(4) + a_6 \\
\bar{\Psi}(1) &= \Psi(4) + a_5
\end{aligned} \tag{C.2}$$

$$\bar{\Omega}(1) = \bar{\Omega}(3) - \bar{M}(3) + a_2$$

$$\bar{V}(1) = \bar{V}(6) + 3\alpha(a_4 + \bar{v}_e - \bar{v}(6))$$

3) Fixed-Grips Boundary Element

$$\begin{aligned} \bar{w}(1) &= \bar{\delta} \\ \bar{m}(1) &= 0 \\ \bar{v}(1) &= 0 \\ \bar{\Psi}(1) &= \bar{\Psi}(4) + a_5 \\ \bar{\Omega}(1) &= \bar{\Omega}(3) - \bar{M}(3) + a_2 \\ \bar{V}(1) &= \bar{V}(6) - 3\alpha(a_4 - \bar{v}(6)) \end{aligned} \qquad (C.3)$$

4) Free-End Boundary Element

$$\begin{aligned} \bar{V}(1) &= 0 \\ \bar{M}(1) &= 0 \\ \bar{w}(1) &= \bar{w}(4) + a_6 \\ \bar{\Psi}(1) &= \bar{\Psi}(4) + a_5 \\ \bar{\Omega}(1) &= \bar{\Omega}(2) + \bar{M}(2) + a_1 \\ \bar{v}(1) &= \bar{v}(5) - a_3 - \frac{1}{3\alpha}\bar{V}(5) \end{aligned} \qquad (C.4)$$

where a_1 through a_6 are the integrals given in the previous appendix.

APPENDIX D

FIXED-GRIPS END-DISPLACEMENTS AND THEIR CORRESPONDING APPLIED LOADS

The equilibrium equations for the semi-infinite DCB model as given in Appendix A may be solved to yield

$$\bar{w}(0) = -\ \tfrac{1}{2}\,(\sqrt{5}/2 + \bar{a})\ \bar{P}$$

$$\bar{\psi}(0) = (\sqrt{5}\ \bar{a} + 1/2)\ \bar{P} \qquad \text{(D.1)}$$

$$\bar{\delta} = \bar{w}(-\bar{a}) = -\ [4/3\ \bar{a}^3 + \sqrt{5}\ \bar{a}^2 + 2\bar{a} + \sqrt{5}/4]\ \bar{P}$$

where the applied pinching force and restoring moment at the crack tip are assumed to be zero.

The first two equations may now be substituted into the crack extension criterion

$$\bar{U}^* = \bar{w}^2(0) + 1/12\ \bar{\psi}^2(0) \qquad \text{(D.2)}$$

Thus

$$\bar{U}^* = (1/3)(1 + \sqrt{5}\ \bar{a} + 2\bar{a}^2)\ \bar{P}^2 \qquad \text{(D.3)}$$

This relation may now be expressed in terms of the boundary displacement, $\bar{\delta}$, through use of the third equation. Thus

$$\bar{U}^* = \frac{(+1/3)(1 + \sqrt{5}\ \bar{a} + 2\bar{a}^2)}{[4/3\ \bar{a}^3 + \sqrt{5}\ \bar{a}^2 + 2\bar{a} + \sqrt{5}/4]^2}\ \bar{\delta}^2\ . \qquad \text{(D.4)}$$

Assuming $\bar{a} = 1.45$ as given in Table 1, the following values result.

$\bar{U}^*$	$\bar{P}$	$\bar{\delta}$
1.0	0.5959	- 7.285
2.0	0.8428	- 10.30
3.0	1.1919	- 14.57
4.0	1.4598	- 17.85

For the analysis of Bilek and Burns problem

$$\bar{a} = 0.10$$

Thus

$\bar{U}^*$	$\bar{P}$
1.0	1.5532

APPENDIX E

VALUES OF FORCE AND MOMENT APPLIED AT THE CRACK TIP OF THE DCB MODEL

The values of force and moment applied at the crack tip are determined so that the prescribed deflections are identical to those calculated in Appendix D, but $\bar{U}^* = 1$ at the crack tip for all of these deflections. This is accomplished by forcing $\bar{w}(0)$ and $\bar{\psi}(0)$ to take on the identical values they naturally attain when the force and moment are not imposed and $\bar{U}^* = 1$ at the crack tip.

The problem then reduces to solving the simpler problems. Figure 25 shows the situation being discussed. Problem (a) is solved in the preceding appendix. The unknown force and moment to be applied at the crack tip are simply the reactions at the wall in problem (b) that is

$$\bar{Q}_T = \frac{3}{4\bar{a}^3 + 3a}\ \bar{\delta}_b$$

$$\bar{M}_T = \frac{12}{4\bar{a}^2 + 3}\ \bar{\delta}_b \qquad \text{(E.1)}$$

$\bar{\delta}_b$ is known, as $\bar{\delta}$ and $\bar{\delta}_a$ are given.

$\bar{\delta}$	$\bar{\delta}_b$	$\bar{Q}_T$	$\bar{M}_T$
- 7.285	0	0	0
- 10.30	- 3.018	0.5472	3.1742
- 14.57	- 7.285	1.321	7.662
- 17.85	- 10.56	1.915	11.11

The selection of values for the applied force and moment at the crack tip used in the analysis conducted at the Battelle Laboratories differ from those involved in this analysis. The Battelle analysis selects the force and moment such that the critical crack extension criteria is met ($\bar{U}^* = 1$ at the crack tip) and "the strain energy of the system is initially a minimum" [22]. The meaning of this statement, or the physical principle involved are not obvious to the author. As all equilibrium configurations produce a minimum in the strain energy functional, the logic behind minimizing the strain energy with respect to the force and moment is not at all clear.

APPENDIX F

SYSTEM ENERGY AND WORK CALCULATIONS

For each problem considered in the DCB analysis, an energy balance equation can be written as

$$E_T = U_o = U + T + A_b - W \qquad (F.1)$$

E_T	Total System Energy
U_o	Initial Strain Energy
U	Strain Energy
T	Kinetic Energy
A_b	Energy Absorbed due to crack extension
W	Work done by external forces

For Kanninen's DCB model the strain energy, kinetic energy, and energy absorbed due to crack extension can be expressed as

$$U = \int_X \left(\frac{M^2}{EI} + \frac{v^2}{kGA} + k_e w^2 + k_r \psi^2 \right) dx$$

$$T = \int_X (\rho A \dot{w}^2 + \rho I \dot{\Psi}^2) dx \,, \qquad A_b = Rb\ \Delta a$$

where the elastic foundation stiffness is taken to be zero for the integration performed over the unsupported section of the beam.

Introducing the dimensionless variables as defined in the text, and replacing the integration with a summation, the resulting equations are

$$\bar{U} = \frac{U}{Rbh} = \sum_j \left(\frac{\bar{M}_j^2}{24} + \frac{\bar{V}_j^2}{6} + \bar{K}_e \bar{w}_j^2 + \bar{K}_r \frac{\bar{\Psi}_j^2}{2} \right) \Delta\tau$$

$$\bar{T} = \frac{T}{Rbh} = \sum_j \left(\frac{\bar{v}_j^2}{2} + \frac{\bar{\Omega}_j^2}{24} \right) \Delta\tau \qquad \text{(F.3)}$$

$$\bar{A}_b = \frac{A_b}{Rbh} = \sum_j \Delta\bar{a}$$

where j is summed over the number of nodes occurring in the network of characteristic curves at a τ = constant line.

In addition, the calculation of work done by the external load at the boundary of the DCB arm is easily accomplished. Writing the expression for work as

$$W = \int_t \underset{\sim}{F} \cdot \underset{\sim}{v} \, dt \qquad \text{(F.4)}$$

Three cases occur

1) Dead-Load presumes F = P, where P is constant.

Therefore

$$W = 2P \int_X v \, dt \qquad \text{(F.5)}$$

The factor of two appears because both halves of the model are included.

In dimensionless form

$$\bar{W} = \frac{W}{Rbh} = \frac{\bar{P}}{3} \sum_{\ell} \Delta \bar{w}_{\ell} \qquad (F.6)$$

where the summation is performed along the boundary $\xi = 0$.

2) Constant End-Deflection Rate

Presumes $v = v_e$, where v_e is constant.

Thus

$$W = 2v_e \int_t V \, dt \qquad (F.7)$$

That is

$$\bar{W} = \frac{W}{Rbh} = \frac{2}{3} \bar{v}_e \sum_{\ell} \bar{V}_{\ell} \Delta\tau \quad . \qquad (F.8)$$

3) Fixed-Grips conditions presumes $w = \delta$ or $v = 0$

$$W \equiv 0 \qquad (F.9)$$

APPENDIX G

DIMENSIONLESS VELOCITIES FOR THE CONSTANT END-DEFLECTION-RATE DCB PROBLEMS

The dimensionless velocity is given in equation (2.8) as

$$\bar{v} = \left(\frac{2\rho h}{R}\right)^{1/2} v \tag{G.1}$$

Typical values for velocity, density and stress-intensity factor are found in [16].

$$\begin{aligned} \rho &= .00874 \text{ slug/in}^3 \\ v_e &= 51.5 \text{ in/sec.} \\ K_q &= 16.52 \text{ ksi}\sqrt{\text{in}} \end{aligned} \tag{G.2}$$

Using the relation

$$G_q = K_q^2/E \tag{G.3}$$

Then

$$G_q = R = 8.538 \text{ in.lb./in}^2 \tag{G.4}$$

yielding

$$\bar{v} = 1.06 \tag{G.5}$$

A second value of $\bar{v}$, $\bar{v} = 2.12$, is also used in the analysis to ascertain the sensitivity of the crack behavior to the input dimensionless velocity.

APPENDIX H

THE EQUIVALENCE OF $\bar{U}^*$ AND G_q/R

By definition the static strain energy release rate, is given by

$$G_q = \frac{\partial U}{\partial A} \tag{H.1}$$

where U is the strain energy and A is the area produced by crack extension. For the DCB specimen subject to a shear load, P, imposed upon the ends of the specimen arm, the strain energy may be written as

$$U = \frac{1}{2} P \delta \tag{H.2}$$

where δ is the end-deflection of the specimen arm. In terms of the dimensionless quantities (2.8), this expression becomes

$$U = Rbh(1/12\ \bar{P}\ \bar{\delta}) \tag{H.3}$$

Now regard δ or $\bar{\delta}$ to be prescribed, that is assuming fixed-displacement conditions, and using equation (D.1) of Appendix D to eliminate $\bar{P}$, the strain energy becomes

$$\bar{U} = Rbh(-1/12)\ \frac{\bar{\delta}^2}{(4/3\bar{a}^3 + \sqrt{5}\bar{a}^2 + 2\bar{a} + \sqrt{5}/4)} \tag{H.4}$$

Thus

$$\frac{\partial U}{\partial A_c} = \frac{\partial U}{bh\partial \bar{a}} = R(+\ 1/12)\ \frac{(4\bar{a}^2 + 2\sqrt{5}\ \bar{a} + 2)}{(4/3\bar{a}^3 + \sqrt{5}\ \bar{a}^2 + 2\bar{a} + \sqrt{5}/4)^2}\ \bar{\delta}^2 \tag{H.5}$$

Thus, remembering that two beams are included in the DCB model, we obtain

$$\frac{G_q}{R} = (+\,1/3)\,\frac{2\bar{a}^{-2} + \sqrt{5}\,\bar{a} + 1}{(4/3\,\bar{a}^{3} + \sqrt{5}\,\bar{a}^{-2} + 2\bar{a} + \sqrt{5}/4)^{2}}\,\bar{\delta}^{2} \qquad \text{(H.6)}$$

which is identical to the equation for $\bar{U}^{*}$ given in Appendix B. Thus specifying values of G_q/R amounts to specifying the strain energy density in the elastic foundation at the crack tip.

APPENDIX I

EXTRACTION OF STRESS-INTENSITY FACTORS FROM FINITE ELEMENT NODAL DISPLACEMENTS

The extraction of stress-intensity factors from finite-element nodal displacements essentially involves simple matrix manipulations. Once a particular nodal pattern has been selected, the x and y displacement component may be assembled in a vector denoted by $\underset{\sim}{u}$. For example

$$\underset{\sim}{u} = \begin{Bmatrix} u_x \\ u_y \\ u_x \\ \vdots \end{Bmatrix} \tag{I.1}$$

If a node is restrained from motion in a particular direction, the identically zero component of displacement is not included in $\underset{\sim}{u}$.

For each node in the pattern we may express the displacement components as

$$u_x = \sum_{n=0}^{N} u_{x_n}$$

$$u_y = \sum_{n=0}^{N} u_{y_n} \tag{I.2}$$

where N is a preselected number of the eigenfunctions to be used to approximate the displacements, and

$$u_{x_n} = \frac{4}{3\sqrt{2\pi}} \frac{K_n}{\mu} \frac{(1 + s_2^2)}{4s_1 s_2 - (1 + s_2^2)^2} \left(\tfrac{1}{2} n + 1\right)\left[r_1^{\frac{1}{2}n} \cos\left(\tfrac{1}{2} n\ \theta_1\right)\right.$$

$$\left. - \tfrac{1}{2}\ g(n) r_2^{\frac{1}{2}n} \cos\left(\tfrac{1}{2} n\ \theta_2\right)\right] \qquad \text{(I.3)}$$

$$u_{y_n} = \frac{4}{3\sqrt{2\pi}} \frac{K_n}{\mu} \frac{(1 + s_2^2)}{4s_1 s_2 - (1 + s_2^2)^2} \left(\tfrac{1}{2} n + 1\right)\left[-s_1 r_1^{\frac{1}{2}n} \sin\left(\tfrac{1}{2} n\ \theta_1\right)\right.$$

$$\left. - \frac{g(n)}{2s_2} r_2^{\frac{1}{2}n} \sin\left(\tfrac{1}{2} n\ \theta_2\right)\right]$$

where

$$g(n) = \begin{cases} 4s_1 s_2/(1 + s_2^2) & n \text{ odd} \\ 1 + s_2^2 & n \text{ even} \end{cases}$$

For a given problem the material properties and crack speed will be known, thus s_1 and s_2 can be determined. The location (r,θ) of each node in the pattern is also known relative to the crack tip, such that (r_1,θ_1) and (r_2,θ_2) are known.

Thus we may write

$$\underset{\sim}{u} = \underset{\approx}{F}\ \underset{\sim}{K} \qquad \text{(I.4)}$$

where $\underset{\sim}{K}$ is the vector of the coefficient K_N. K_1 is the stress-intensity factor which we wish to determine.

Clearly if $\underset{\approx}{F}$ is a square matrix, that is, the number of eigenfunctions used equals the number of displacement components in the pattern, a simply matrix inversion may be applied.

$$\underset{\sim}{K} = \underset{\approx}{F}^{-1} \underset{\sim}{u} \tag{I.5}$$

For those situations in which fewer eigenfunctions are used than there are displacement components. A least-squares solution [42] is sought.

$$\underset{\sim}{K} = (\underset{\sim}{F}^{T} \underset{\sim}{F})^{-1} \underset{\sim}{F}^{T} \underset{\sim}{u} \tag{I.6}$$

APPENDIX J

TABLES

Table 1. DCB Specimen Geometry.

Battelle Specimen		DCB Model		Bilek and Burns Model	
Dimensional	Dimensionless	Dimensional	Dimensionless	Dimensional	Dimensionless
a_o = 92.4 mm (3.628 in)	$\bar{a}_o$ = 1.4551	a_o = 92.1 mm (3.625 in)	$\bar{a}_o$ = 1.45	a_o = 6.35 mm (0.25 in)	$\bar{a}_o$ = 0.10
L = 360.7 mm (14.201 in)	$\bar{L}$ = 5.6803	L = 358.8 mm 14.125 in)	$\bar{L}$ = 5.65		
h = 63.5 mm (2.5 in)		h = 63.5 mm (2.5 in)		h = 63.5 mm (2.5 in)	

$$\bar{a} = \frac{a}{h}$$

$$\bar{L} = \frac{L}{h}$$

Table 2. Comparison of DCB Crack Behavior.

q/R		(1) 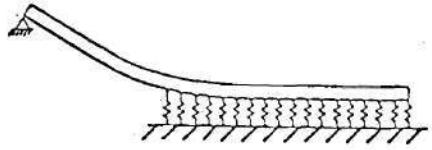	(2) 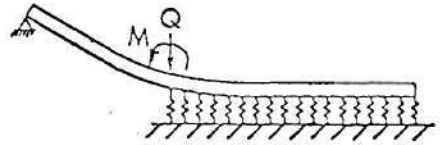	ϵ
2	c/c_o	0.087	0.125	35%
	$\bar{a}_r$	2.30	2.45	6%
4	c/c_o	0.152	0.212	33%
	$\bar{a}_r$	3.55	4.15	16%
6	c/c_o	0.191	0.254	28%
	$\bar{a}_r$	4.60	*	-

*Arrest did not occur.

$$\epsilon = \frac{(2) - (1)}{\frac{(2) + (1)}{2}} \cdot 100\%$$

Table 3. Stress-Intensity Factor Errors

Percent Difference Between Calculated Stress-Intensity Values and Broberg's Values

	COD CALCULATION		INNER NODAL PATTERN			MIDDLE NODAL PATTERN					OUTER NODAL PATTERN		
v/c_2	1st Node	2nd Node	9T	2T	4T	13T	2T	3T	4T	5T	11T	2T	4T
0.2	41	36	82	36	31	28	17	20	16	16	6	17	8
0.4	22	28	29	16	14	22	12	17	10	10	17	17	5
0.6	27	24	30	20	29	9	16	20	10	11	16	22	4
0.8	18	40	18	19	18	18	20	22	16	28	28	24	3

2T, 4T, etc. indicates the number of eigenfunctions which are used to fit the finite-element nodal displacements.

APPENDIX K

ILLUSTRATIONS

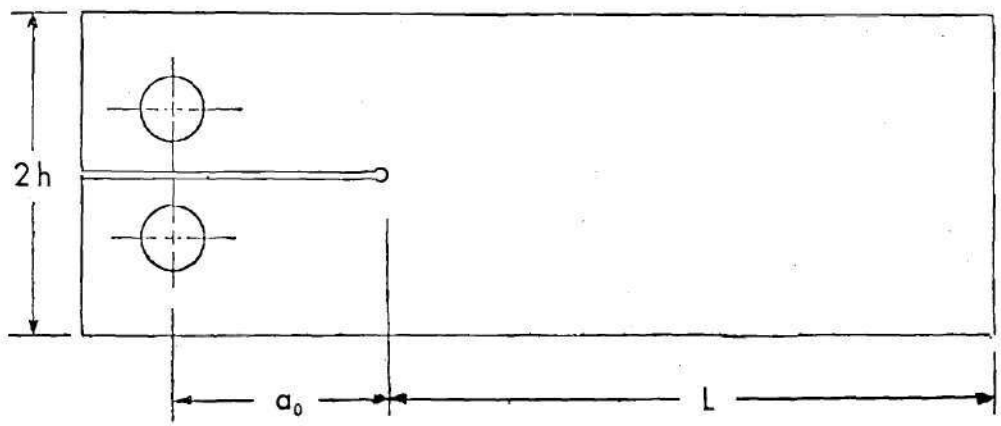

Figure 1. The DCB Test Specimen.

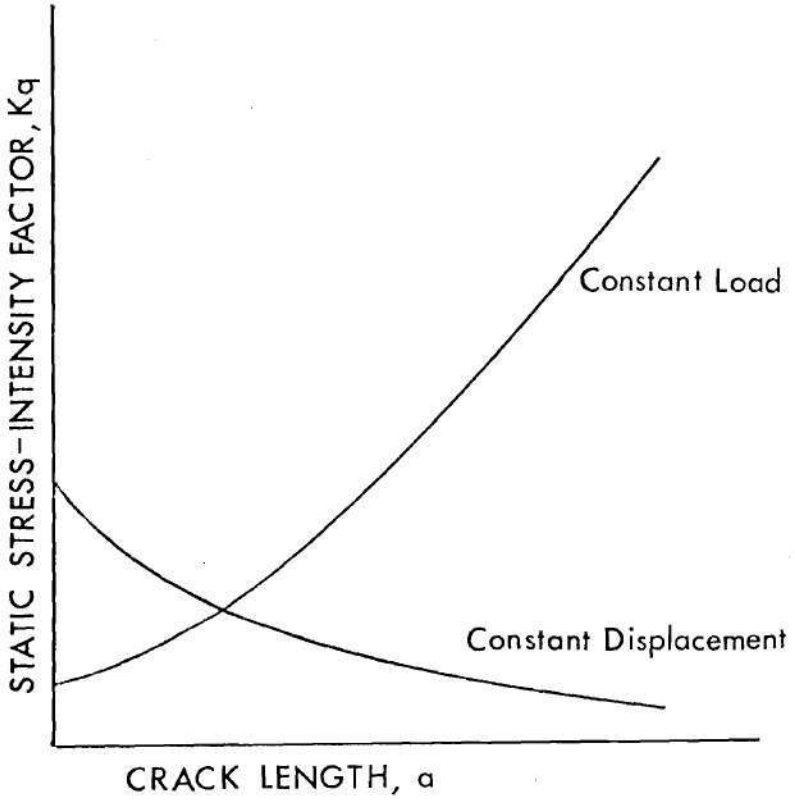

Figure 2. Static Stress-Intensity Factor as a Function of Crack Length for a DCB Specimen.

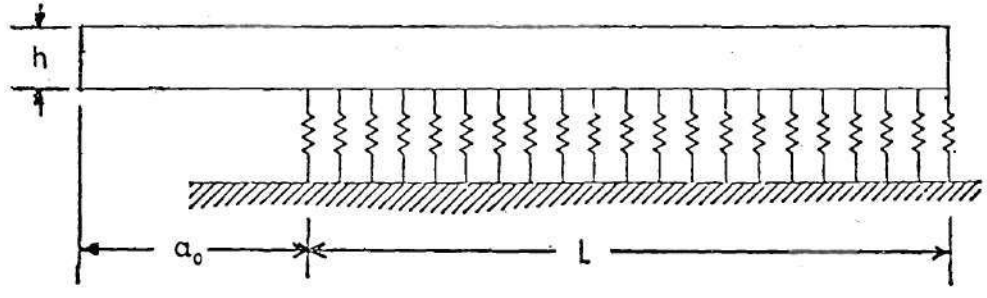

Figure 3. Kanninen's DCB Model.

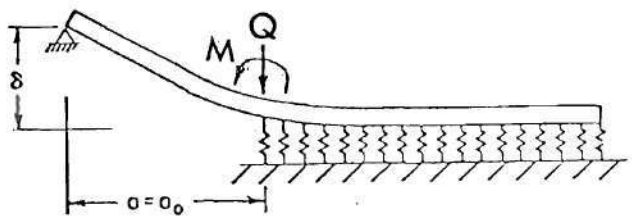

(a) Equilibrium Configuration

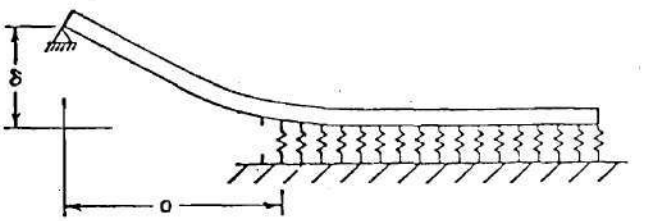

(b) Configuration Just After Initiation.

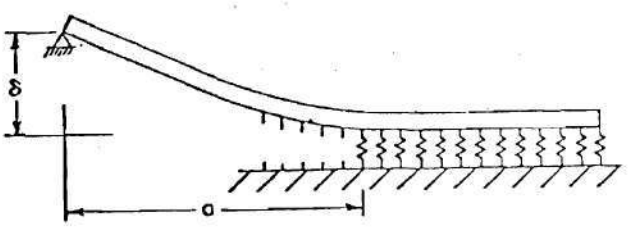

(c) Configuration at Crack Arrest.

Figure 4. Crack Propagation Sequence in the Battelle Analysis.

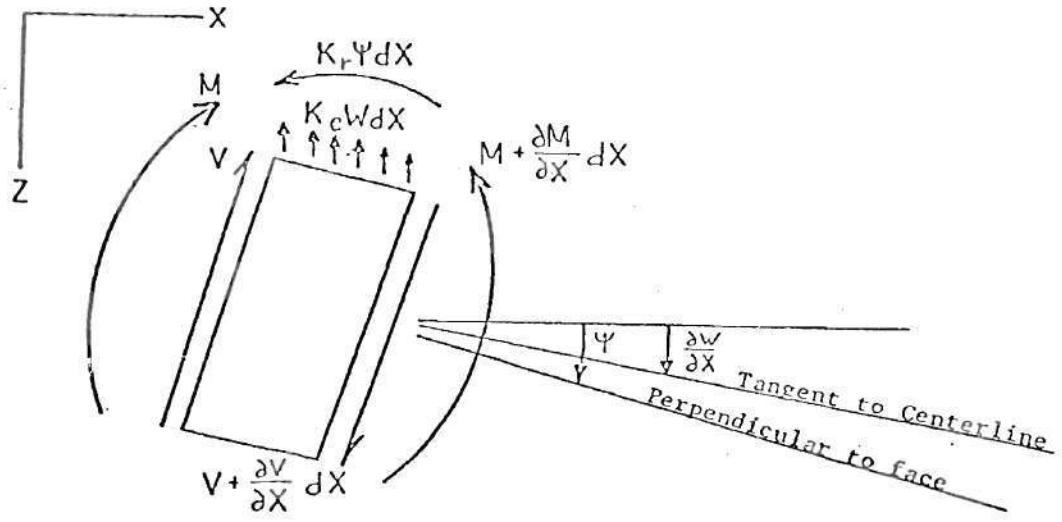

M = bending moment

V = transverse shear

w = average deflection of the cross section

Ψ = mean angle of rotation of the cross section about neutral axis

b = thickness of beam

h = height of beam

L = length of uncracked segment of beam

a_o = initial crack length

E = elastic modulus

G = shear modulus

ν = Poisson's ratio

ρ = mass density

A = cross sectional area of the beam (= bh for a rectangular cross section)

I = moment of inertia (= $bh^3/12$ for a rectangular cross section)

k_e = extensional stiffness of the foundation

k_r = rotational stiffness of the foundation

k = shear deflection coefficient of the beam

Figure 5. DCB Model Notation.

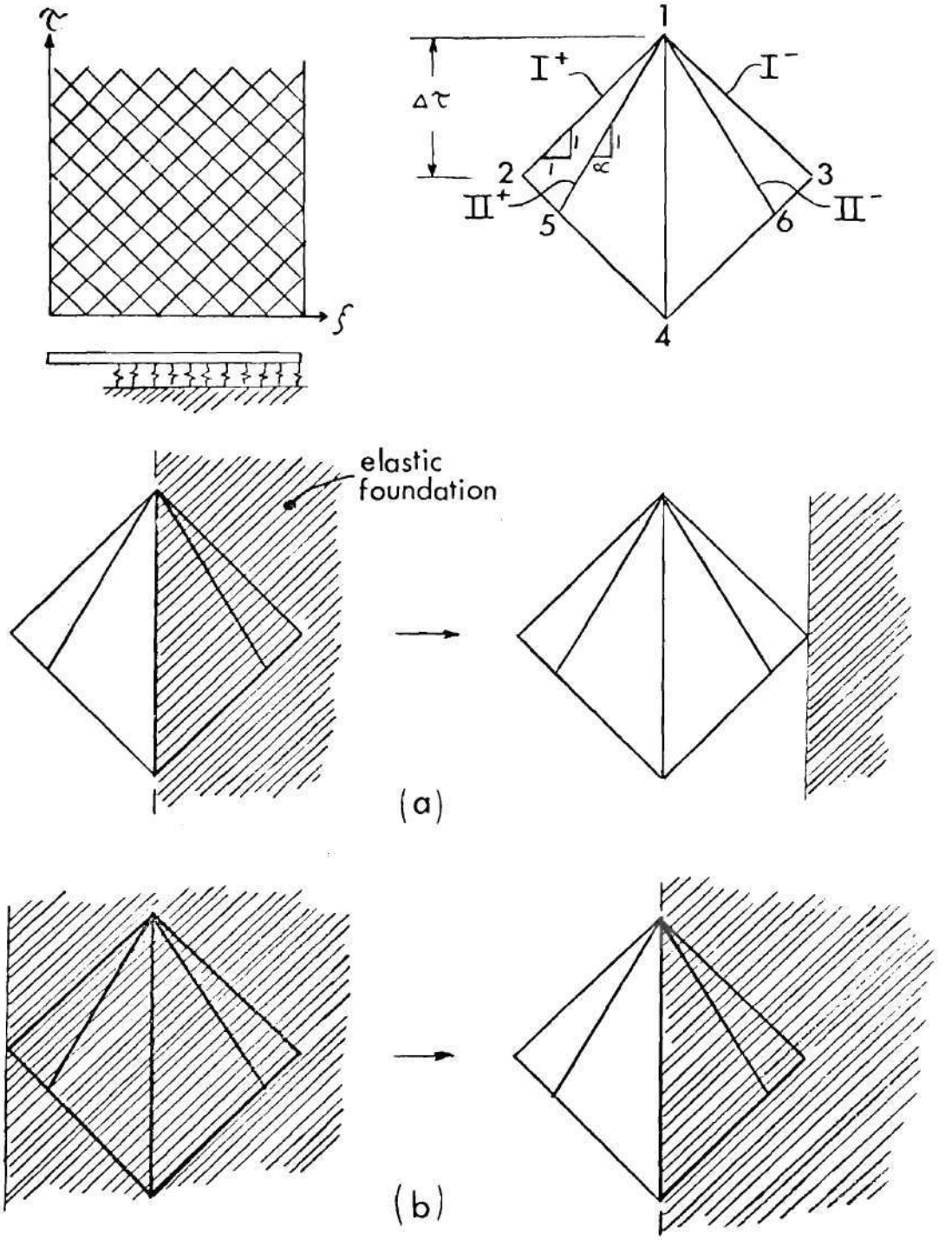

Figure 6. The Network of Characteristic Curves.

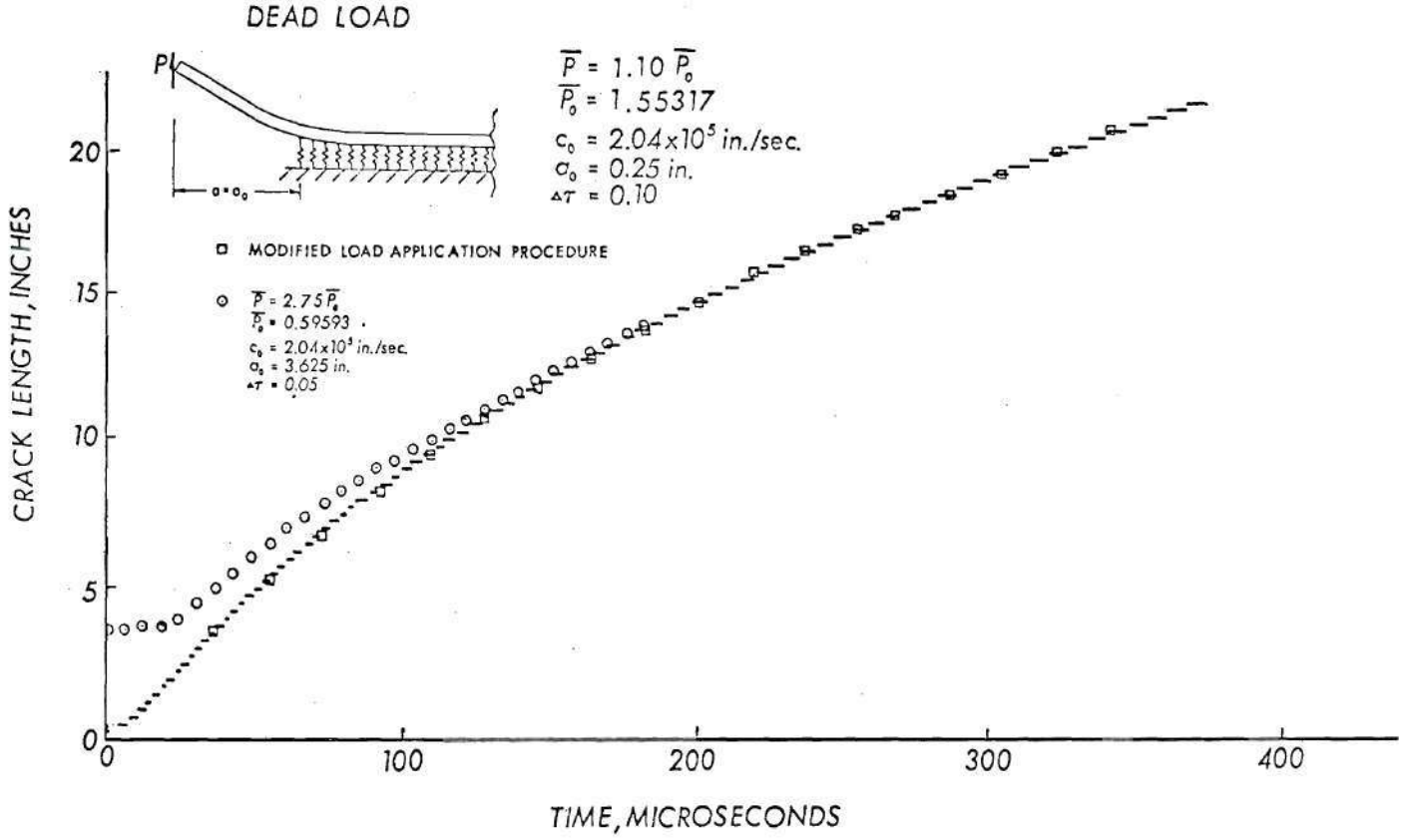

Figure 7. Semi-Infinite Model, Dead-Load.

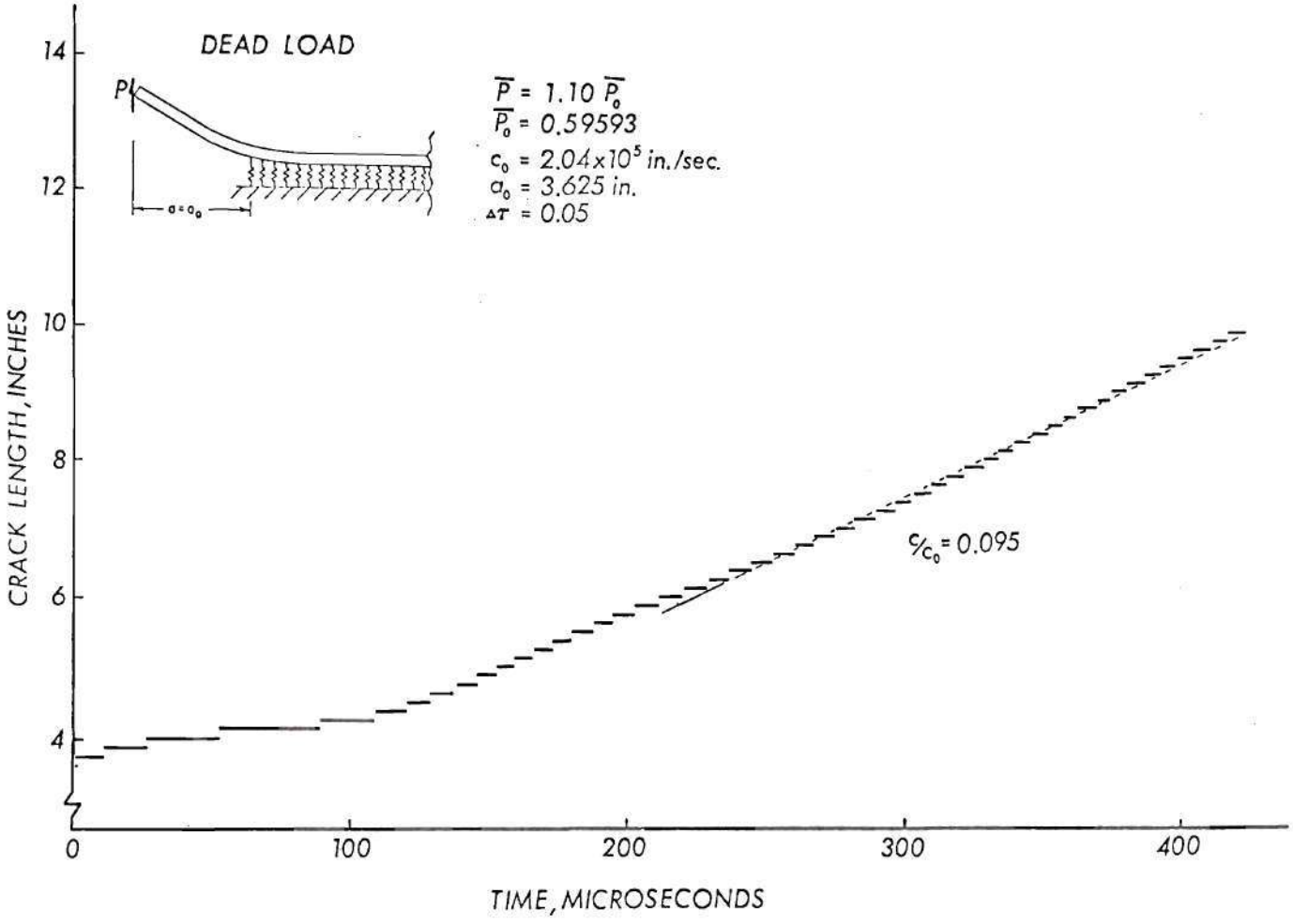

Figure 8. Semi-Infinite Model, Dead-Load, 10 percent Overload.

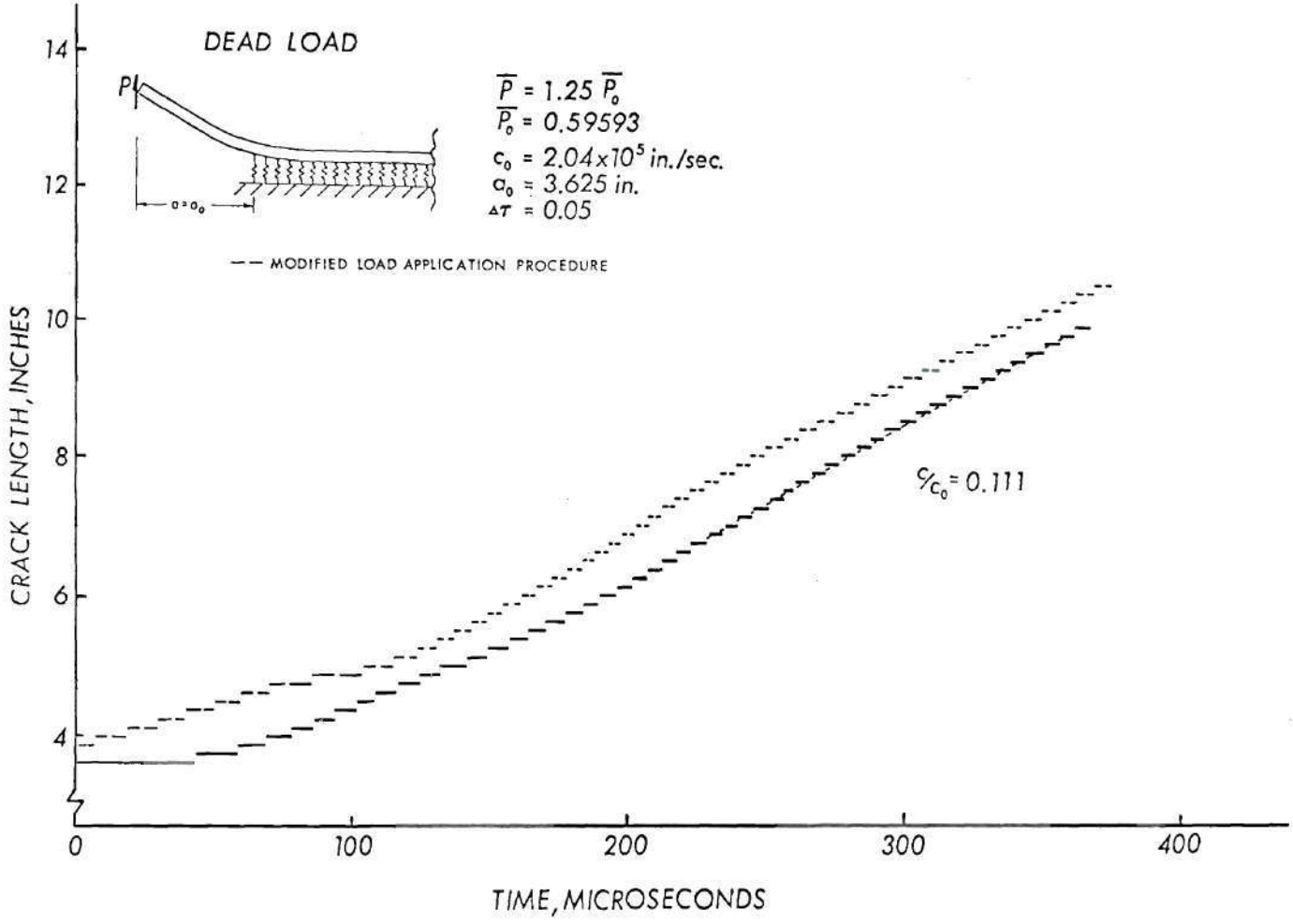

Figure 9. Semi-Infinite Model, Dead-Load, 25 percent Overland.

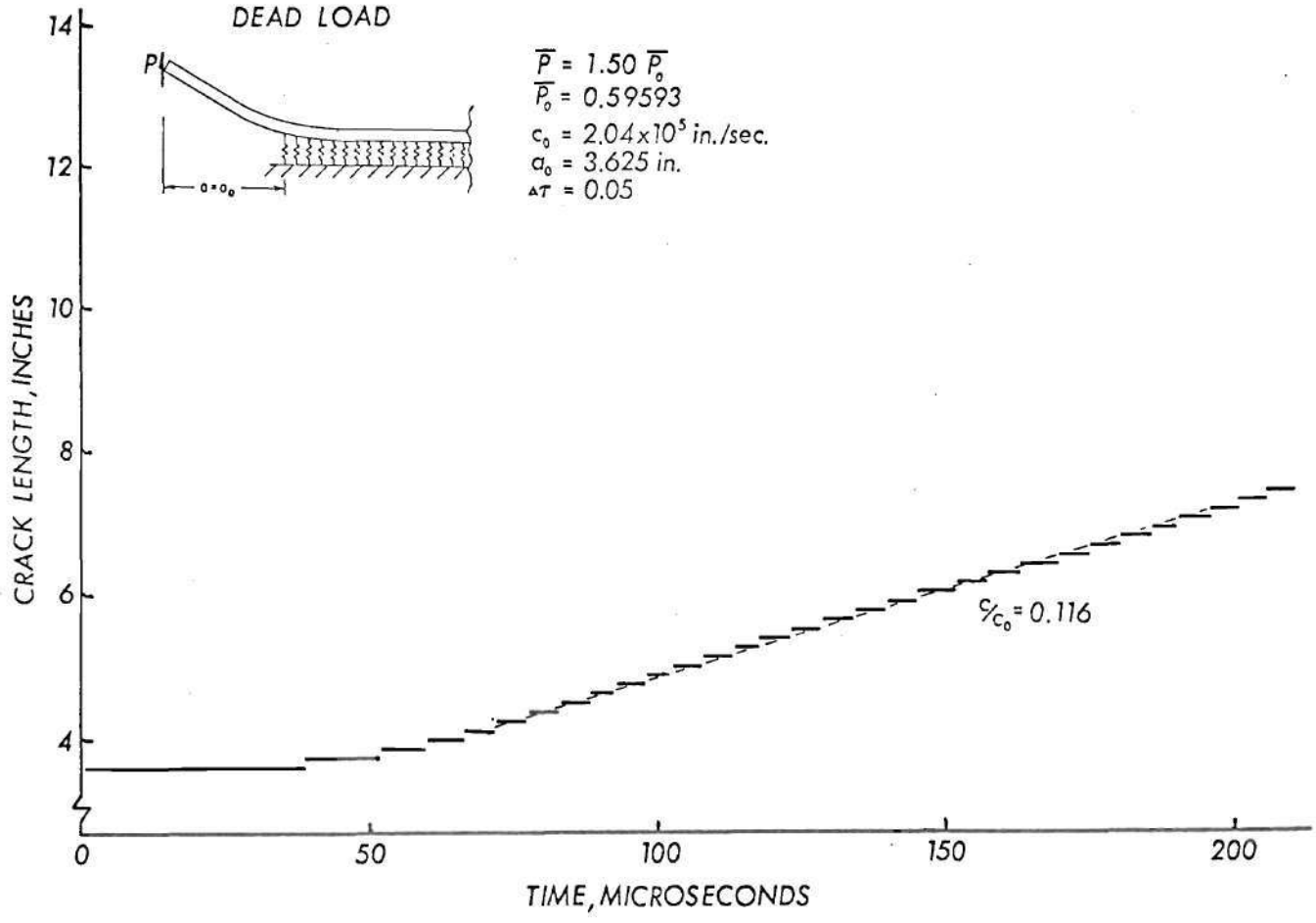

Figure 10. Semi-Infinite Model, Dead-Load, 50 percent Overload.

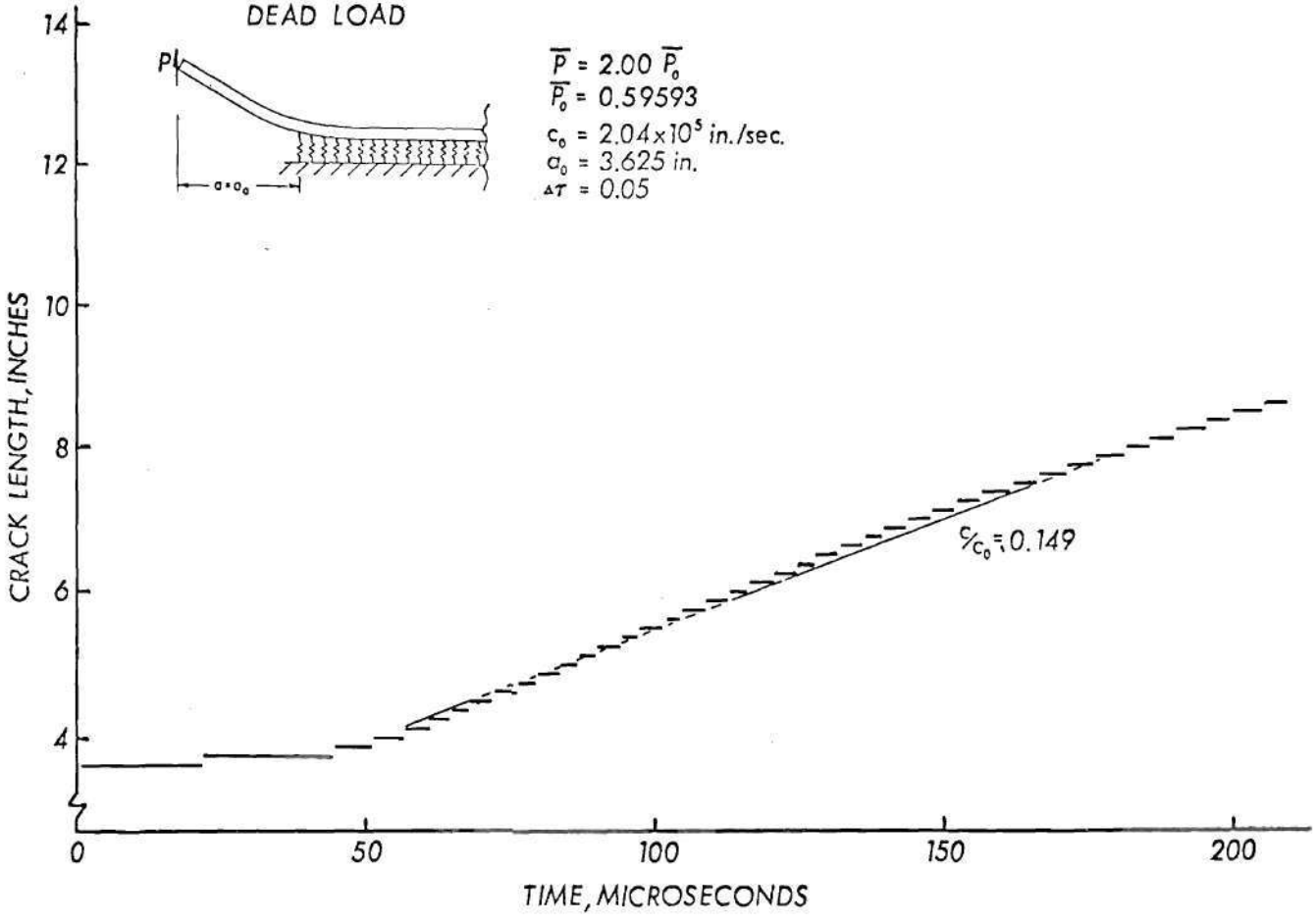

Figure 11. Semi-Infinite Model, Dead-Load, 100 percent Overload.

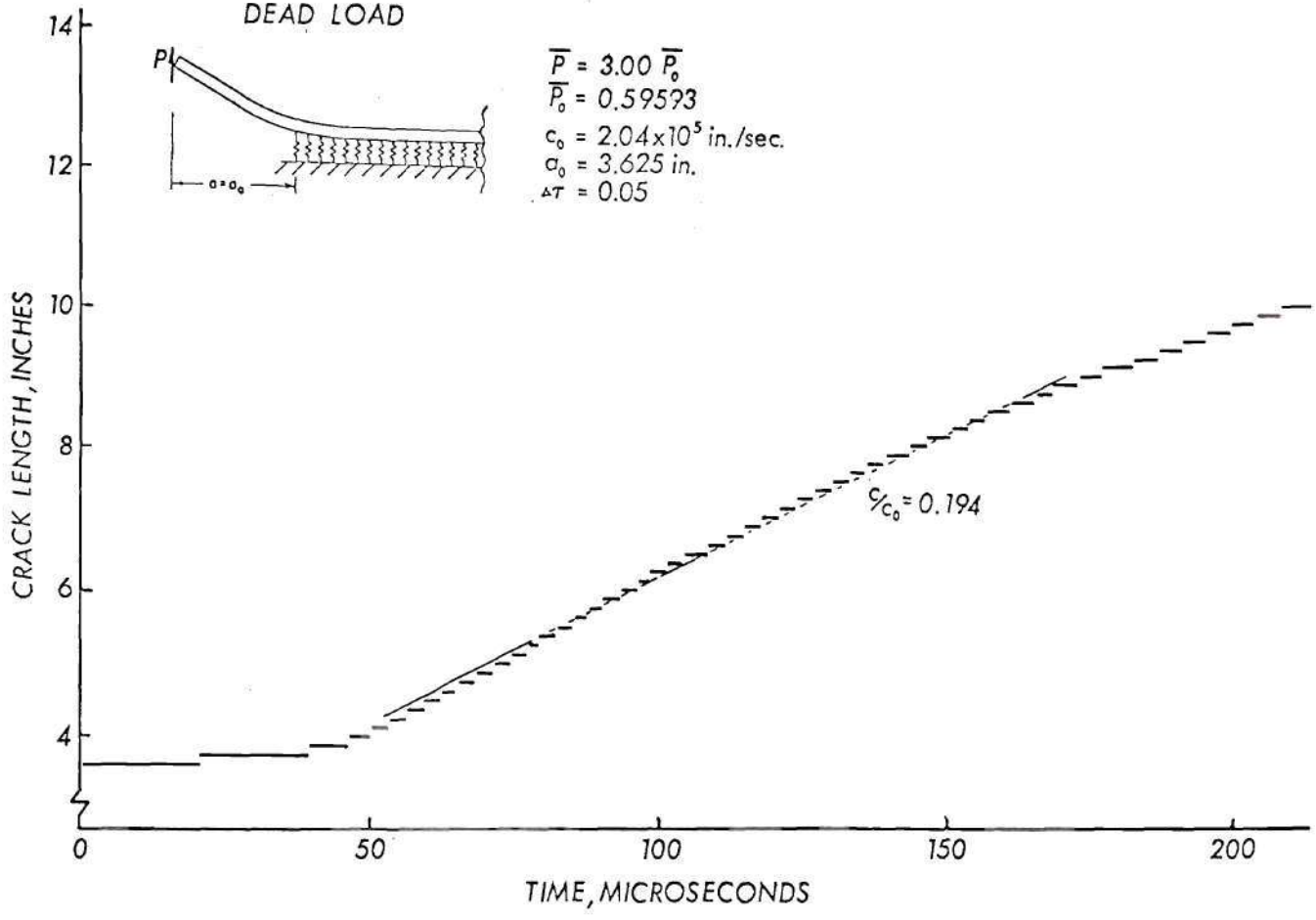

Figure 12. Semi-Infinite Model, Dead-Load, 200 percent Overload.

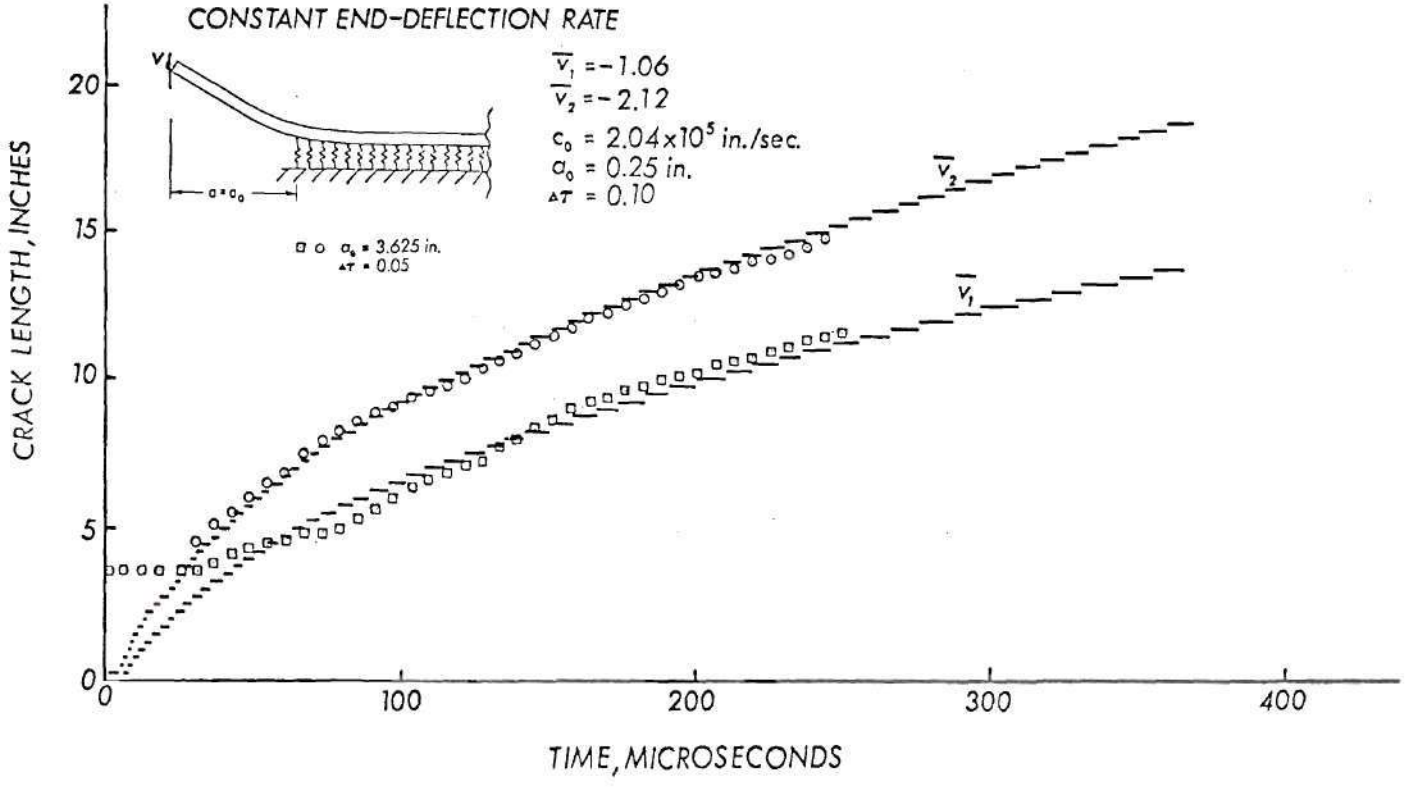

Figure 13. Semi-Infinite Model, Constant End-Deflection-Rate.

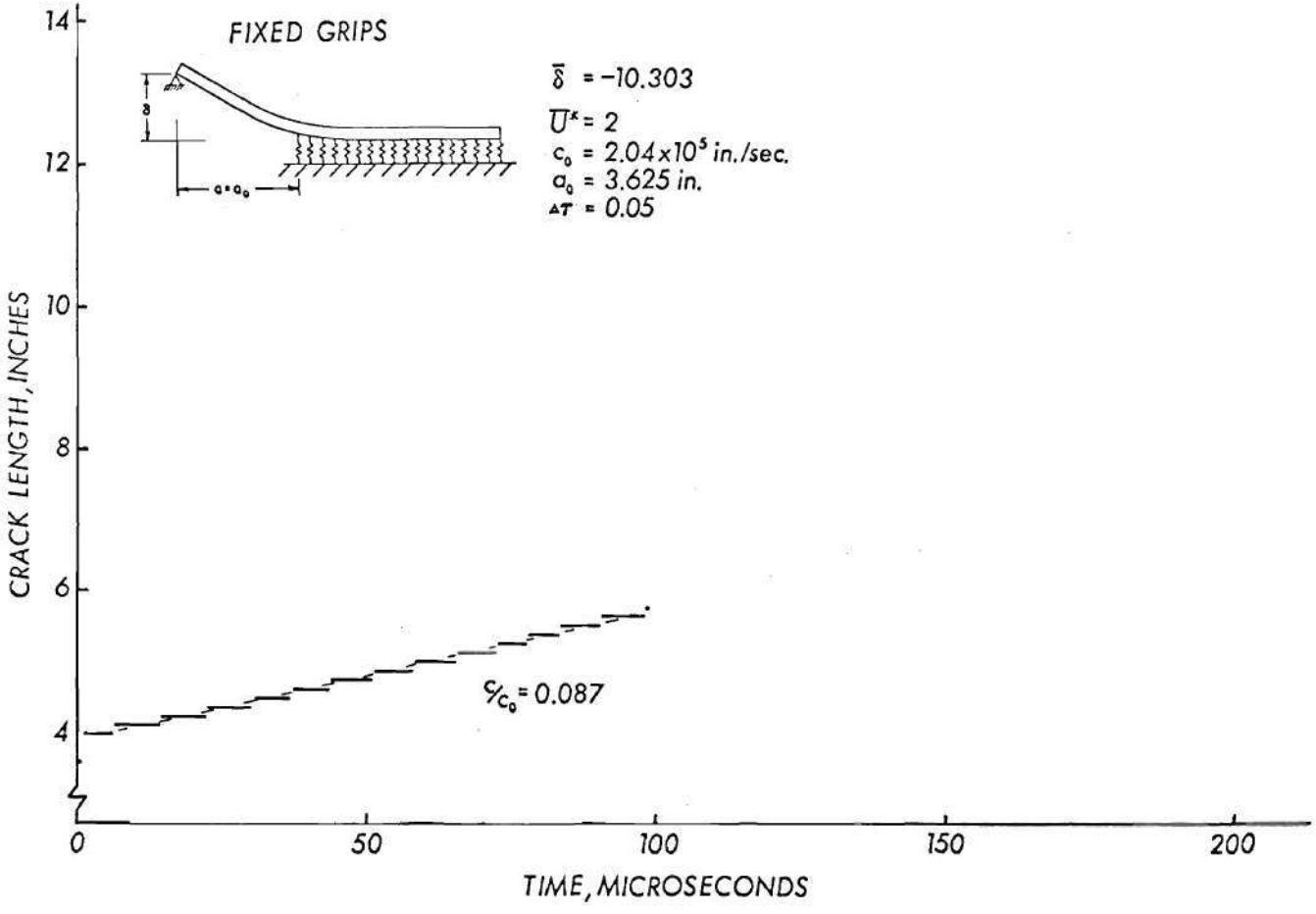

Figure 14. Finite Model, $G_q/R = 2$, Overstretch Foundation.

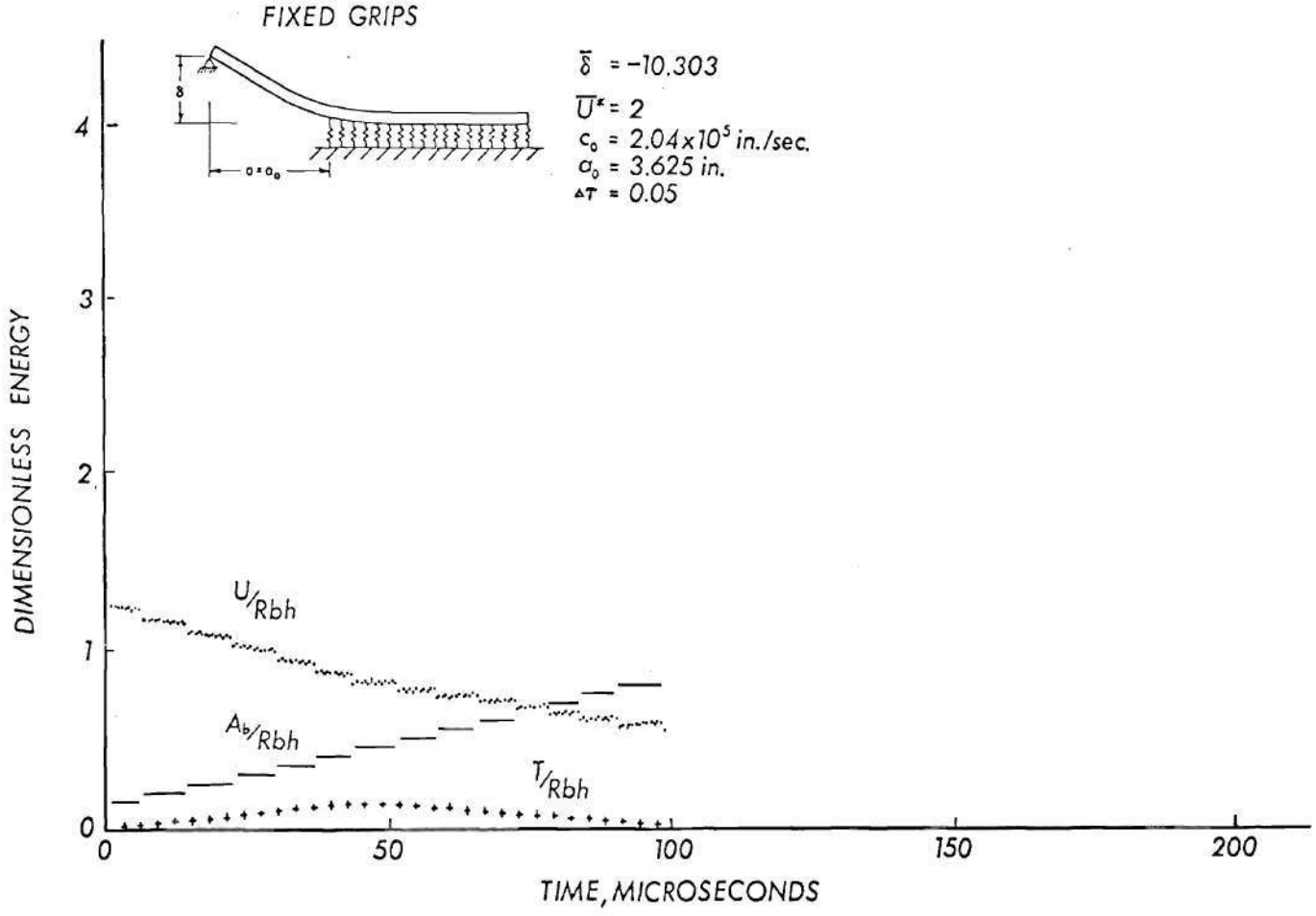

Figure 15. System Energy, $G_q/R = 2$.

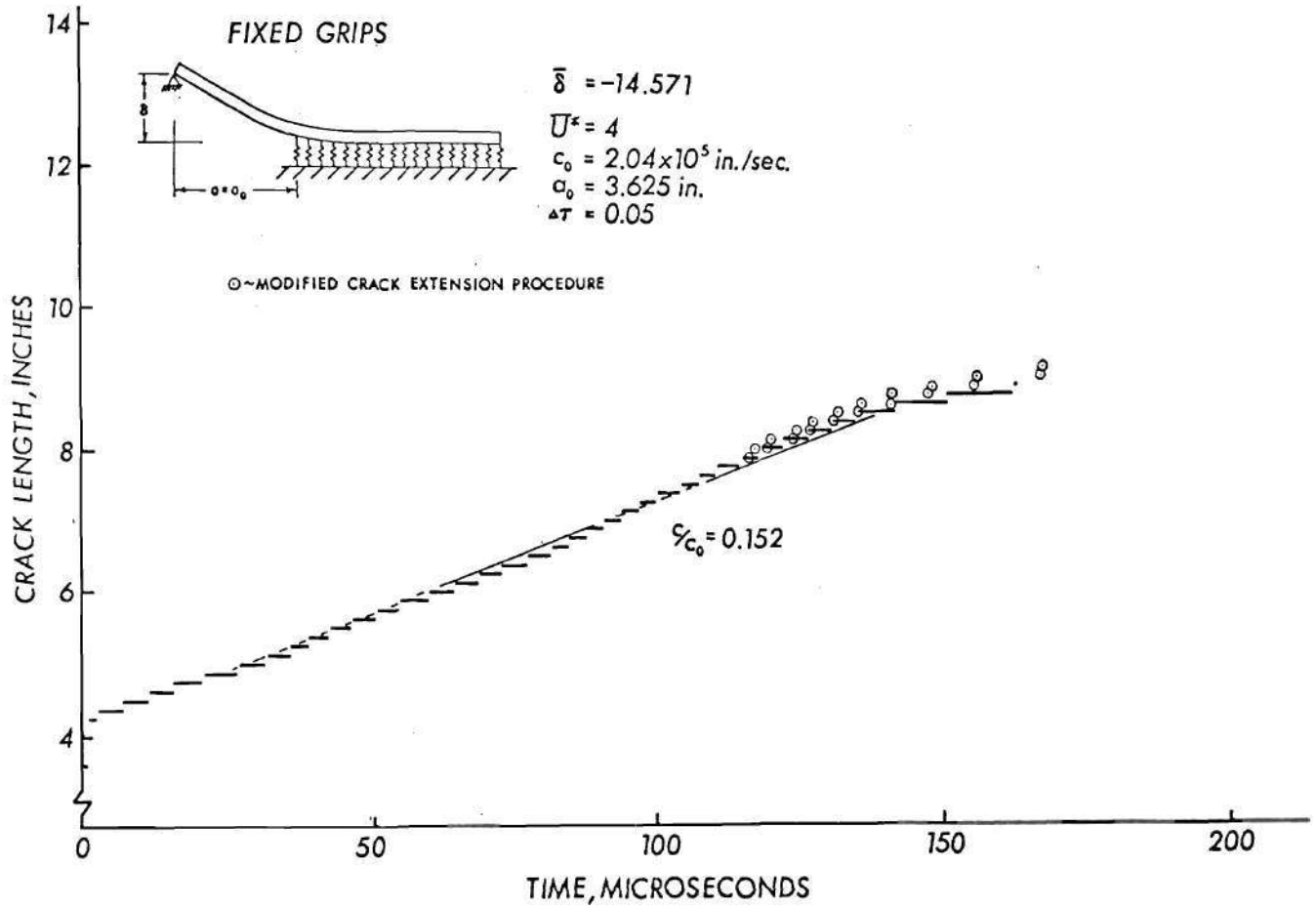

Figure 16. Finite Model, $G_q/R = 4$, Overstretch Foundation.

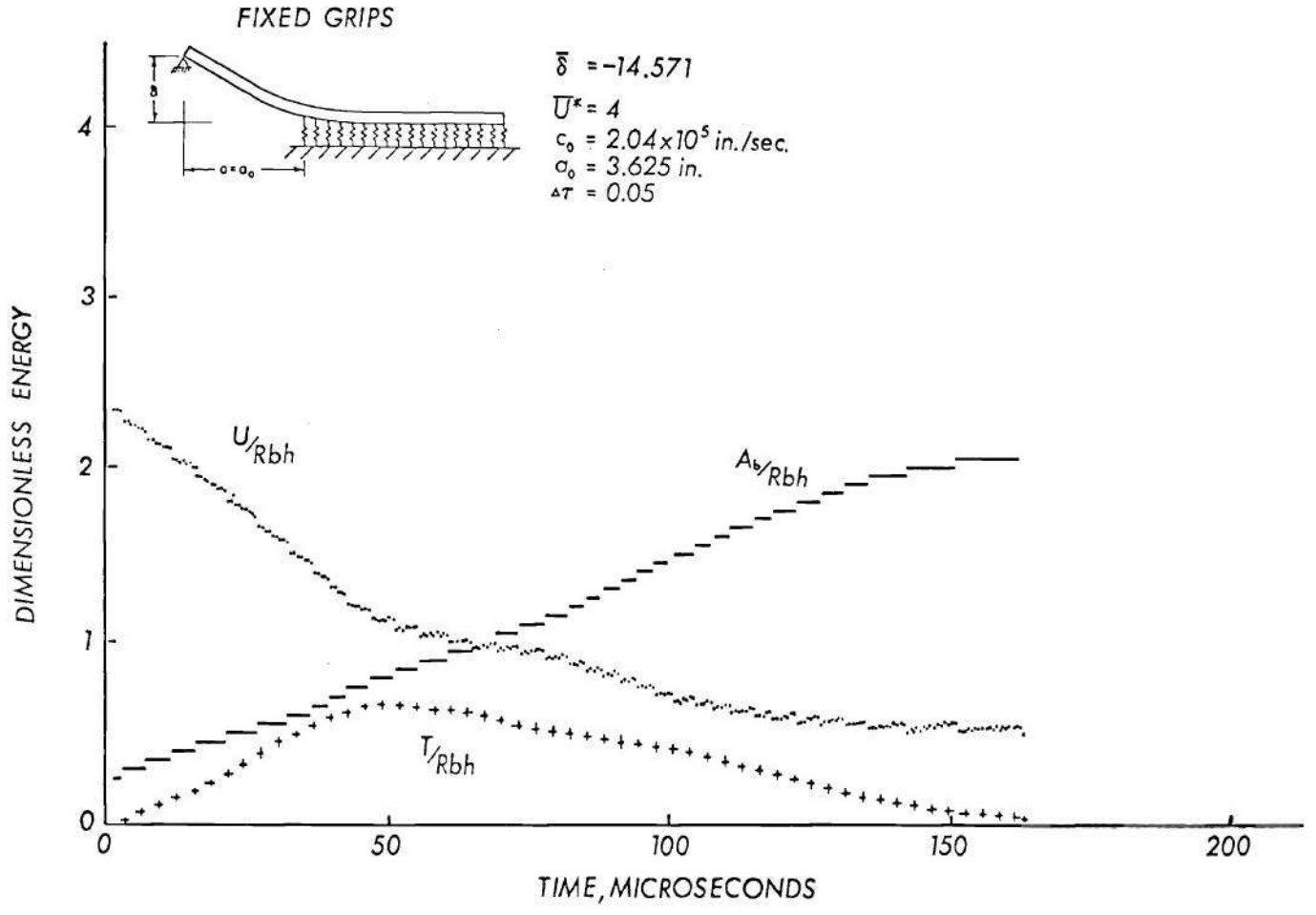

Figure 17. System Energy, $G_q/R = 4$.

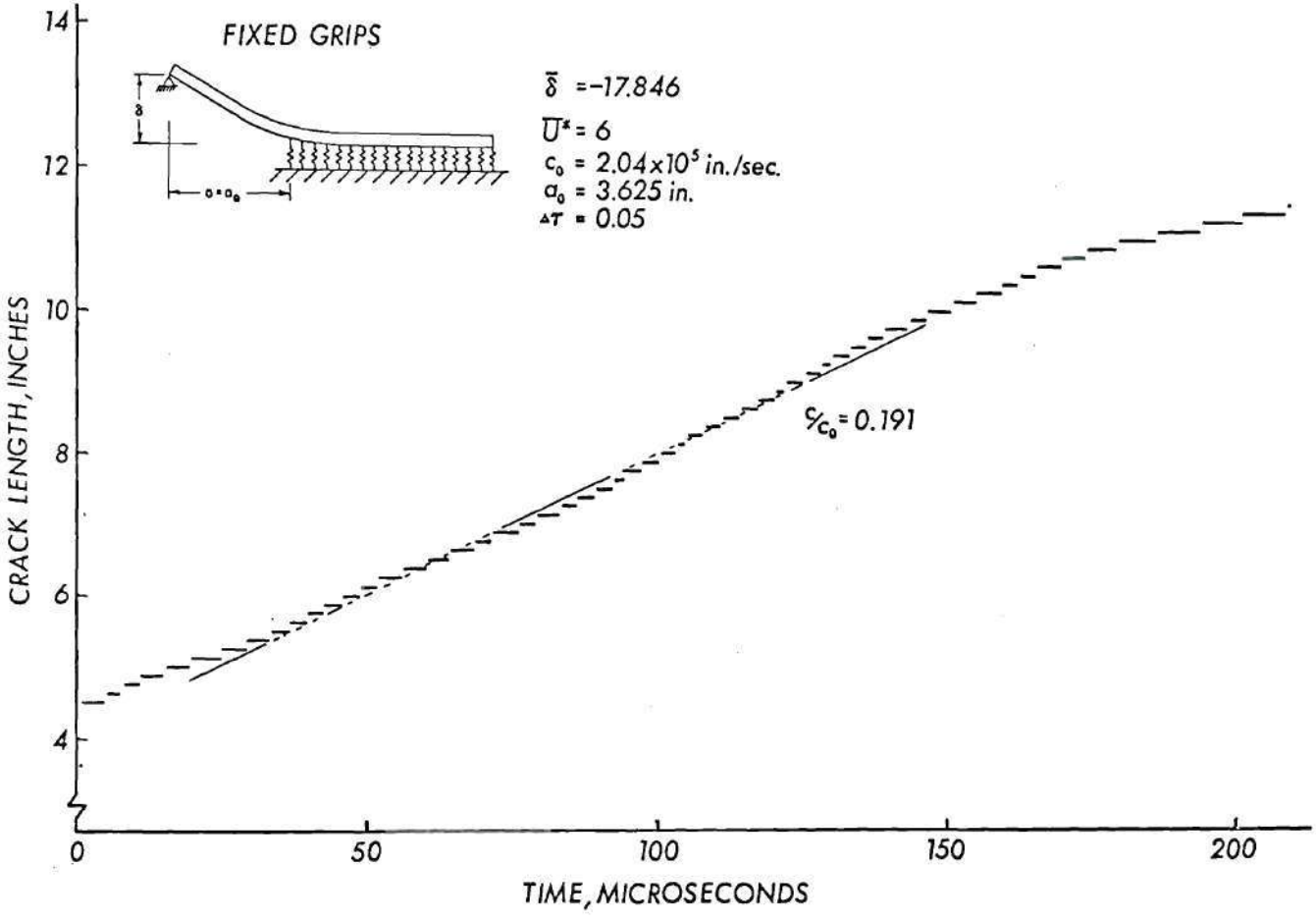

Figure 18. Finite Model, $G_q/R = 6$, Overstretched Foundation.

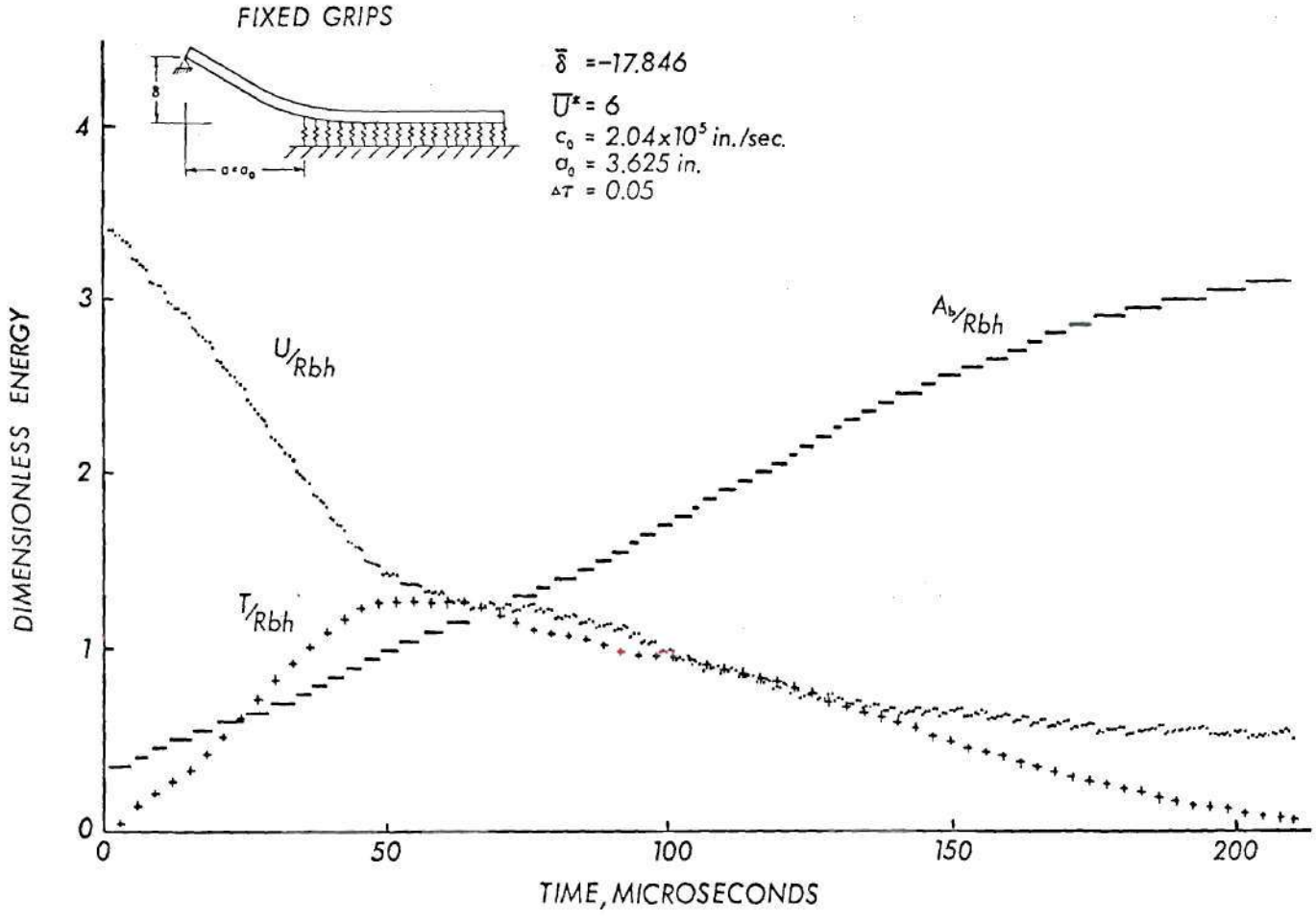

Figure 19. System Energy, $G_q/R = 6$.

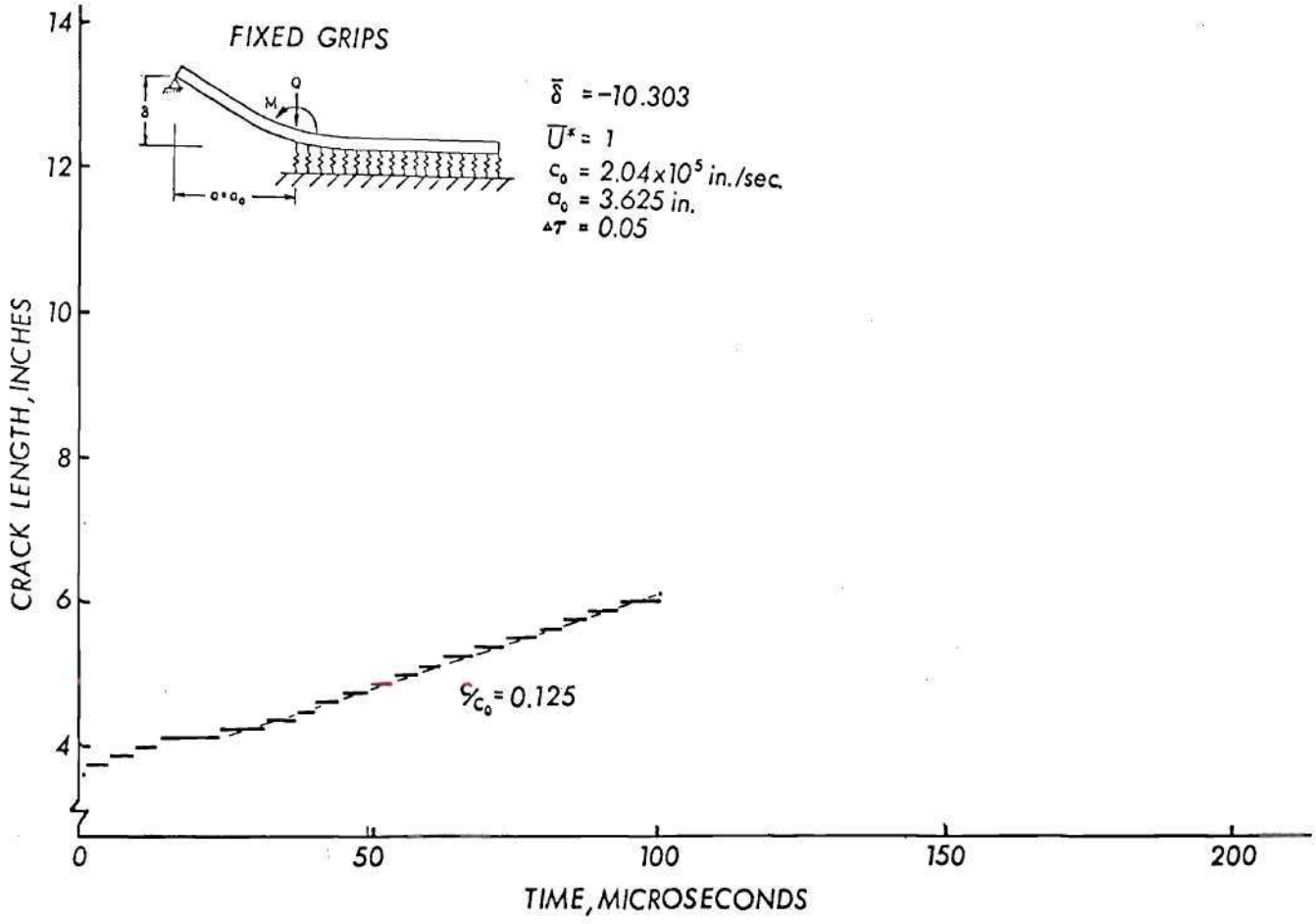

Figure 20. Finite Model, $G_q/R = 2$, Imposed Loads at Crack Tip.

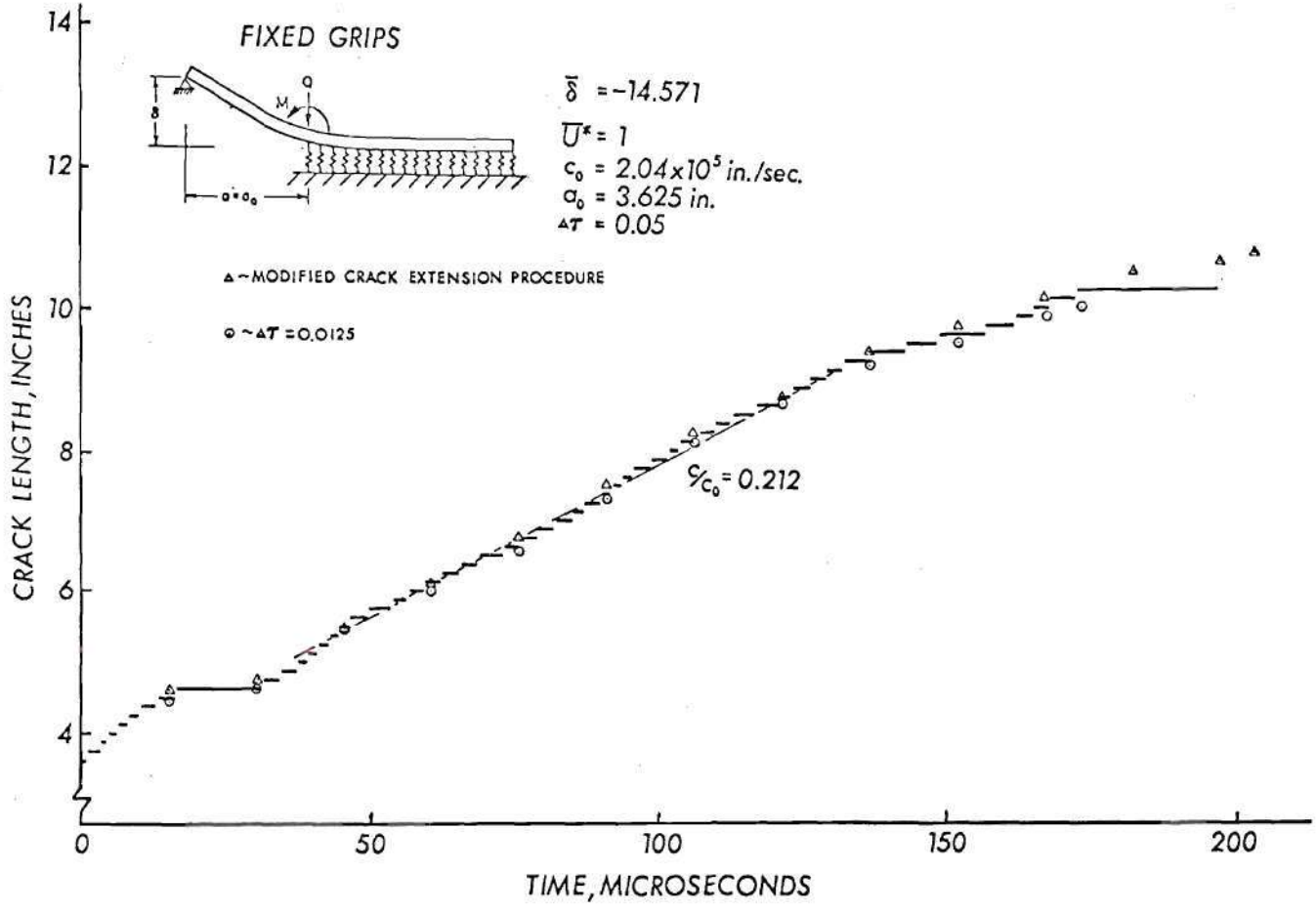

Figure 21. Finite Model, $G_q/R = 4$, Imposed Loads at Crack Tip.

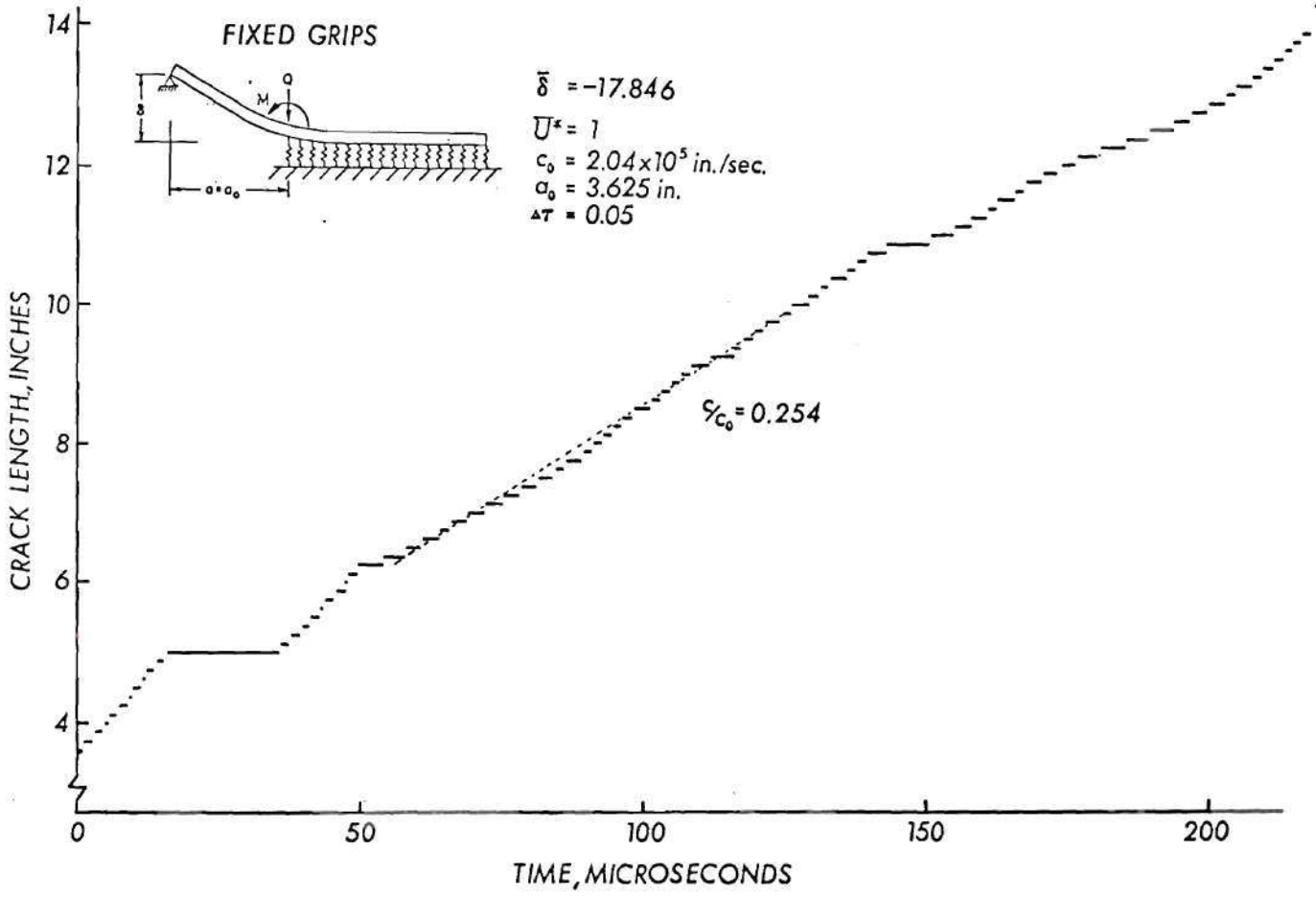

Figure 22. Finite Model, $G_q/R = 6$, Imposed Loads at Crack Tip.

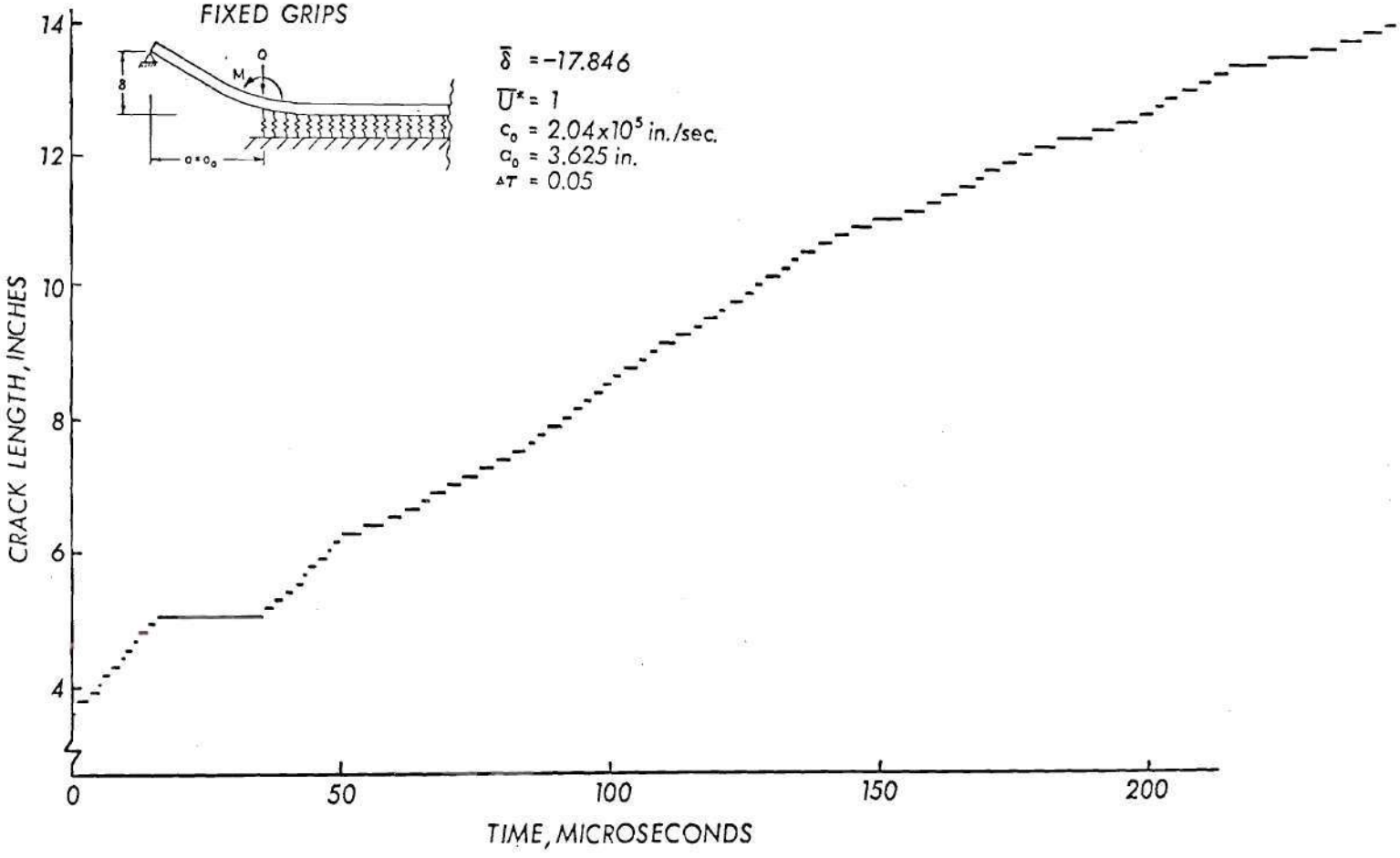

Figure 23. Semi-Infinite Model, $G_q/R = 6$, Imposed Loads at Crack Tip.

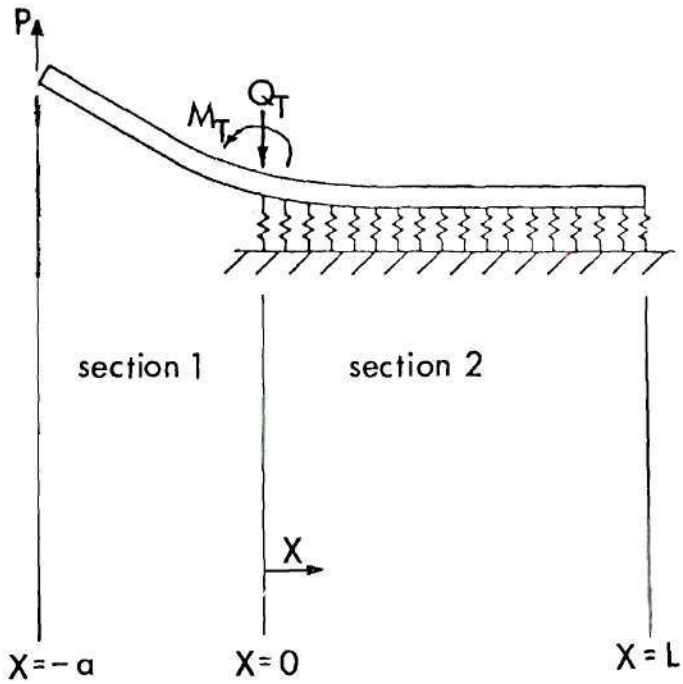

Figure 24. Configuration for the Static DCB Solution.

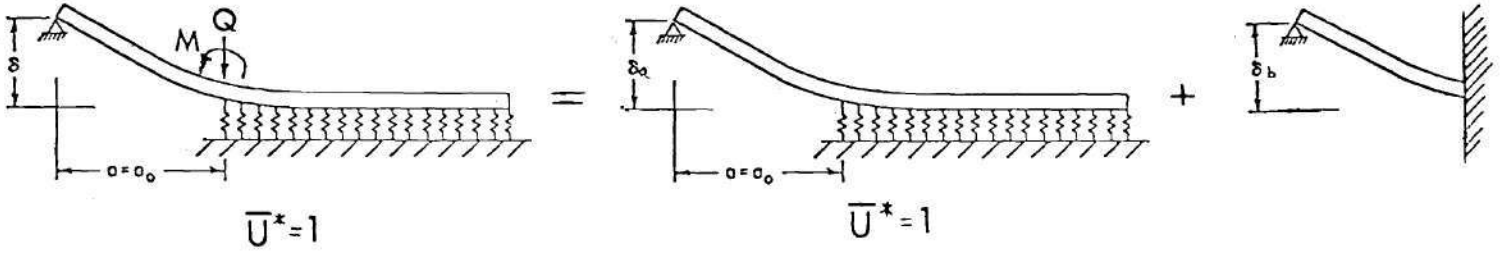

$$\delta = \delta_a + \delta_b$$

Figure 25. Procedure for Determining the Crack Tip Loads.

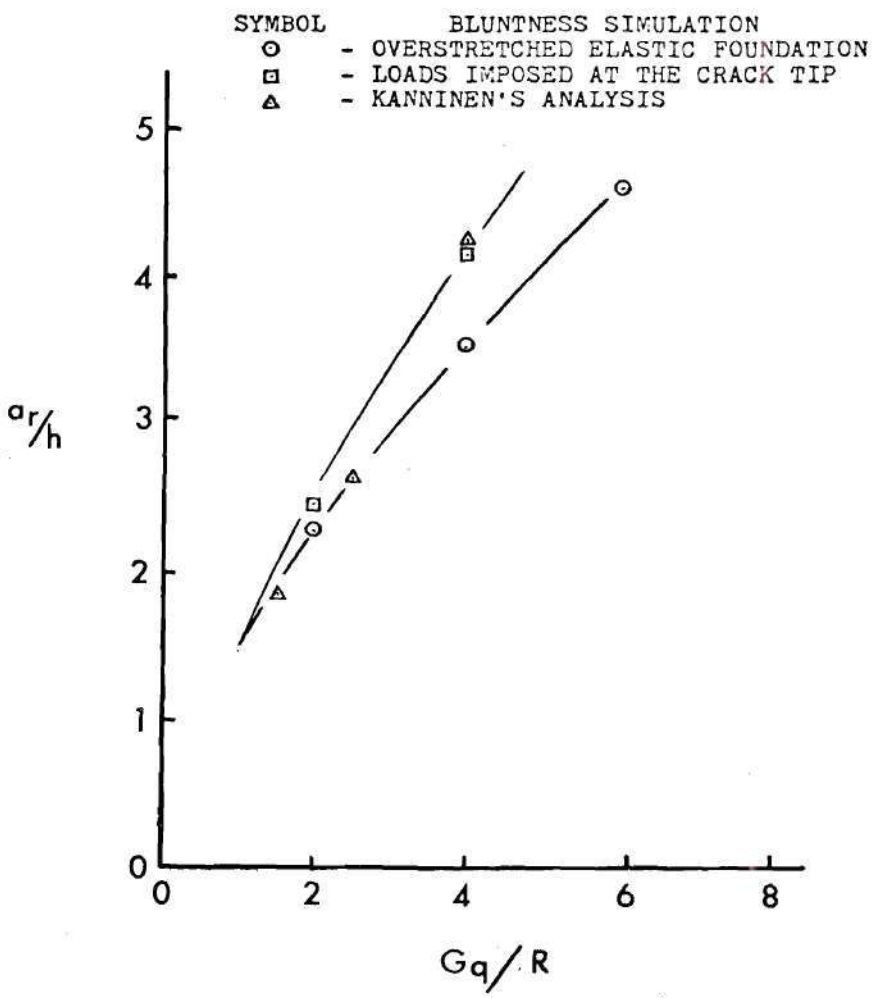

Figure 26. Crack Arrest Length versus Energy Overstorage in the DCB Model.

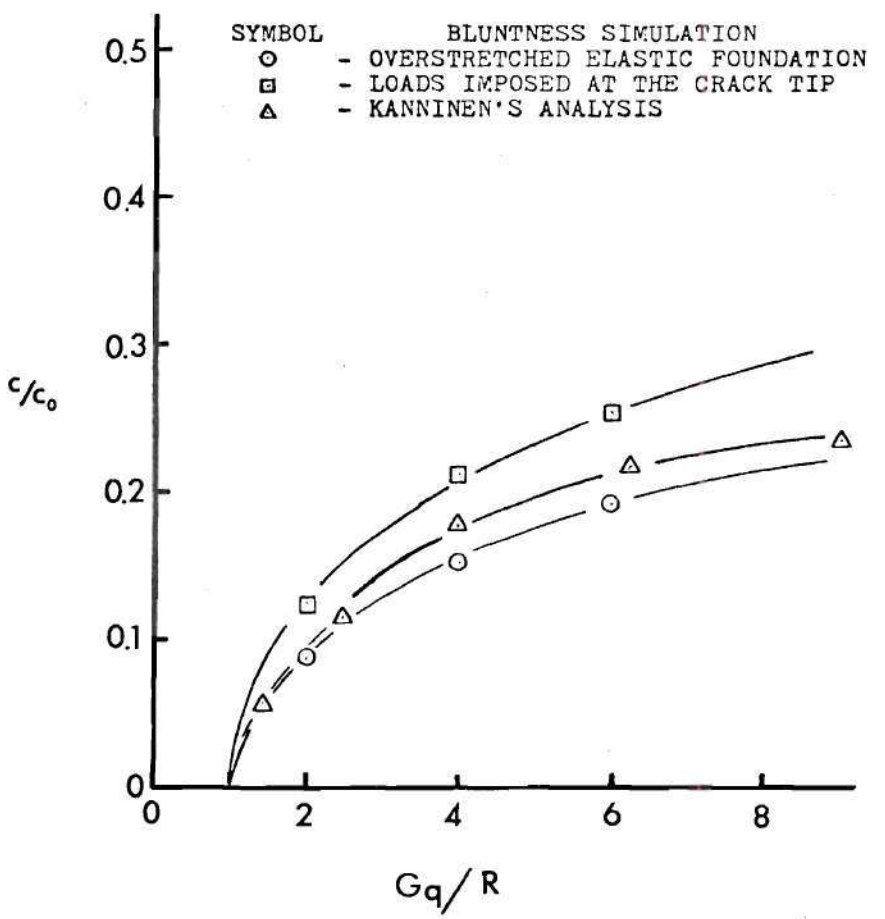

Figure 27. Crack Speed versus Energy Overstorage in the DCB Model.

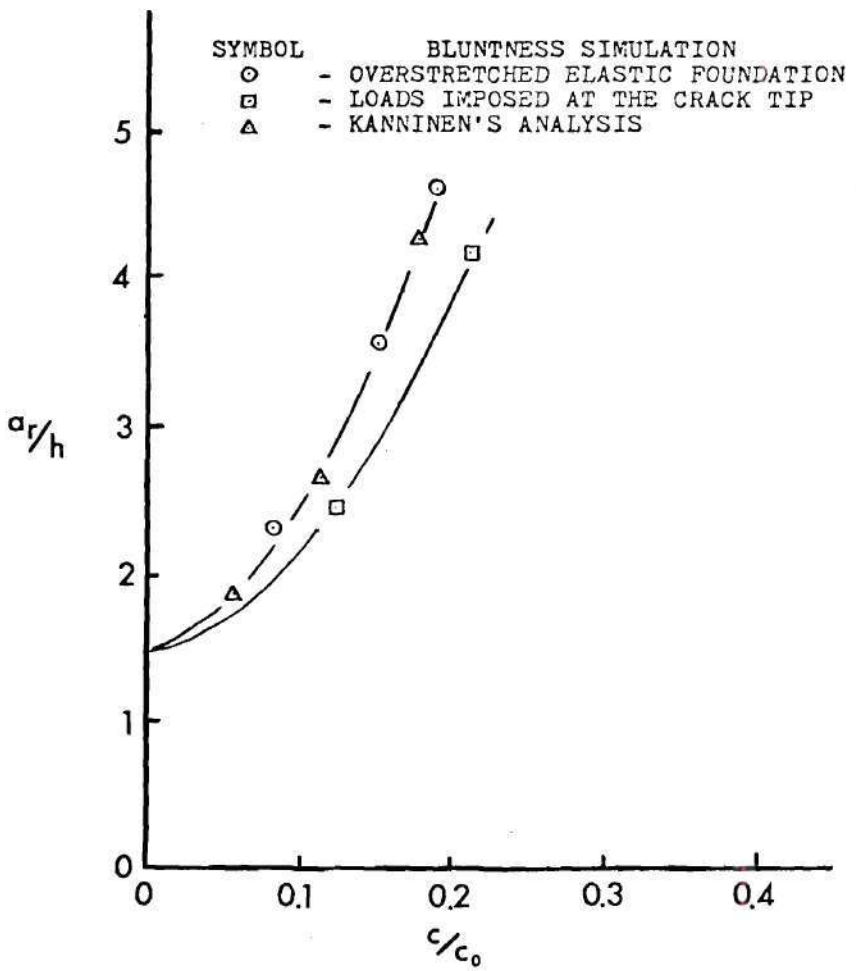

Figure 28. Crack Arrest Length versus Crack Speed for the DCB Model.

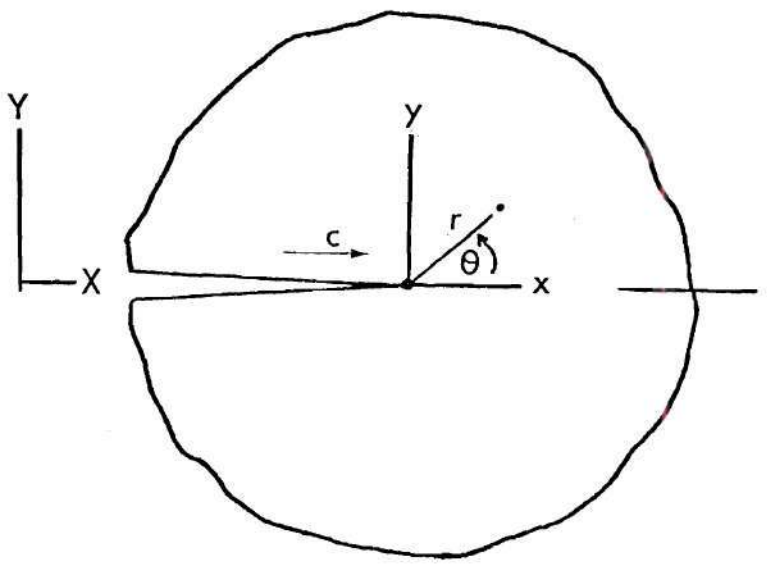

Figure 29. Notation for the Constant Velocity Eigenfunctions.

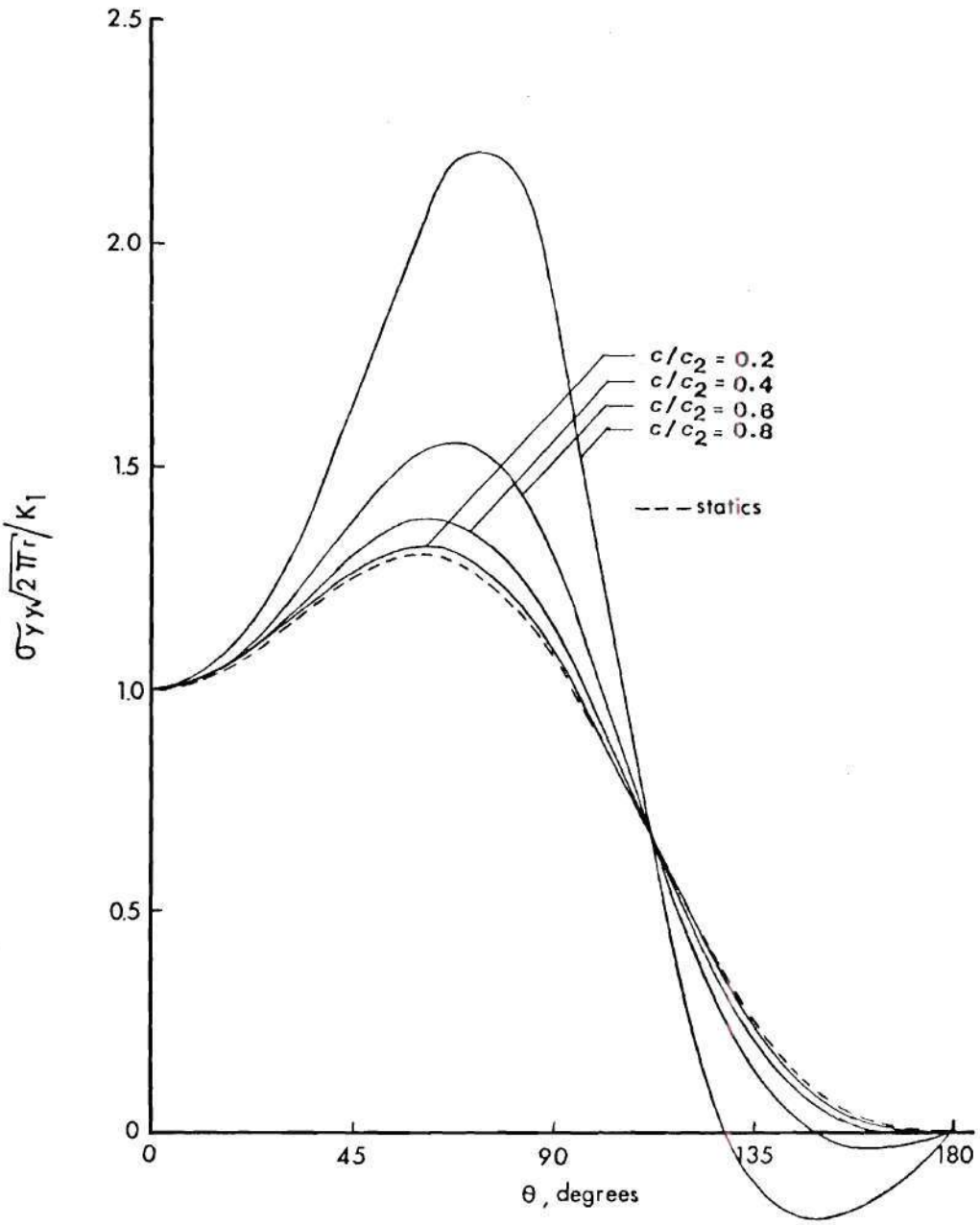

Figure 30. Angular Behavior of σ_{yy}.

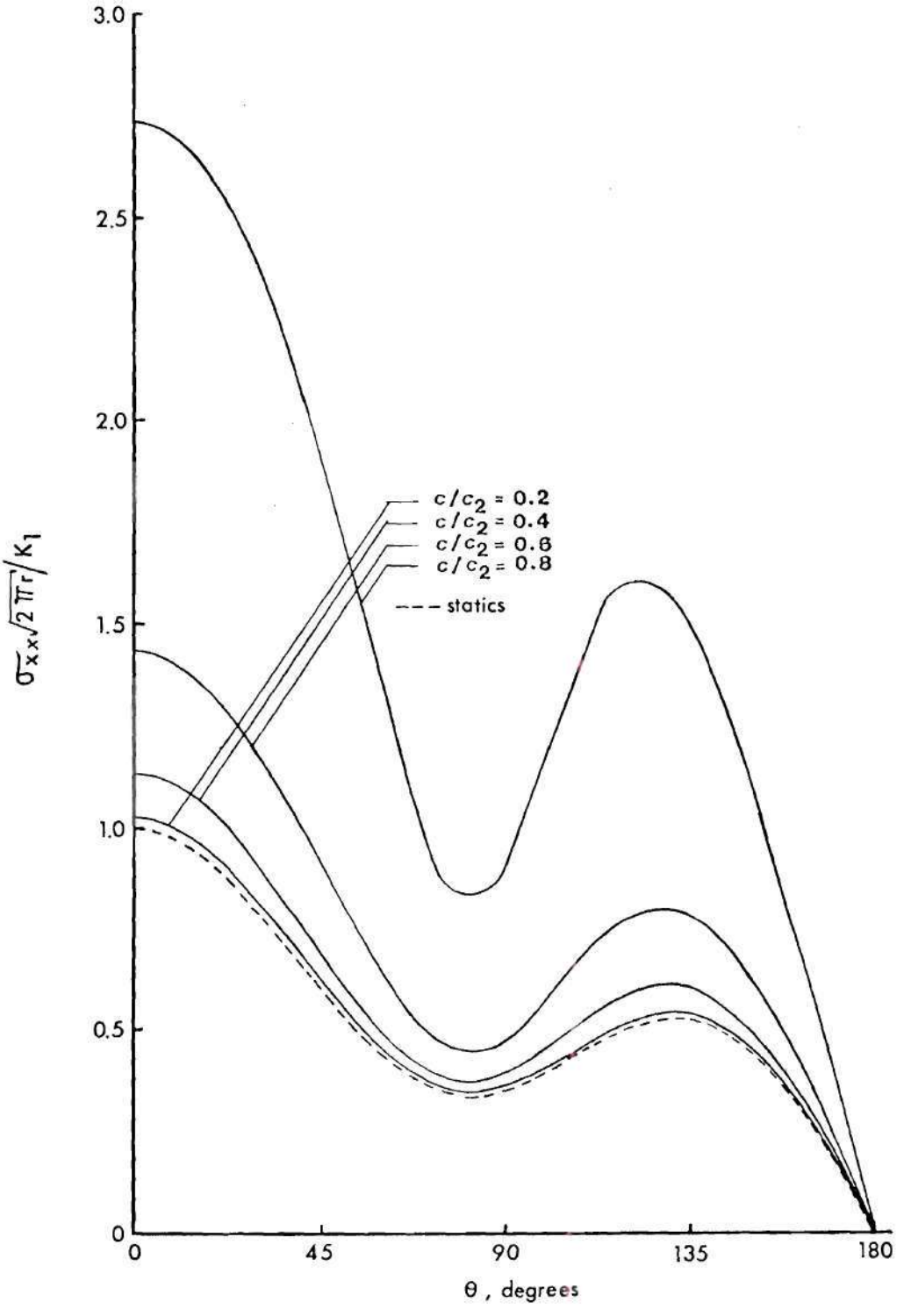

Figure 31. Angular Behavior of σ_{xx}.

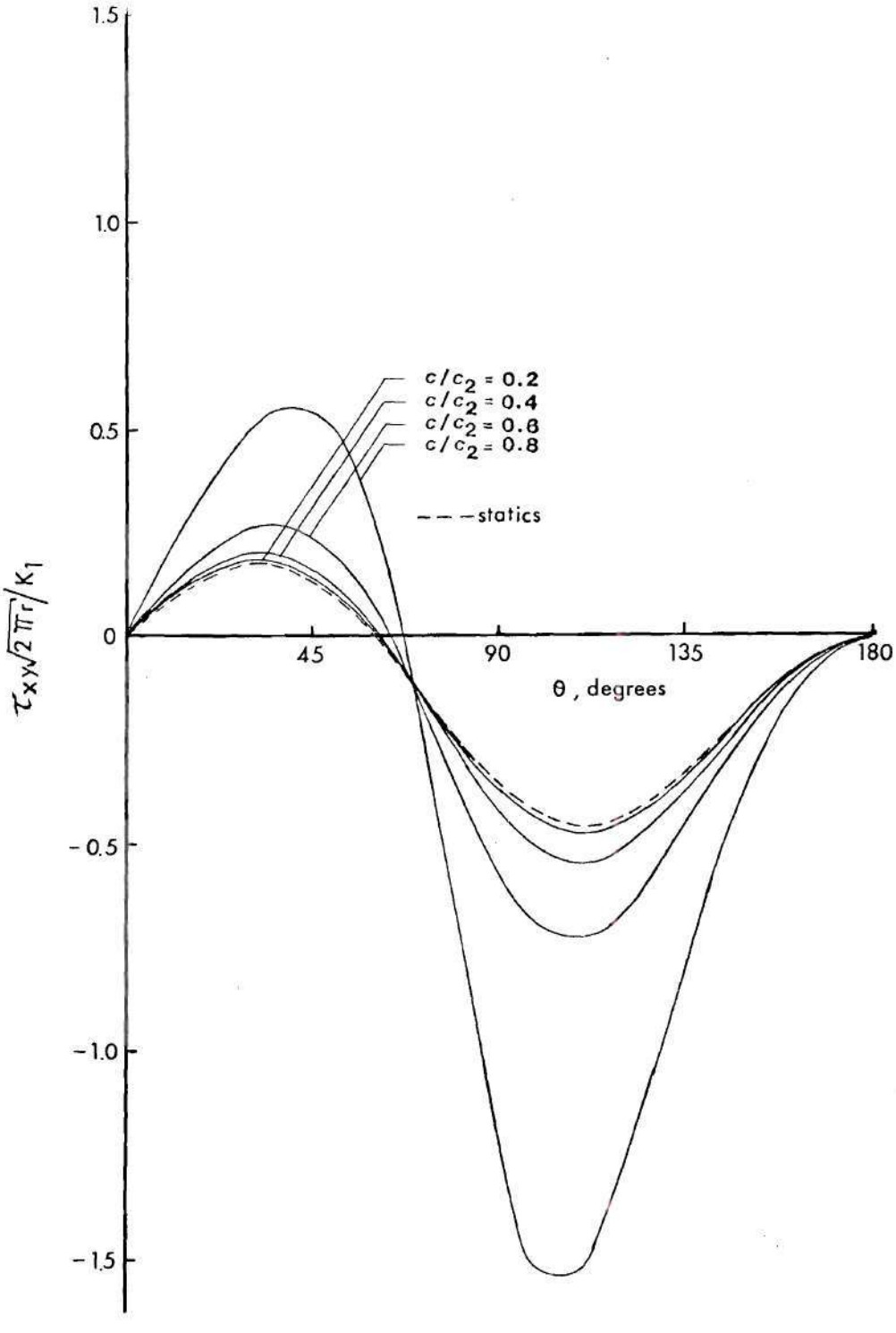

Figure 32. Angular Behavior of τ_{xy}.

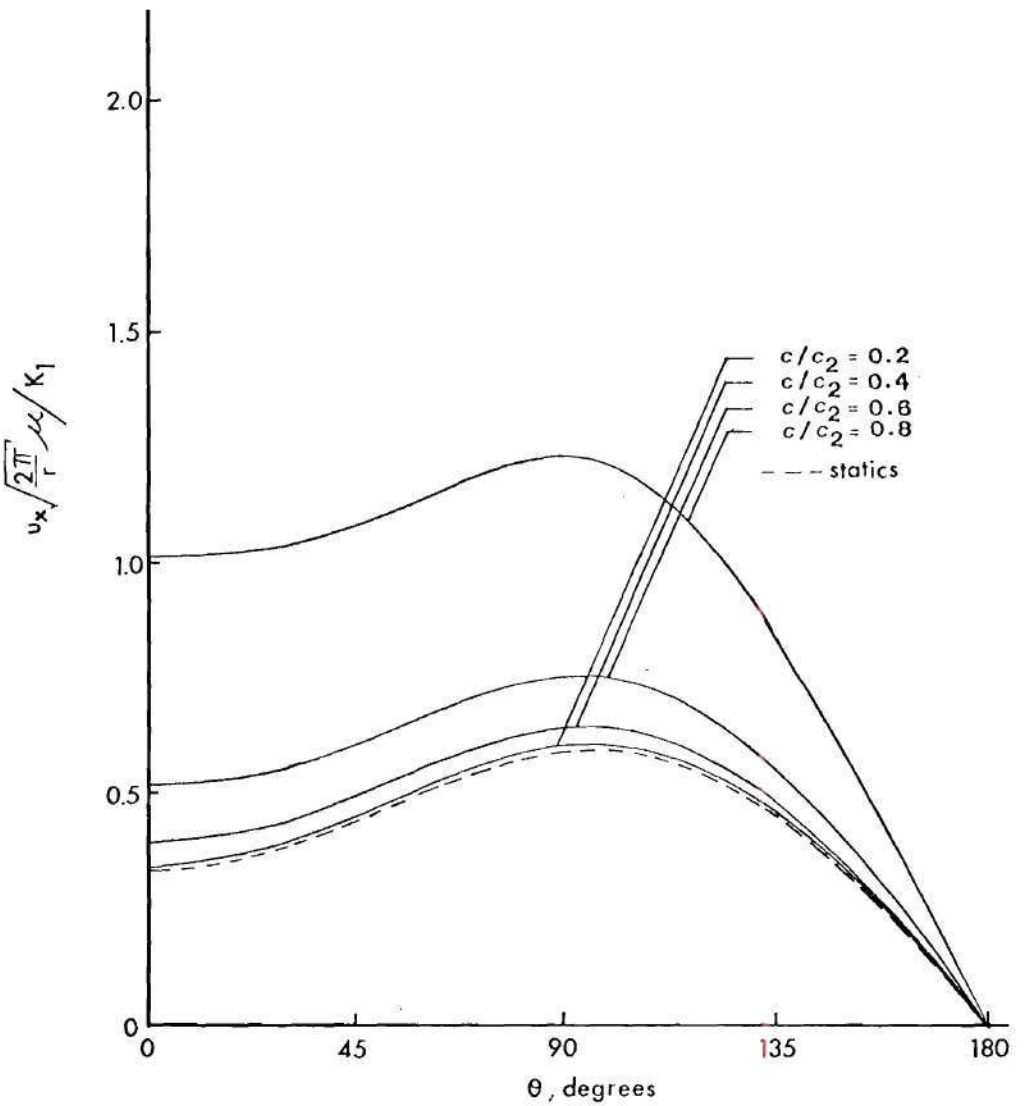

Figure 33. Angular Behavior of u_x.

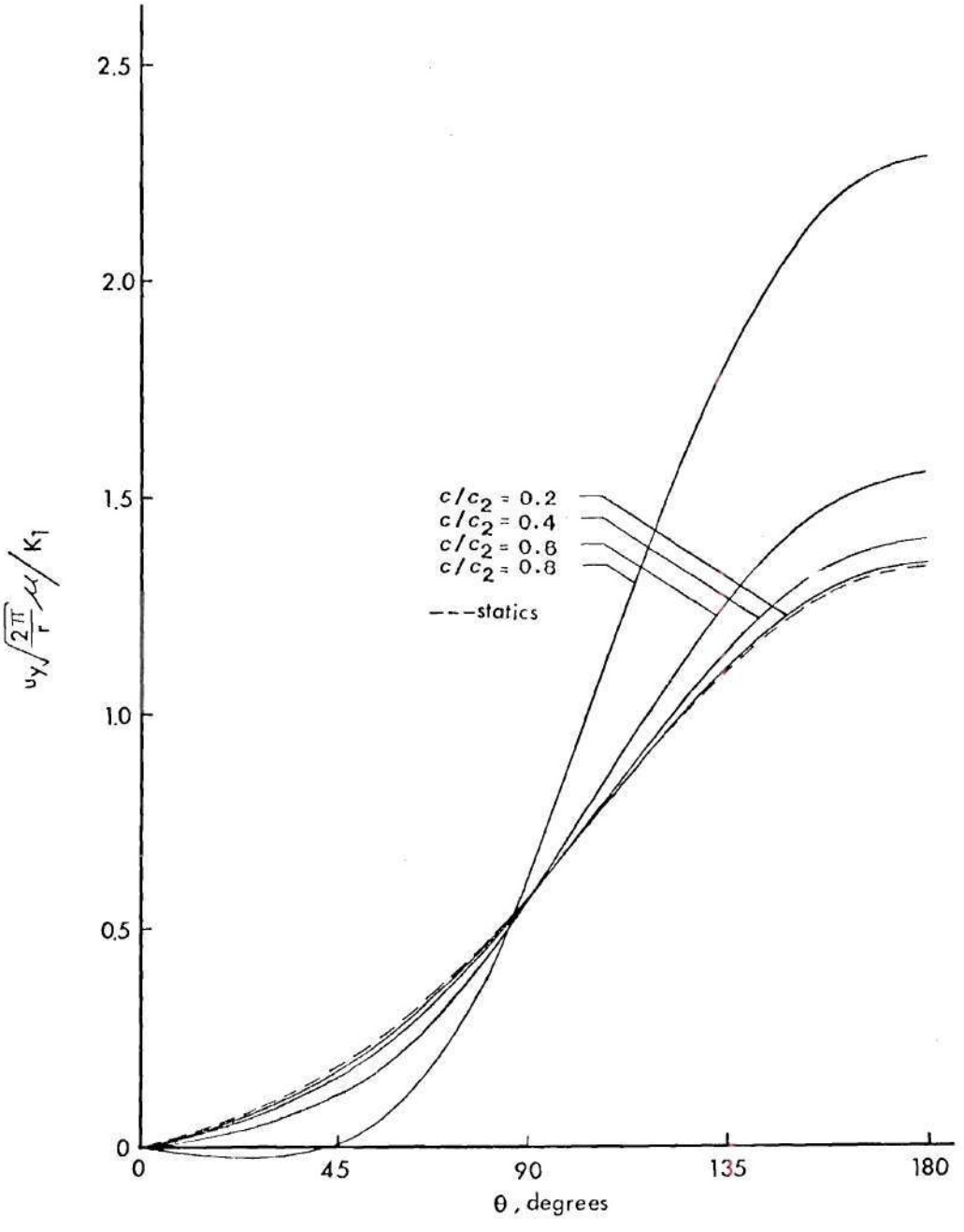

Figure 34. Angular Behavior of u_y.

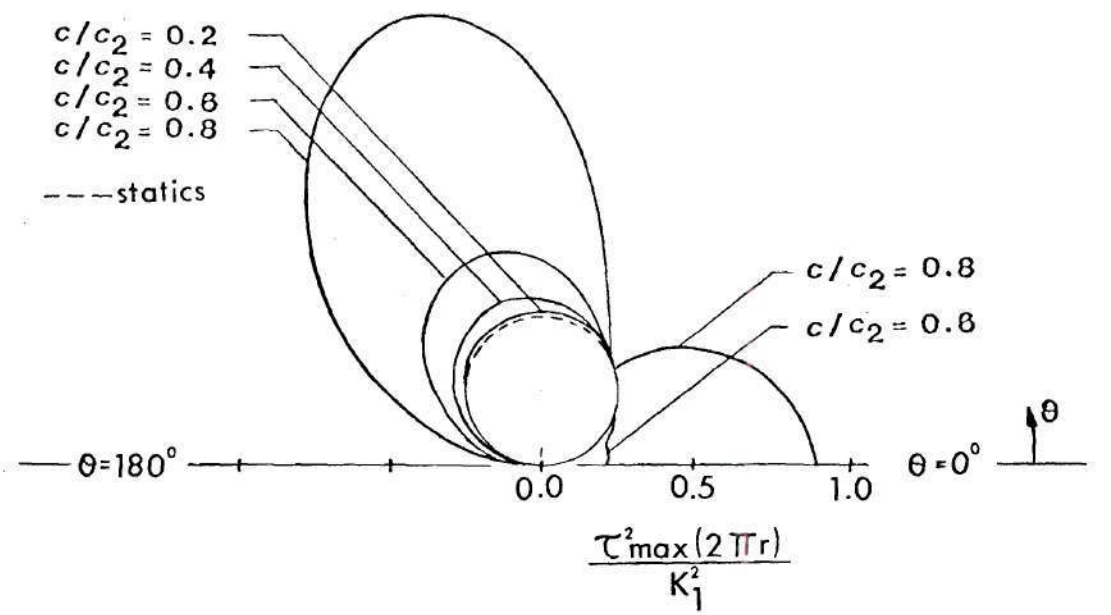

Figure 35. Dynamic Isochromatics.

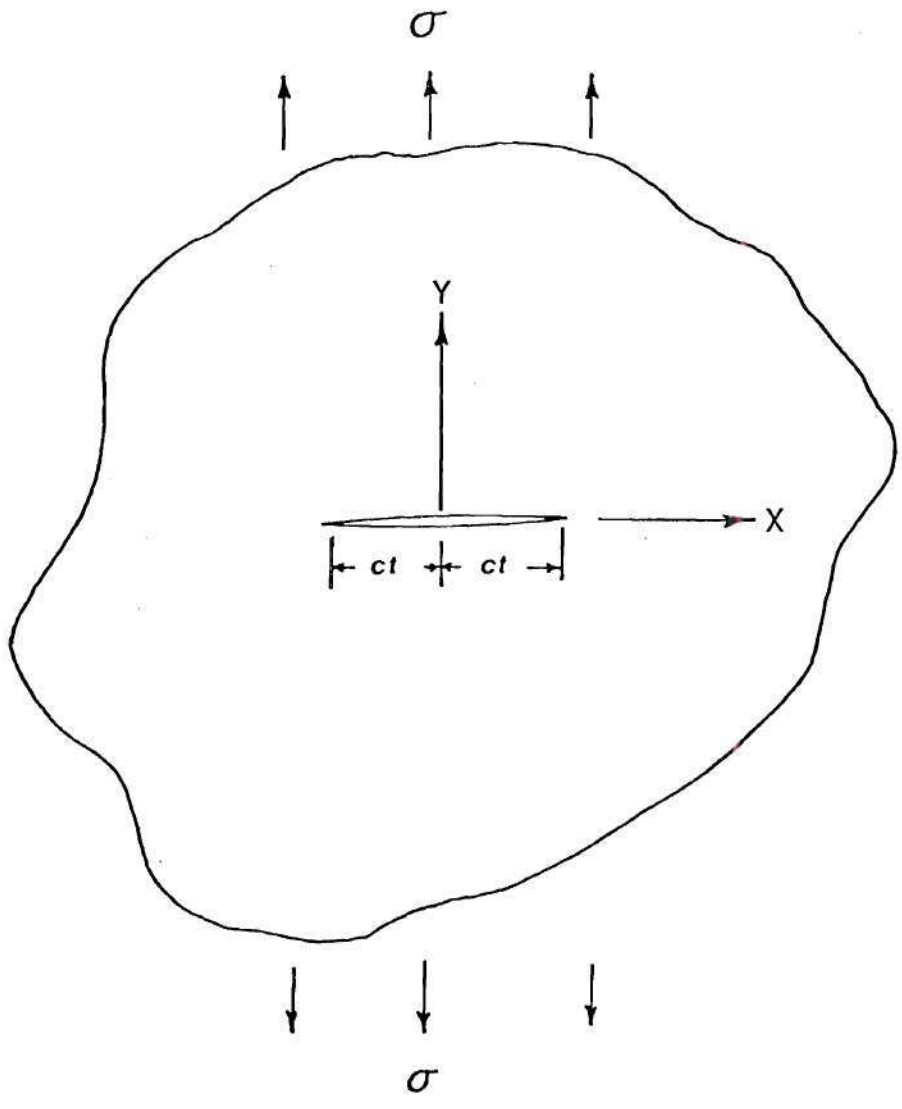

Figure 36. Broberg's Problem.

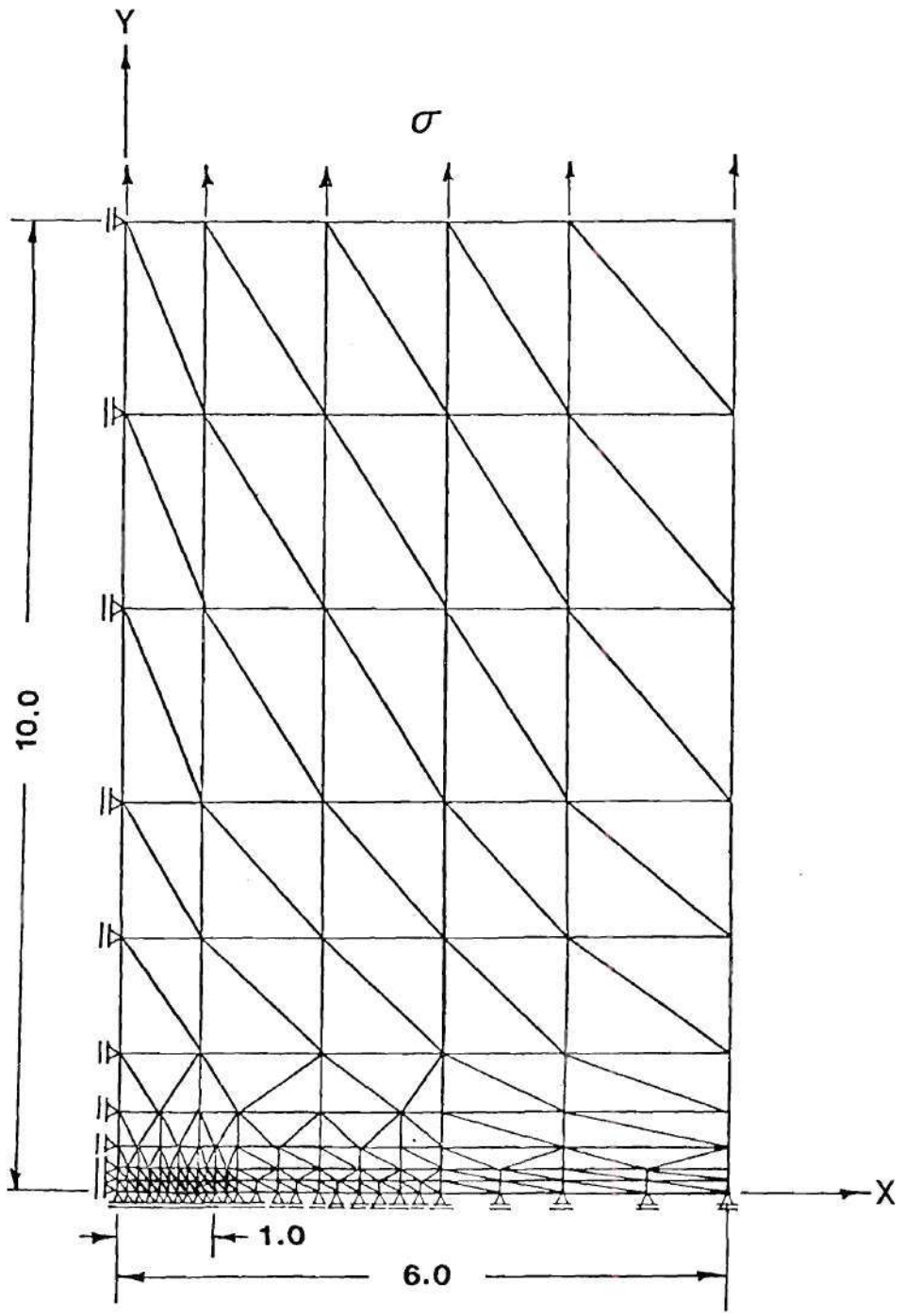

Figure 37. Finite-Element Model for Broberg's Problem.

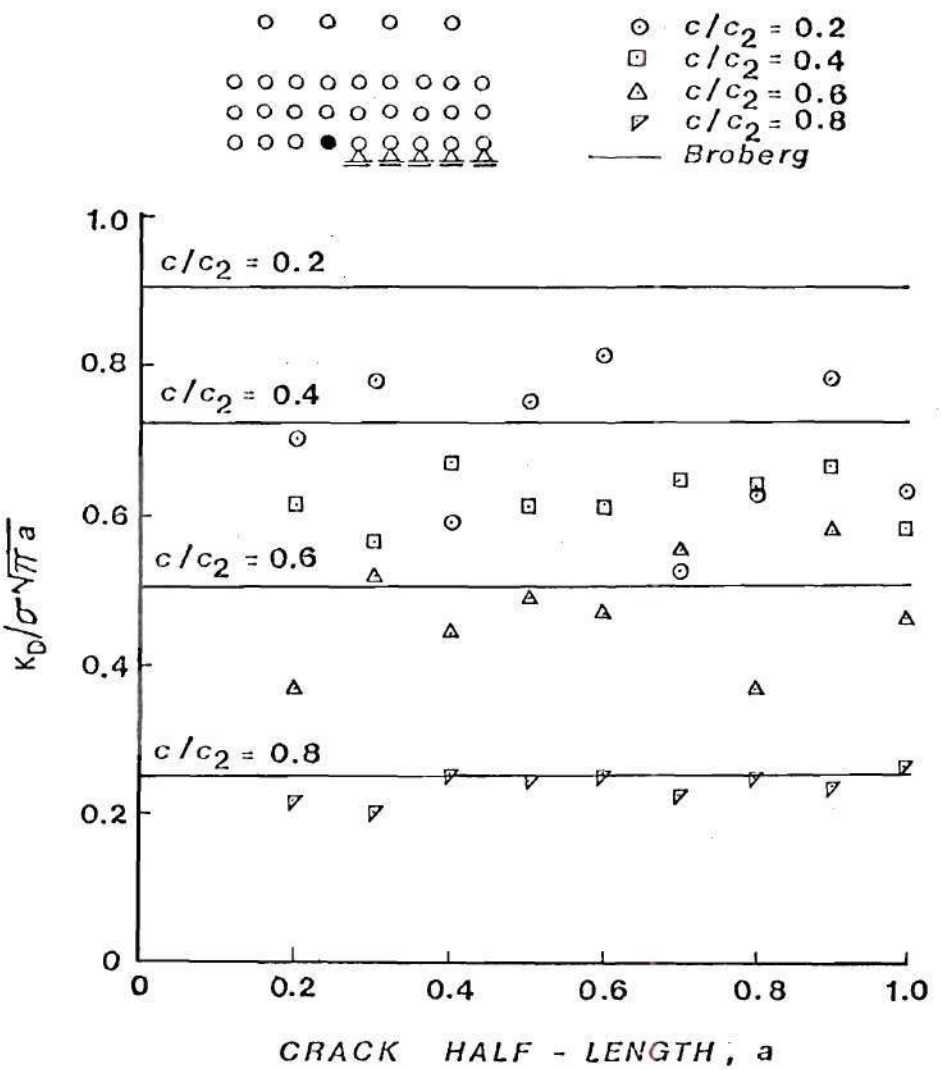

Figure 38. Stress-Intensity Factors, COD, First Node.

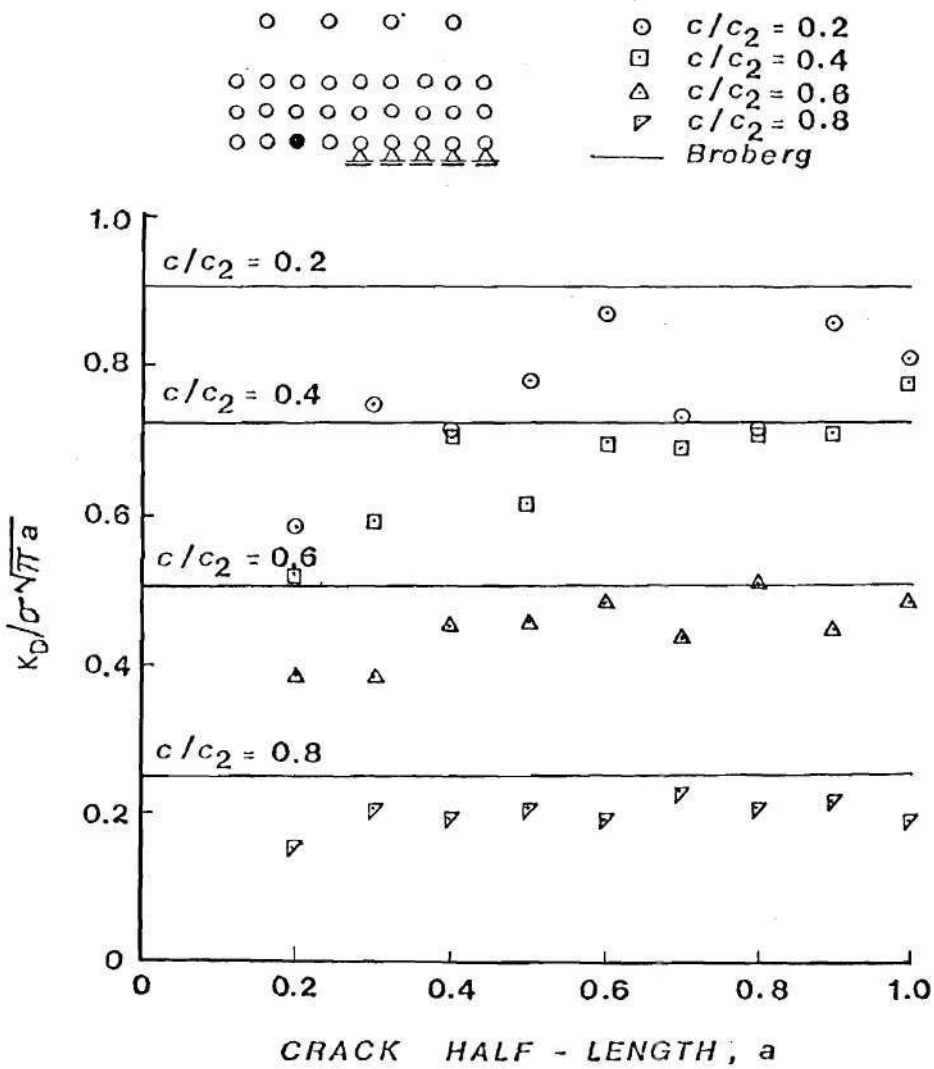

Figure 39. Stress-Intensity Factors, COD, Second Node.

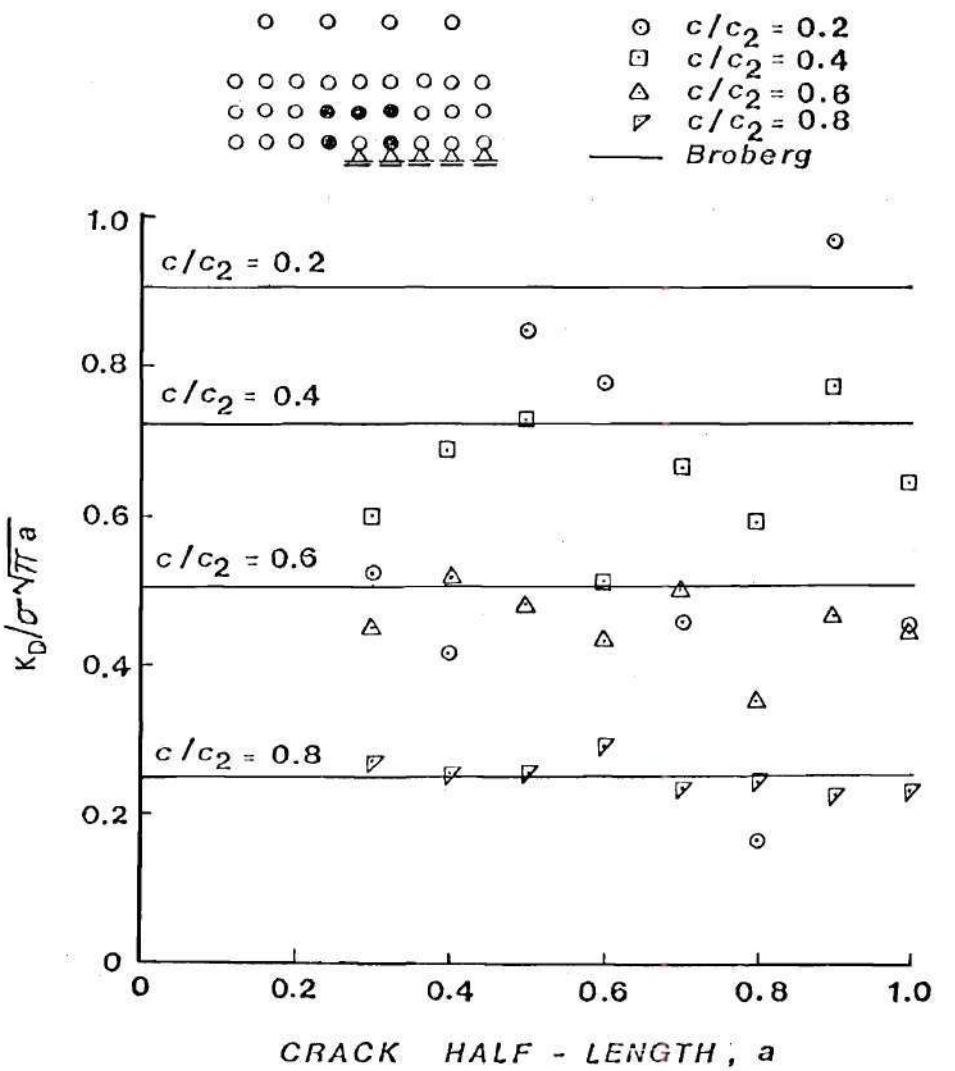

Figure 40. Stress-Intensity Factors, Inner Nodes, 9 Term Fit.

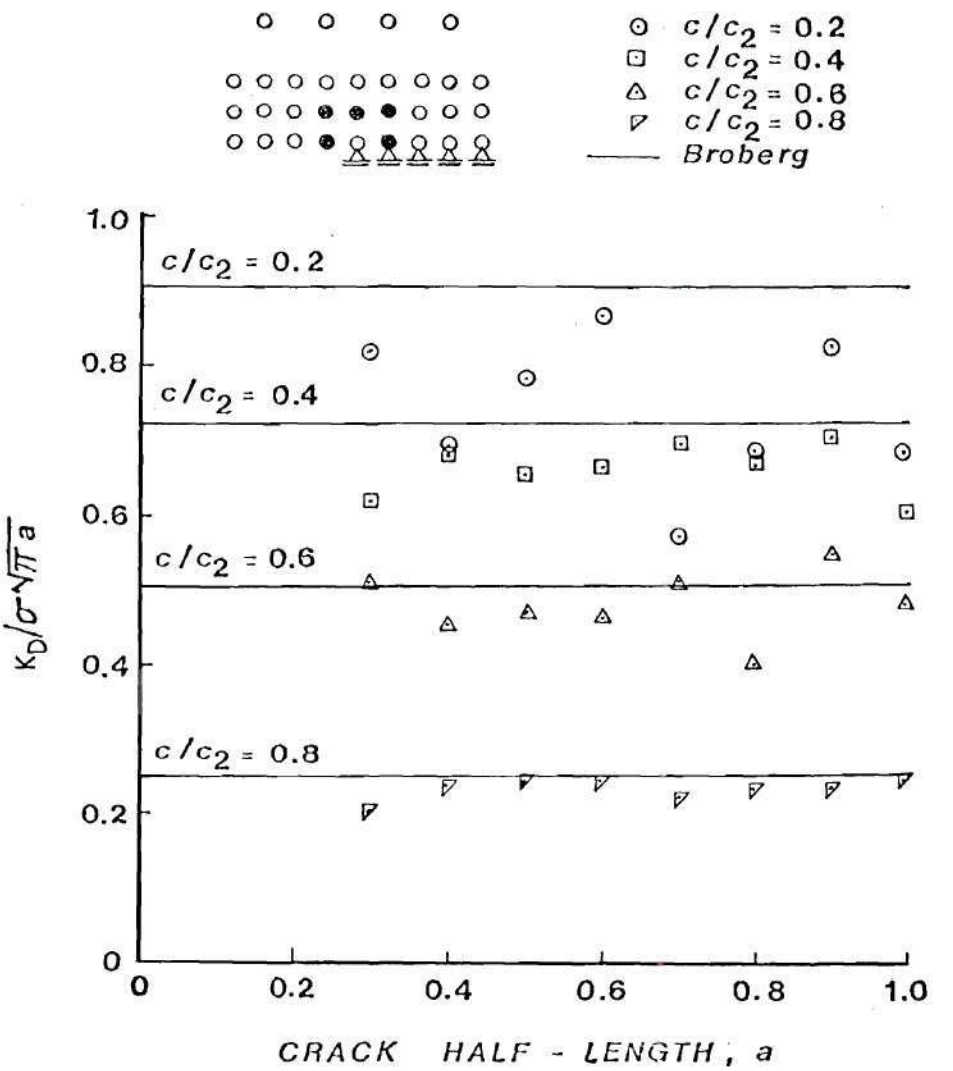

Figure 41. Stress-Intensity Factors, Inner Nodes, 2 Term Fit.

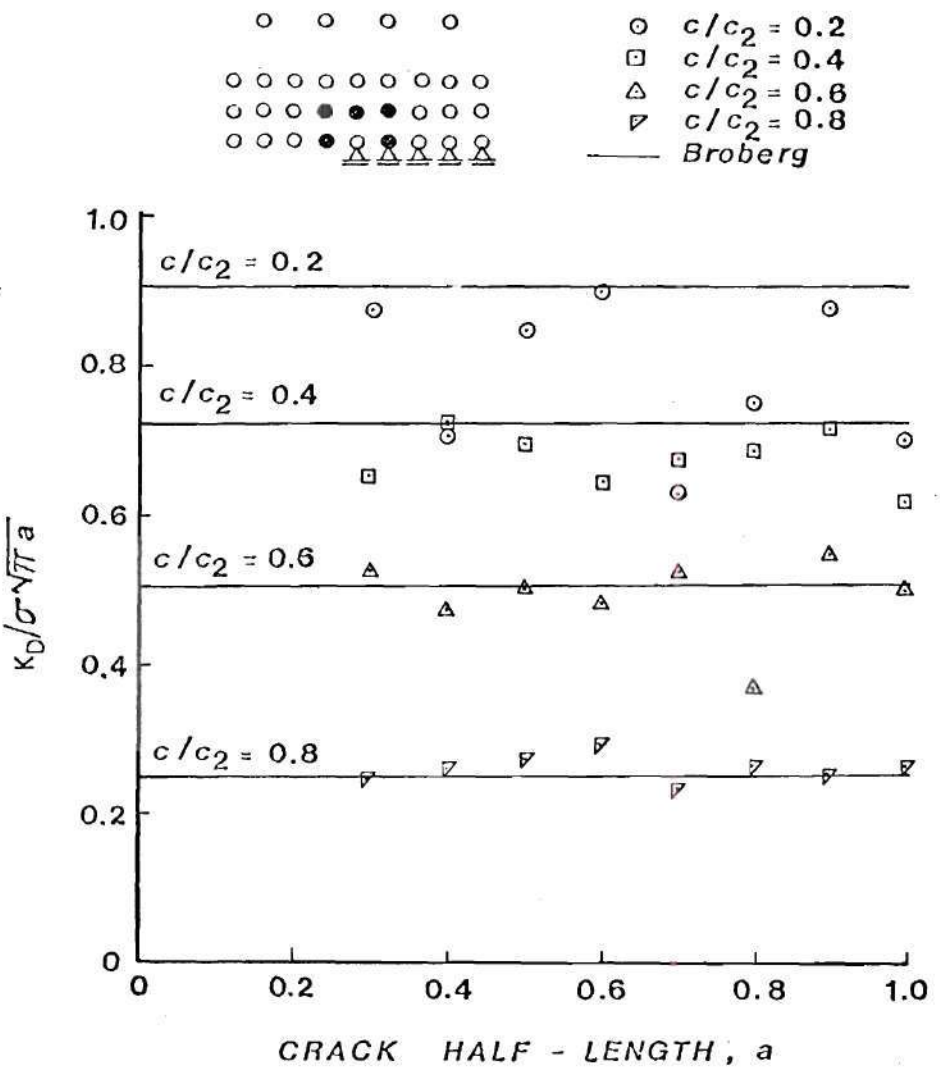

Figure 42. Stress-Intensity Factors, Inner Nodes, 4 Term Fit.

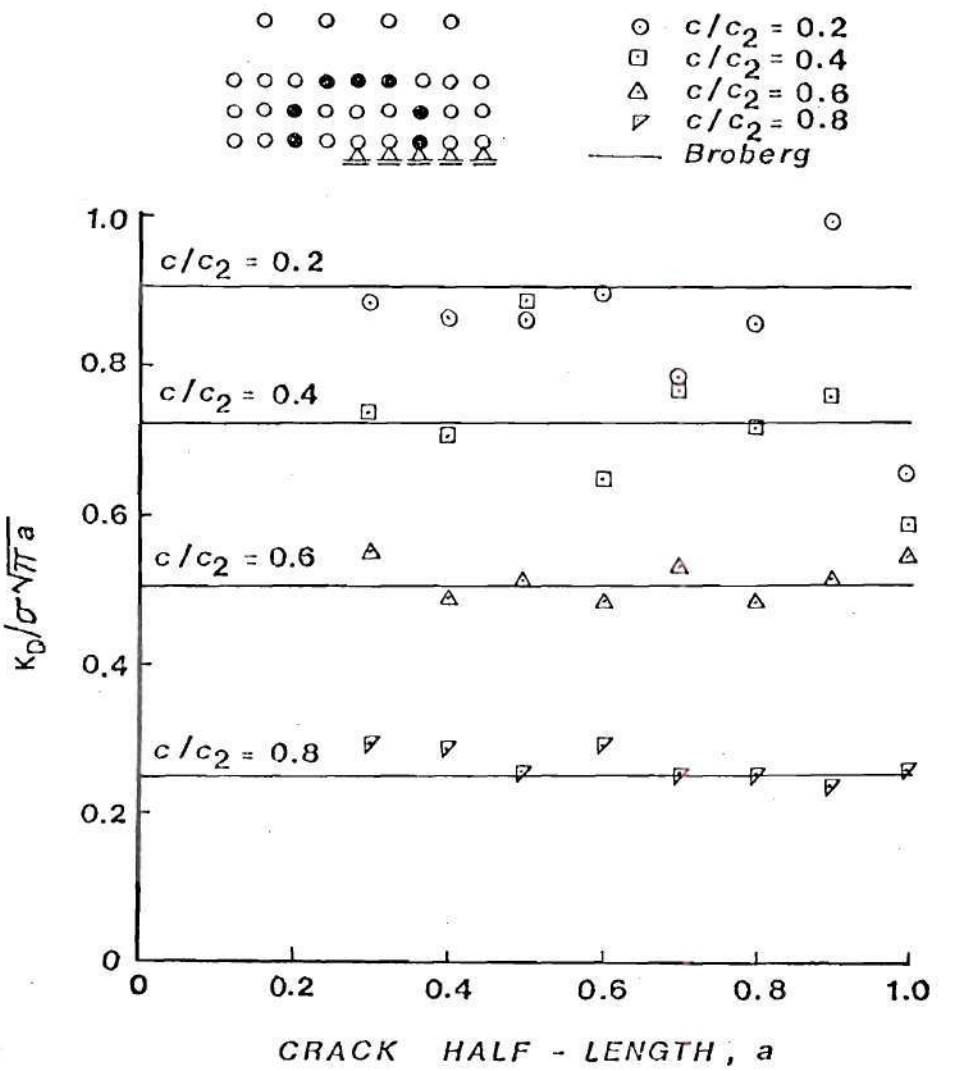

Figure 43. Stress-Intensity Factors, Middle Nodes, 13 Term Fit.

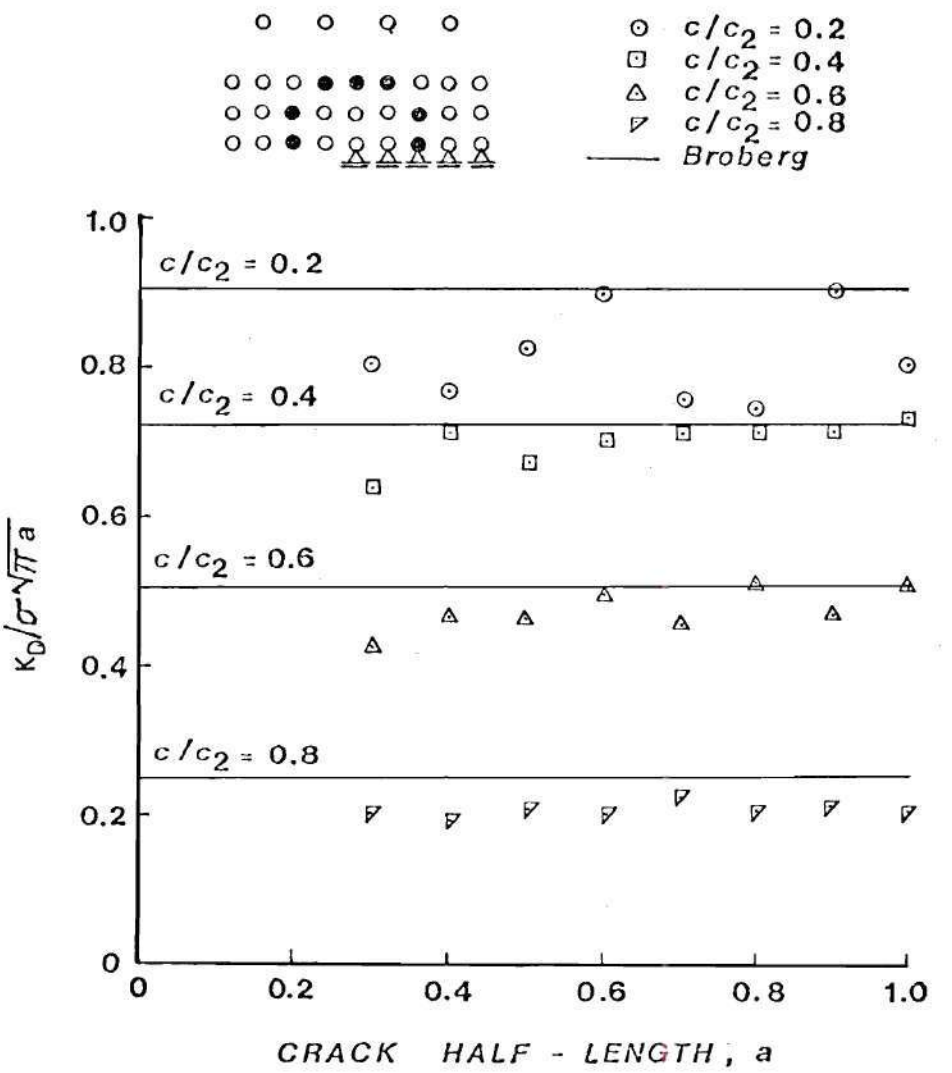

Figure 44. Stress-Intensity Factors, Middle Nodes, 2 Term Fit.

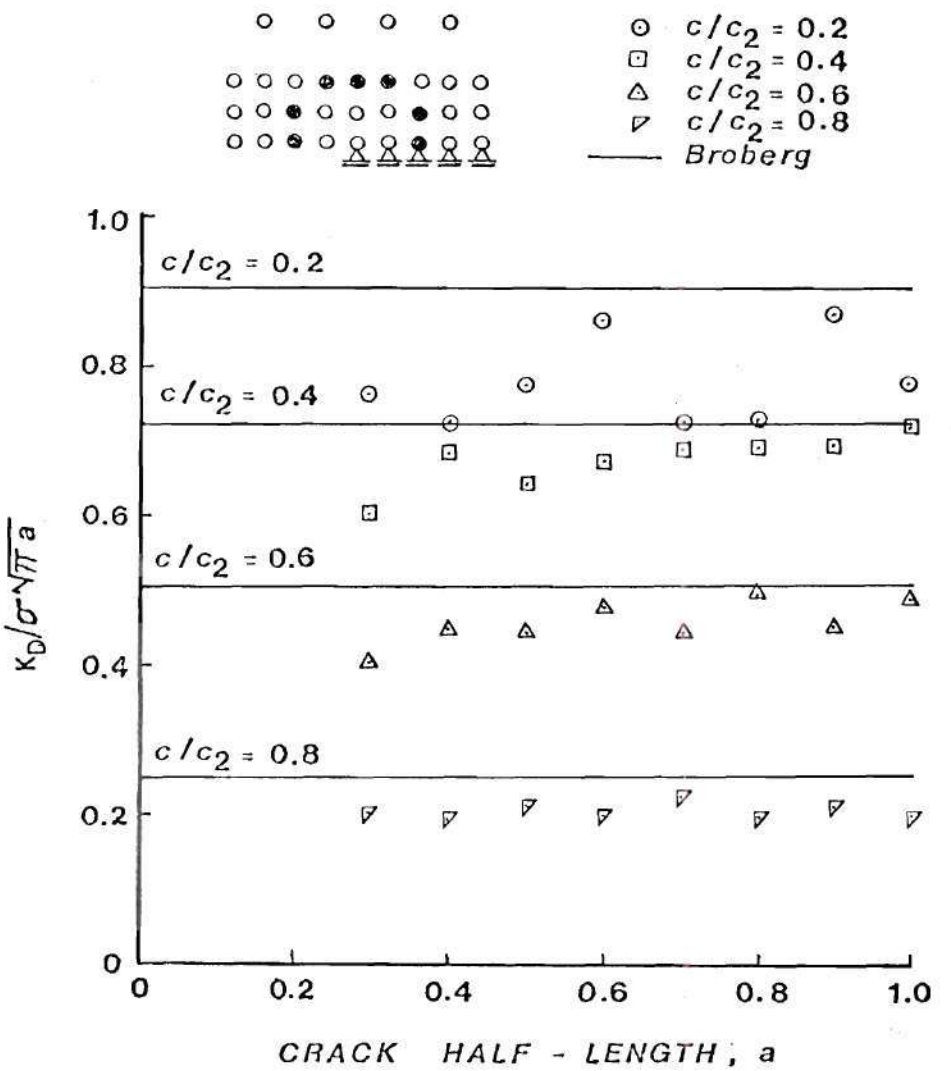

Figure 45. Stress-Intensity Factors, Middle Nodes, 3 Term Fit.

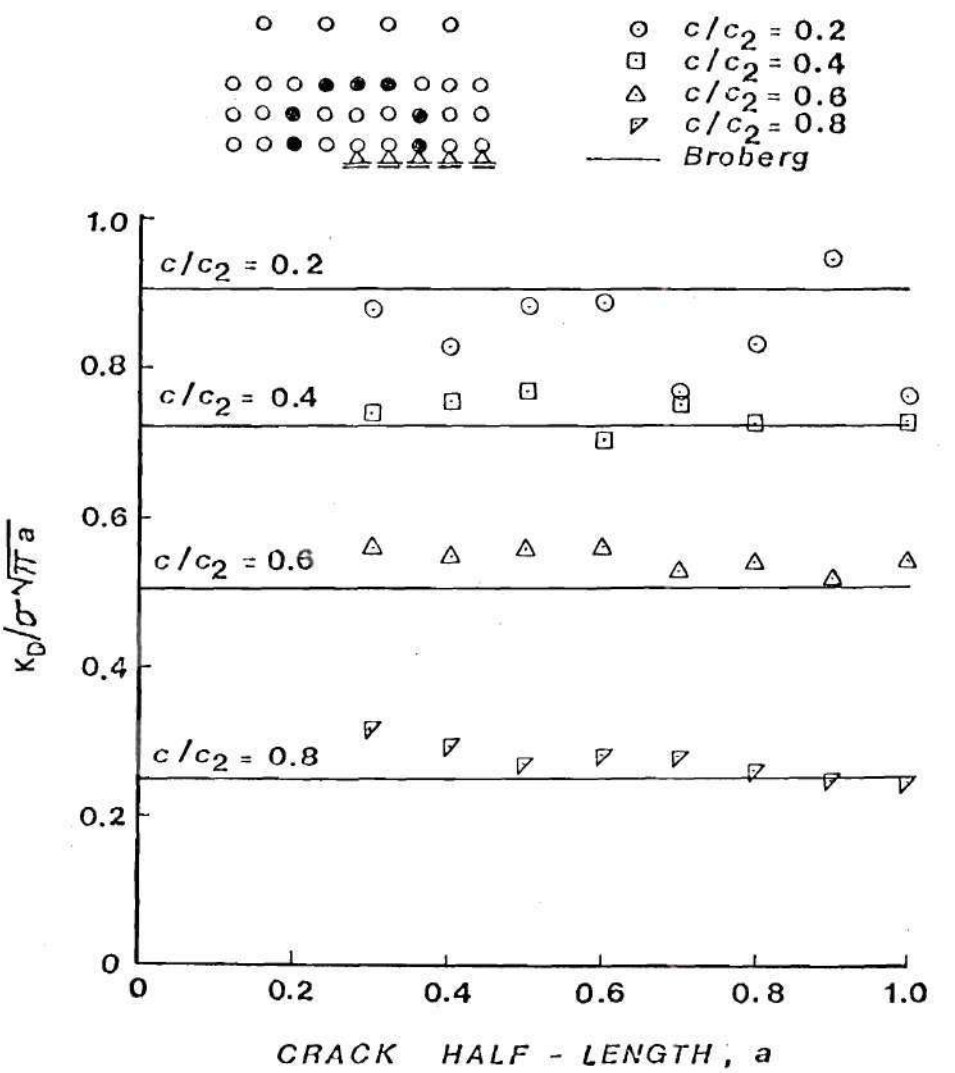

Figure 46. Stress-Intensity Factors, Middle Nodes, 4 Term Fit.

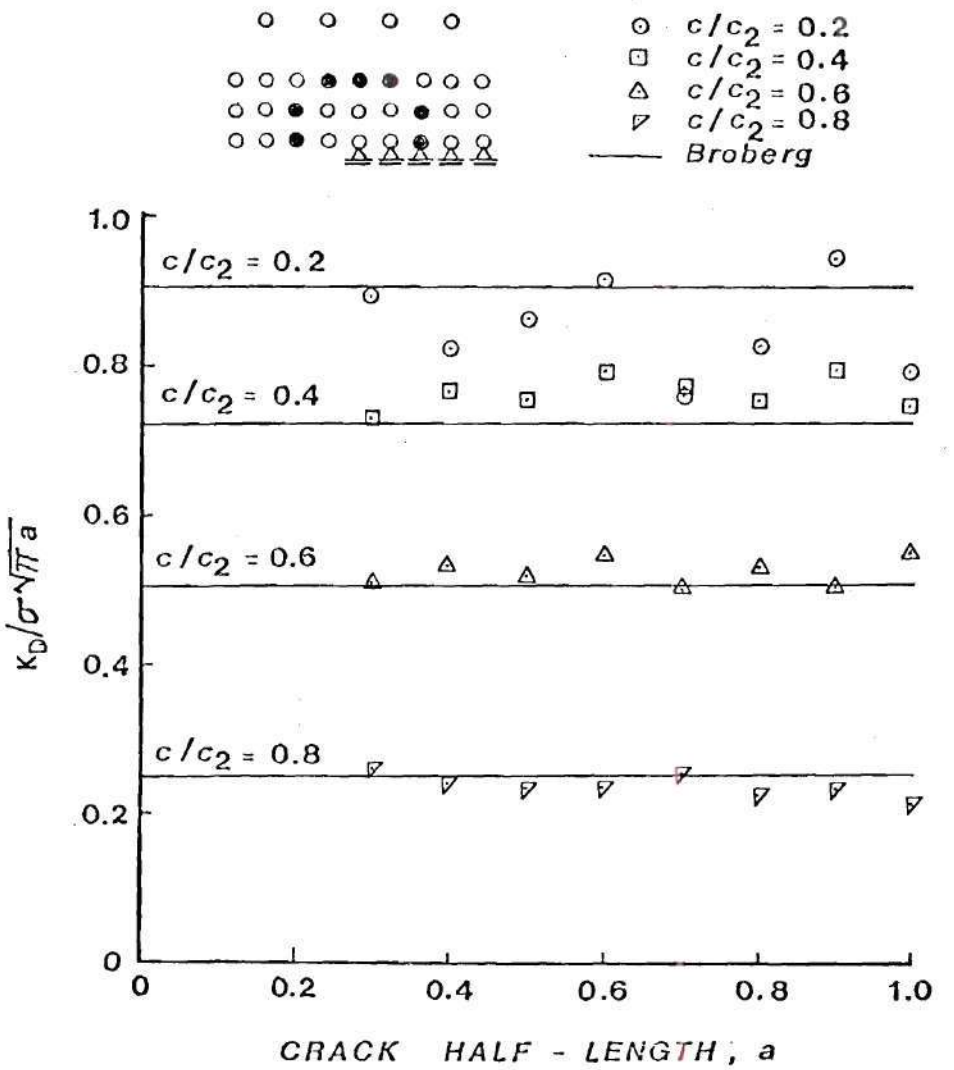

Figure 47. Stress-Intensity Factors, Middle Nodes, 5 Term Fit.

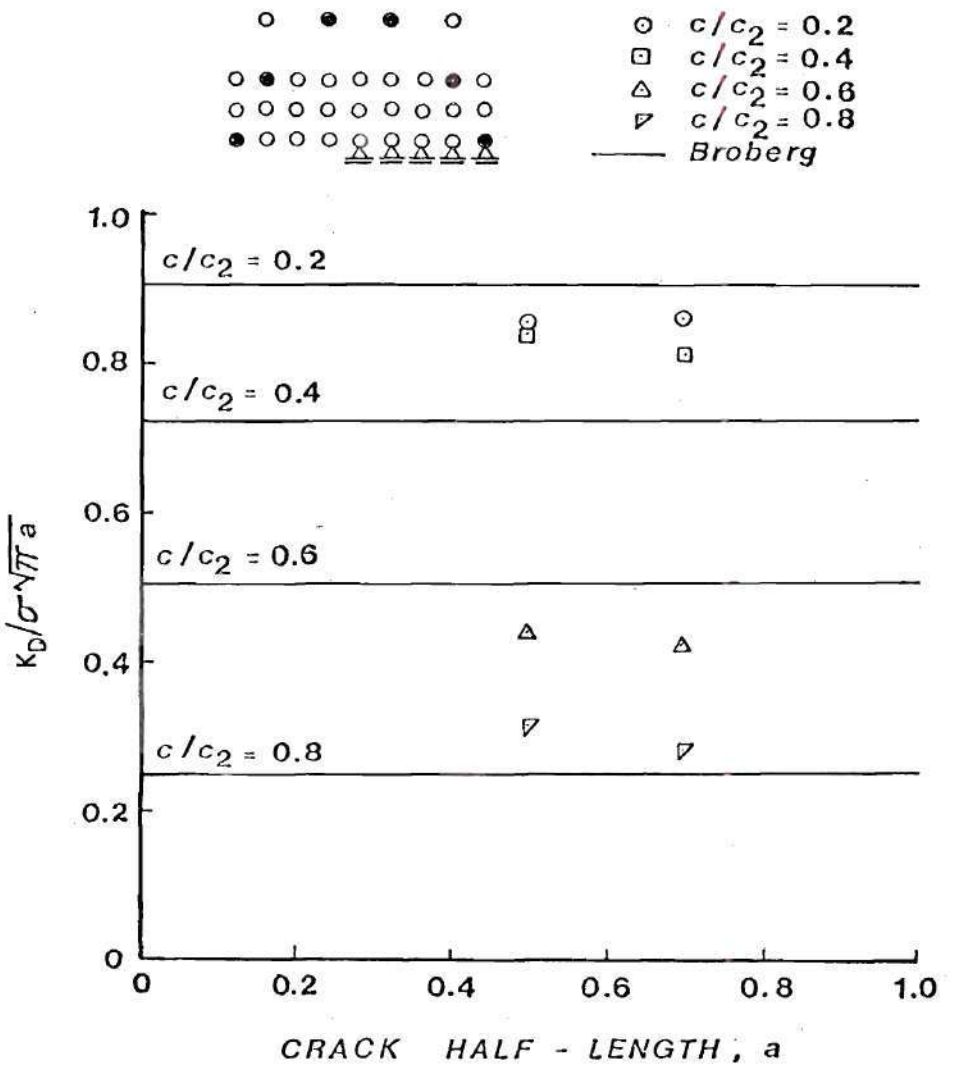

Figure 48. Stress-Intensity Factors, Outer Nodes, 11 Term Fit.

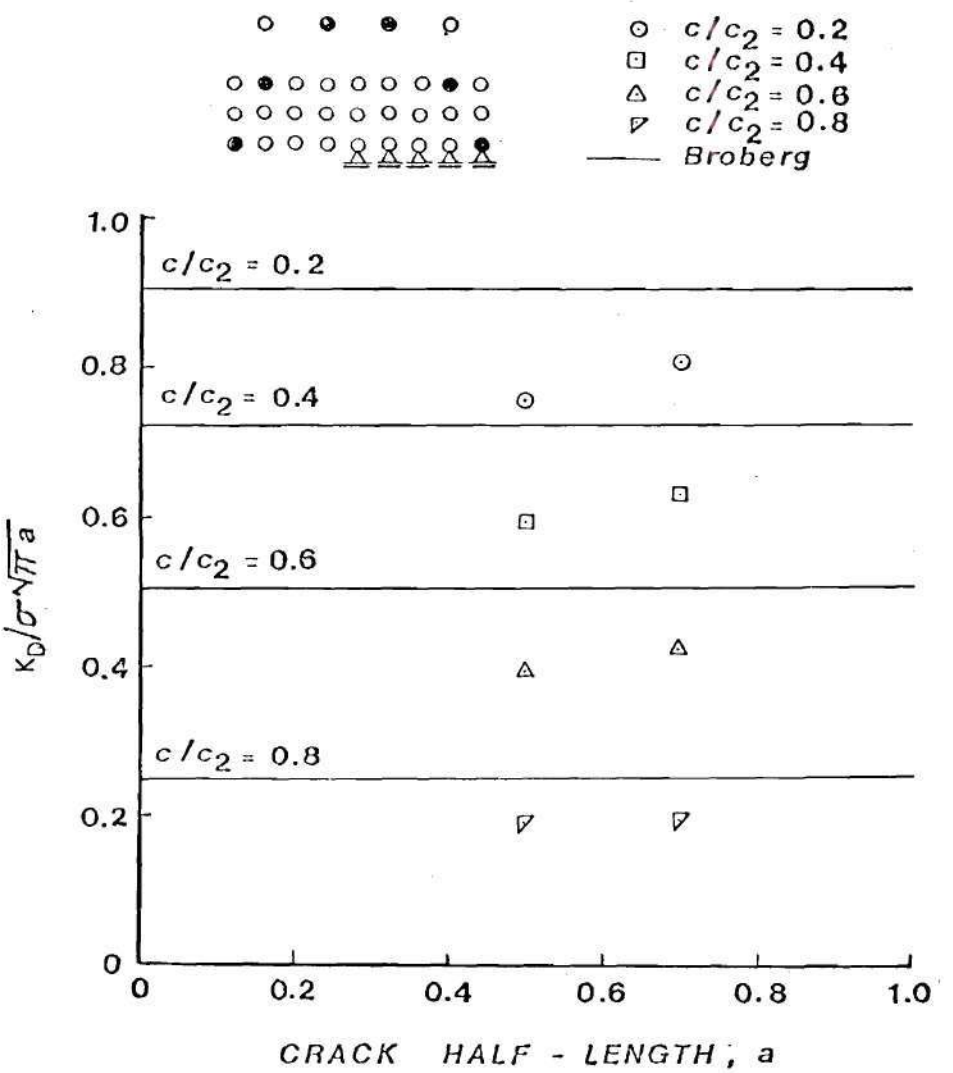

Figure 49. Stress-Intensity Factors, Outer Nodes, 2 Term Fit.

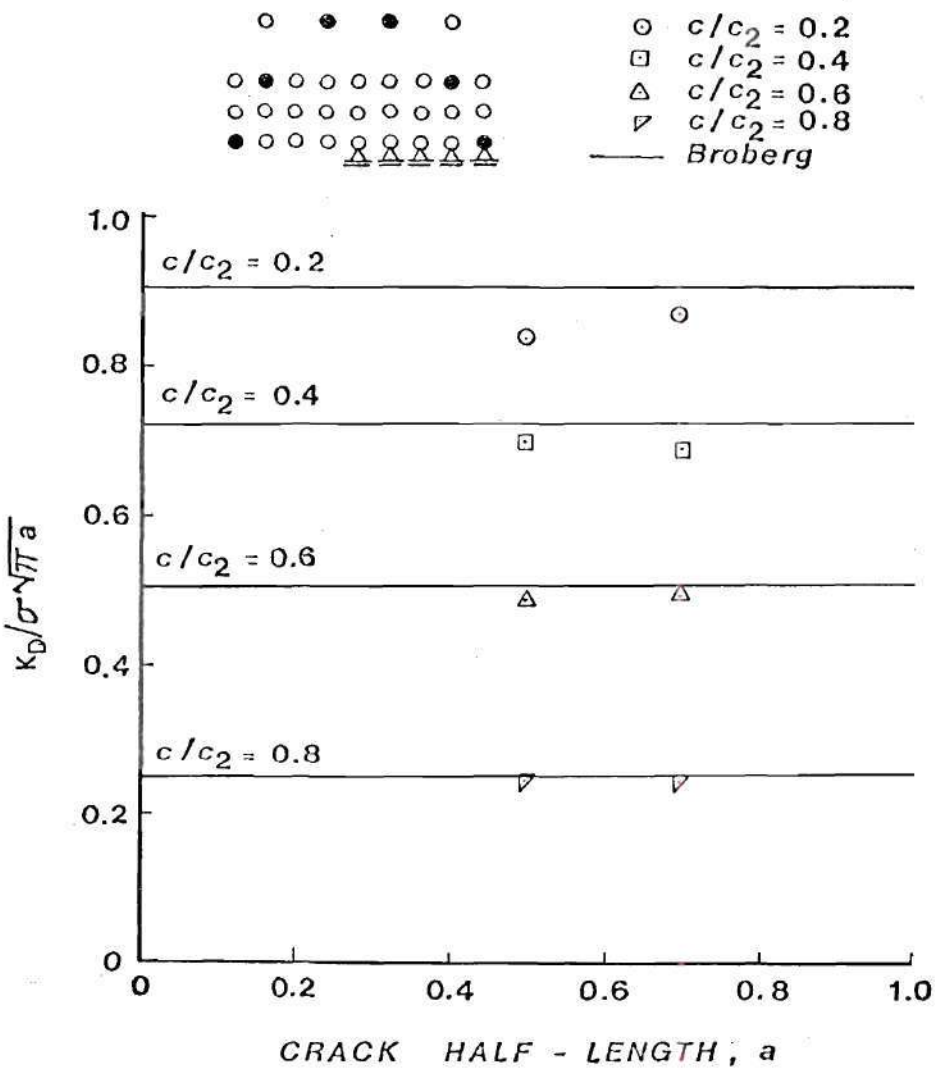

Figure 50. Stress-Intensity Factors, Outer Nodes, 4 Term Fit.

BIBLIOGRAPHY

1. Achenbach, J. D., "Dynamic Effects in Brittle Fracture," Mechanics Today, Vol. 1, Ed. by S. Nemat-Nasser, Pergamon, (1972), pp. 1-57.

2. Yoffe, E. H., "The Moving Griffith Crack," Philosophical Magazine, 42, No. 330, (July 1951), pp. 739-750.

3. Craggs, J. W., "On the Propagation of a Crack in an Elasto-Brittle Material," Journal of the Mechanics and Physics of Solids, Vol. 8, (1960), pp. 66-75.

4. Broberg, K. B., "The Propagation of a Brittle Crack," Arkiv für Fysik, 18, 159, (1960), pp. 159-192.

5. Tsai, Y. M., "Propagation of a Brittle Crack at Constant and Accelerating Speeds," International Journal of Solids and Structures, Vol. 9, (1973), pp. 625-642.

6. Baker, B. R., "Dynamic Stresses Created by a Moving Crack," Journal of Applied Mechanics, Vol. 29, No. 3, (1962), pp. 449-458.

7. Achenbach, J. D., and Nuismer, R., "Fracture Generated by a Dilatation Wave," International Journal of Fracture Mechanics, Vol. 7, No. 1, (March 1971), pp. 77-88.

8. Freund, L. B., "Crack Propagation in an Elastic Solid Subjected to General Loading - I. Constant Rate of Extension," Journal of the Mechanics and Physics of Solids, Vol. 20, (1972), pp. 129-140.

9. Freund, L. B., "Crack Propagation in an Elastic Solid Subjected to General Loading - II. Non-Uniform Rate of Extension," Journal of the Mechanics and Physics of Solids, Vol. 20, (1972), pp. 141-152.

10. Freund, L. B., "Crack Propagation in an Elastic Solid Subjected to General Loading - III. Stress Wave Loading," Journal of the Mechanics and Physics of Solids, Vol. 21, (1972), pp. 47-61.

11. Freund, L. B., "Crack Propagation in an Elastic Solid Subjected to General Loading - IV. Obliquely Incident Stress Pulse," Journal of the Mechanics and Physics of Solids, Vol. 22, (1972), pp. 137-146.

12. Kostrov, B. V., "On the Crack Propagation with Variable Velocity," International Journal of Fracture, Vol. 11, No. 1, (February 1975), pp. 47-56.

13. Gillis, P. P., and Gilman, J. J., "Double-Cantilever Cleavage Mode of Crack Propagation," Journal of Applied Physics, 35, (1964), pp. 647-658.

14. Berry, J. P., "Some Kinetic Considerations of the Griffith Criterion for Fracture - I. Equations of Motion at Constant Force," Journal of the Mechanics and Physics of Solids, Vol. 8, (1960), pp. 194-206.

15. Berry, J. P., "Some Kinetic Considerations of the Griffith Criterion for Fracture - II. Equations of Motion at Constant Deformation," Journal of the Mechanics and Physics of Solids, Vol. 8, (1960), pp. 207-216.

16. Burns, S. J., and Bilek, Z. J., "The Dependence of the Fracture Toughness of Mild Steel on Temperature and Crack Velocity," Metallurgical Transactions, Vol. 4, (April 1973), pp. 975-984.

17. Bilek, Z. J. and Burns, S. J., "Crack Propagation in Wedged Double Cantilevered Beam Specimens," Journal of the Mechanics and Physics of Solids, Vol. 22, (1974), pp. 85-95.

18. Bilek, Z. J., and Burns, S. J., "The Dynamics of Crack Propagation in Double Cantilevered Beam Specimens," Proceedings of the Conference on Dynamic Crack Propagation, Noordhoff International Publishers, Leyden, The Netherlands, (1973), pp. 371-385.

19. Kanninen, M. F., "An Augmented Double Cantilever Beam Model for Studying Crack Propagation and Arrest," International Journal of Fracture, Vol. 9, No. 1, (March 1973), pp. 83-91.

20. Hahn, G. T., Hoagland, R. G., Kanninen, M. F., and Rosenfield, A. R., "A Preliminary Study of Fast Fracture and Arrest in the DCB-Test Specimen," Proceedings of the Conference on Dynamic Crack Propagation, Noordhoff International Publishers, Leyden, The Netherlands, (1973), pp. 649-662.

21. Kanninen, M. F., Rosenfield, A. R., and Hoagland, R. G., "Fast Fracture in PMMA," Deformation and Fracture in High Polymers, H. Kausch et al. ed., Plenum Press, New York (1973), pp. 471.

22. Kanninen, M. F., "A Dynamic Analysis of Unstable Crack Propagation and Arrest in the DCB Test Specimen," International Journal of Fracture, Vol. 10, No. 3, (September 1974), pp. 415-430.

23. Hahn, G. T., Hoagland, R. G., Kanninen, M. F., Rosenfield, A. R., and Sejnoha, R., "Fast Fracture Resistance and Crack Arrest in Structural Steels," Naval Ship Systems Command, Report Number SSC-242 (1973).

24. Kanninen, M. F., "An Analysis of Dynamic Crack Propagation and

Arrest for a Material Having a Crack Speed Dependent Fracture Toughness," Conference on the Prospects of Fracture Mechanics, Delft, The Netherlands, 1974, pp. 251-266.

25. Wilkins, M. L., "Computer Simulation of Fracture," Sagamore Army Materials Research Conference Proceedings, Vol. 17, Shock Waves and the Mechanical Properties of Solids, Syracuse University Press, (1970), pp. 387-394.

26. Shmuely, M., and Alterman, Z. S., "Crack Propagation Analysis by Finite Differences," Journal of Applied Mechanics, Vol. 40, No. 4, (December 1973), pp. 902-908.

27. Shmuely, M., and Peretz, D., "Static and Dynamic Analysis of the DCB Problem in Fracture Mechanics," International Journal of Solids and Structures, Vol. 12, (1976), pp. 67-79.

28. Kobayashi, A. S., Emery, A. F., and Mall, S., "Dynamic Finite Element and Dynamic Photoelastic Analysis of Two Fracturing Homalite - 100 Plates," ONR Technical Report No. 23, (December 1975).

29. Williams, M. L., "On the Stress Distribution at the Base of a Stationary Crack," Journal of Applied Mechanics, Vol. 24, No. 1, (March 1957), pp. 109-114.

30. Aberson, J. A., and Anderson, J. M., "Cracked Finite Elements Proposed for NASTRAN," NASA TMX-2893, NASA Langley Research Center, Hampton, Virginia (September 1973).

31. Anderson, J. M., Aberson, J. A., and King, W. W., "Finite Element Analysis of Cracked Structures Subjected to Shock Loads," Computational Fracture Mechanics, Ed. by E. F. Rybicki and S. E. Benzley, American Society of Mechanical Engineers, New York, (1975).

32. Cotterell, B., "On the Nature of Moving Cracks," Journal of Applied Mechanics, Vol. 31, No. 1, (March 1964), pp. 12-16.

33. Rice, J. R., "Mathematical Analysis in the Mechanics of Fracture," Fracture, ed. by H. Liebowitz, Academic Press, (1968), pp. 191-200.

34. Nilsson, F., "A Note on the Stress Singularity at a Non-Uniformly Moving Crack Tip," Journal of Elasticity, Vol. 4, No. 1, (March 1974), pp. 73-75.

35. Leonard, R. W., and Budiansky, B., "On Traveling Waves in Beams," NACA Report 1173, (1955).

36. Shah, R. C., "Exploratory Investigation of Rapid Crack Propagation and Crack Arrest," Technical Report AFFDL-TR-73-95, Boeing

Aerospace Company, Seattle, Washington, (1973).

37. Fung, Y. C., Foundations of Solid Mechanics, Prentice-Hall (1965), pp. 186-189.

38. Kolsky, N., Stress Waves in Solids, Dover Publications, (1963), pp. 16-23.

39. Kobayashi, A. S., "Photoelasticity Techniques," Experimental Techniques in Fracture Mechanics, Ed. by A. S. Kobayashi, Society for Experimental Stress Analysis, (1973), pp. 126-145.

40. Sih, G. C., "Dynamic Aspects of Crack Propagation," Inelastic Behavior of Solids, ed. by M. F. Kanninen et al., McGraw-Hill, New York, (1970), pp. 607-639.

41. Chan, S. P., Cox, H. L., and Benfield, W. A., "Transient Analysis of Forced Vibrations of Complex Structural-Mechanical Systems," Journal of the Royal Aeronautical Society, Vol. 66, (July 1962), pp. 457-460.

42. Pipes, L. A., and Harvill, L. R., Applied Mathematics for Engineers and Physicists, McGraw-Hill, (1970), pp. 562-567.

VITA

John F. Malluck was born in Providence, Rhode Island on March 21, 1949. John entered Georgia Tech in June, 1967. He received a Bachelor of Aerospace Engineering in June, 1972 under the co-operative program. His co-op training was undertaken at the General Dynamics Corporation in Fort Worth, Texas. In September 1972, John enrolled as a graduate student in The School of Engineering Science and Mechanics at Georgia Tech. He received a Master of Science in Engineering Mechanics in September, 1973. John is currently employed in the Aeronautical Research Department of the Lockheed-Georgia Company.

John is married to the former Sandra Michele Giuliani, also from Providence, Rhode Island. They have one child, Lisa Michele, born in 1974.